SAPIENZA
UNIVERSITÀ DI ROMA

SCUOLA DI DOTTORATO "VITO VOLTERRA"

PhD in Chemical Sciences- XXXII Cycle

Preparation and characterization of screening methods for classification and quality control of olive oils

Daniele Zappi
Matriculation number 1320355

Thesis Advisor: Prof. Claudia Sadun

Ph.D. Program Coordinator: Prof. Osvaldo Lanzalunga

Academic year 2018-2019

Index

1. Purpose of the thesis

The main goal of this Ph.D. research has been the development, characterization, and application of innovative procedures and sensing tools for olive oil quality control, in particular, one or more analytical methods useful to categorize olive oils and detect frauds relating to olive oil quality, composition, and origin have been pointed out.

In order to obtain a friendly platform for users with minimal waste production, all the methodologies had been aimed to minimize the organic solvent use or any other environmental toxic material.

In order to monitor as many parameters as possible concerning olive oils, different approaches to the olive oil quality problem were sought.

The first developed analytical system was constituted by a screen-printed electrode modified with green ionic liquids and nanomaterials. The initial tests were performed to find the best RTIL/nanomaterial combination [1] for the electrode modification. Then the RTIL/nanomaterial proportions in the functionalization mixture were optimized using a chemometric approach. Further studies were performed to understand if the best platform performance could be achieved by the enzyme immobilized on the electrode or incubated with the sample and the resulting mixture dropped on the electrode [2]. Finally, the optimized platform was used to analyze monocultivar oil samples collected over three years from various geographical origins in order to verify a possible classification based on the oil cultivar or geographical origins [3].

A second analytical system was developed to detect if an oil sample was adulterated or replaced with lower quality oils poor in polar antioxidants. To this aim, deep eutectic solvents (DES) were employed as an extraction medium for polar phenolic compounds present in olive oils. A screen-printed electrode was modified using a mixture of nanomaterials suspended in Nafion resin. At the same time, the extraction procedure of the polar phenolic compounds from olive oil was optimized by means of various mechanical steps. The DES phase was analyzed with the modified electrode

to quantify the polar phenols, which are only present in olive oil and not in other edible seed oils.

Finally, WAX and SAX diffraction measurements were performed to search a possible classification of olive oils, based on differences in the structures created by triglycerides aggregates. To this end, oil samples were analyzed using energy-dispersive X-ray diffraction (EDXD), which allowed fast and easy measurements of the oils with no pretreatment of the sample.

2. Introduction

2.1. Olive Oil

Olive oil is defined as the oil obtained from the fruits of the olive tree (*Olea europae L.*) by mechanical means with processes that do not alter the oil organoleptic characteristics.

Olive trees seem to have coexisted alongside with humans since the early Bronze Age (3150 – 1200 BC). The origins of olive cultivation can be traced back to the east Mediterranean zone, nowadays corresponding to Turkey, Syria, Lebanon, Palestine, and Israel. Numerous archaeological finds suggest that olive trees were actively cultivated by the ancient farmers and both olives and olive oil were an integral part of their diet [4].

It is supposed that the Phoenicians (1000 BC) first brought the cultivation of olive trees in southern Spain and Northen Africa coasts, while the Greeks imported olive plants to their colonies in Southern Italy [5]. When the nascent Roman Empire came in contact with the Greek colonies in South Italy, they adopted the olive tree cultivation and, during their subsequent conquest of Europe, were responsible for spreading the tree across the Empire [6]. Romans did not mainly use olive oil for food purposes, preferring its use for personal hygiene, religious rites, as pharmaceutical ointments to treat diseases and as fuel for illumination [7].

Olive oil continued to be one of the central plants in numerous plantation in Southern Europe until the early 20th century where the discovery and development of low-cost solvent extraction of seed oils coupled with the rise of other sources of illumination (gas first and electricity later) marked a sharp decline in olive oil demand.

Olive oil returned in high demand when, in recent years, numerous scientific publications underlined its importance in human nutrition. Olive oil is a central food of the so-called "Mediterranean diet" [38], used both during cooking and poured raw on foods for flavoring. More and more proofs are emerging that this extensive use of

olive oil done by people in the Mediterranean area is correlated with a lower incidence of various illnesses and health problems such as obesity [8], hypertension [9], some types of cancer [10] and a general improvement in the functioning of the immune system [11], [12]. This is because, as opposed to seed oils, olive oil is a complex mixture of substances, mainly triacylglycerols (up to 99% of total weight), and a plethora of minor compounds, such as [6]:

- Pigments (mainly chlorophylls and carotenoids);
- Aliphatic and aromatic alcohols;
- Sterols (mainly cholesterol);
- Antioxidants: polar (various phenolic compounds) and nonpolar (mainly tocopherol group);
- Various volatile and aroma compounds (alcohols, esters, aldehydes, ketones, etc.).

Regarding the fatty acids making up the triacylglycerols, their composition varies strongly depending on genetic profile (*cultivar*) from which the olives have been obtained. The most common fatty acid encountered in olive oils (and relative abundance) are:

- Oleic acid (C18:1 55.0-83.0 %)
- Palmitic acid (C16:0 7.5-20.0 %)
- Linoleic acid (C18:2 3.5-21.0 %)
- Stearic acid (C18:0 0.5-5.0 %)
- Palmitoleic acid (C16:1 0.3-3.5 %)
- Others (less than 1.0 % each)

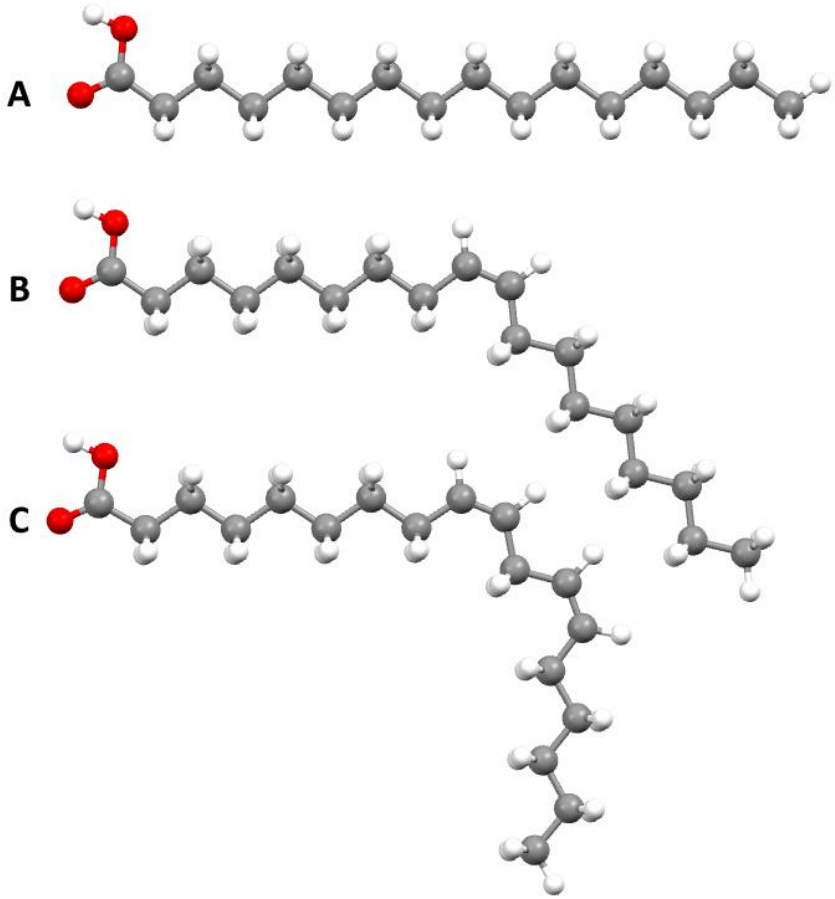

Figure 2.*1* Most prevalent fatty acids forming triglycerides in olive oil: A) Palmitic acid; B) Oleic acid; C) Linoleic acid

As can be seen (Figure 2.1), olive oils are mostly composed of unsaturated fats unlike other traditional fats such as butter rich in saturated fats [13].

2.1.1. Olive oil production

In order to maintain the aforementioned beneficial properties for human health, olive oil must be obtained from olives with methods that minimize the degradation of the final product.

The extraction of oil from olives is mainly carried out by two methods: a discontinuous method carried out with traditional mills and a continuous one performed with "modern" mills.

The operating cycle of a traditional mill requires that the olives are washed (not always defoliated) before grinding. For crushing, ancient stone wheels (molazze) are

used. The olive paste produced is distributed on fiber disks (now synthetic fiber, once made of vegetable fiber) called "fiscoli", which are placed one above the other. The stack thus obtained is then pressed to obtain the oil. The main advantage of a traditional oil mill is that the paste suffers lower heating and less mechanical stress. On the other hand, there are some disadvantages in using this system, such as long processing times, difficult cleaning of the machines used, prolonged exposure of the paste to air and light, all of which can lead to oxidation of the oil.

The modern oil mill with a "continuous cycle" system consists of a set of machines continuously connected to each other, thus excluding any interruption in processing. The phases of the olive oil extraction process are washing, crushing, kneading, centrifugation, and separation. Different extraction methods are used, the most common one is the 3-phase cycle (oil/water/pomace): the olives are washed and defoliated, are sent to the olive press which continuously produces an olive paste that goes to the kneader. The olive paste, appropriately added with water (characteristic of the 3-phase cycle), is sent to the centrifuge, which separates the paste in its three components: pomace, vegetation water, and oil-water emulsion. The emulsion is sent to another centrifugal separator to extract the oil. The main advantages of this method are the speed and cleaning of the process, the main disadvantages are the high cost of machinery and energy. Furthermore, since the machine involved in the process work in a closed-circuit system, the temperature of the olive paste can rise to levels where degradation processes can happen, especially during the crushing and kneading phases.

2.1.2. Olive oil quality regulation

Olive oil quality parameters have been defined by the International Olive Council (IOC) [14]. The three major parameters that are used to categorize an olive oil are:

- *Acidity* (expressed as % m/m of free oleic acid). It is an index of deterioration of the structure of the triglycerides, due to incorrect storage (i.e., oil in an untreated metal container or stored at high humidity/temperature), microbial contamination or low quality of the olives.
- *Peroxide value* (expressed as milliequivalents of peroxide oxygen per oil kg). An index of oxidation of the fatty acids of the oil. A high value could be due to long time exposure of the oil to air/light/high temperature during the grinding phase of production.
- *Absorbance in ultra-violet* (K_{270} - K_{232}). Measurement that gives the abundance of ketonic and aldehydic compounds in the oil. These compounds are produced by the fragmentation and decomposition of the peroxidated free fatty acids of the oil.

Based on the analyses of these factors, the olive oils are thus categorized:

	Acidity (% m/m free oleic acid)	**Peroxide value** (m eq. peroxide per kg/oil)	**UV Absorbance**	
			K270	**K232**
Extra-virgin olive oil	≤ 0.8	≤ 20	≤ 0.22	≤ 2.50
Virgin olive oil	≤ 2.0	≤ 20	≤ 0.25	≤ 2.60
Olive oil	≤ 1.0	≤ 15	≤ 0.90	//
Lampante olive oil	> 3.3	No limit	//	//

Table 2.1 Categorization of olive oils based on analytical parameters according to International Olive Council

For olive oil production in the European Union, the analytical procedures for the determination of these parameters have been defined by Commission Regulations [15], [16]. Furthermore, these regulations define that the label must not contain false, misleading information or anything else to to deliberately mislead the consumers about the origin, the organoleptic qualities and/or the composition of the product.

2.1.3. Olive oil adulteration

Due to the considerable market involved (2,186 million tons of olive oil produced in Europe) and the large request (1,584 million tons consumed only in Europe) [17] the risk of frauds concerning the adulteration of olive oils is high. The problem is further exacerbated by the progressive increase in prices of commercial extra-virgin olive oils caused by worsening climate conditions in Italy, Greece, and Spain so that an increasing portion of the commercialized olive oil comes from extra-European sources. Traceability for these oils is often poor, and scams and frauds are common.

The analytical techniques proposed by the European Union to ascertain olive oil quality and to certify the commercial category, are not useful to classify extra-virgin olive oils according to their geographical origin [18]. Furthermore, scammers have found ways to adulterate the oils sold in ways as to deceive the analyses.

The typical frauds performed in recent years to evade such controls are [19]–[22]:

- replacement of all or part of the olive oil with different seed oils (sunflower, hazelnut, etc.), the oil is then added with chlorophyll/carotenoids to obtain an olive oil-like color
- mixing extra-virgin olive oil with olive oils of lower quality (i.e., virgin or lampante virgin olive oils); if acidity results over the limit for extra-virgin oils, the oil is deacidified by addition of sodium hydroxide and removal (by filtration) of the formed precipitate;
- chemical/physical treatment of low-quality oils to make them look-like extra-virgin ones: oils can be subjected to deodorization (removal of volatile compounds such as aldehydes, alcohol and short-chain carboxylic acids responsible for odor defects [23]), deacidified, added with dyes (for example chlorophyll, carotenoids) to correct color;
- replacement or mixing of the PDO oils (Protected Denomination of Origin) with oils of unknown origin.

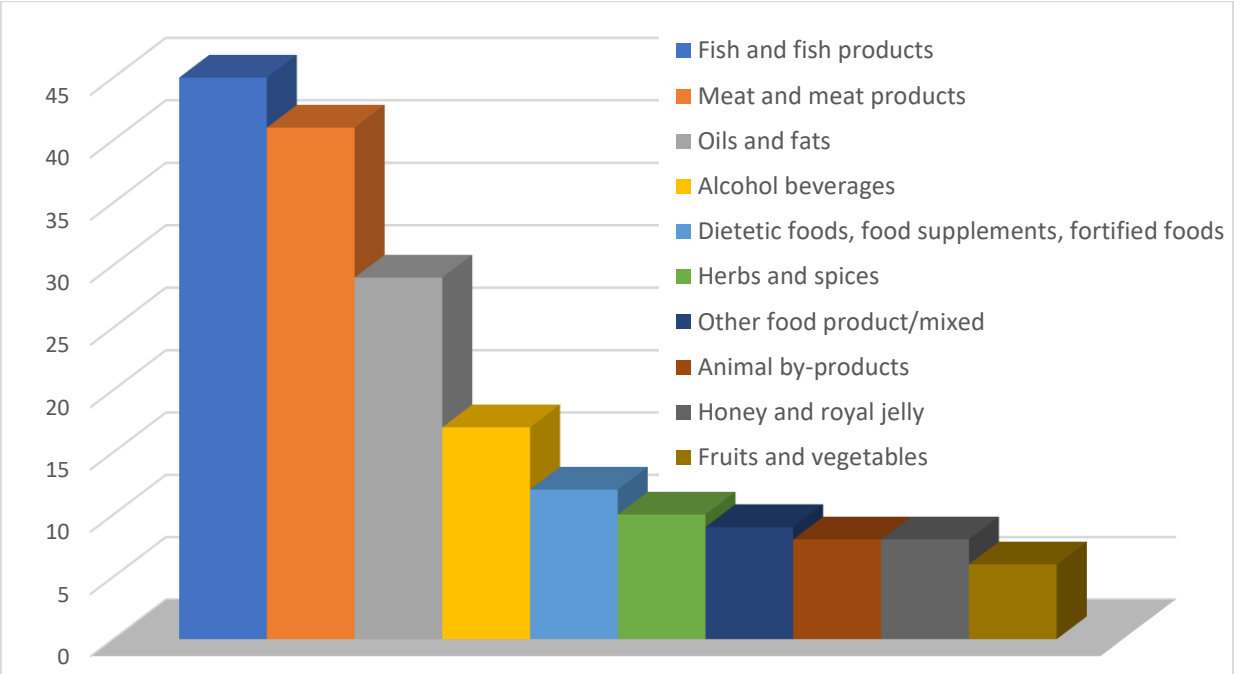

Figure 2.2 Top 10 product categories (number of requests) in the Administrative Assistance and Cooperation System – Agri-Food Chain (AAC-FF) in 2018 (data from "The EU Food Fraud Network and the System for Administrative Assistance - Food Fraud - Annual Report 2018.", European Commission for Health and Food Safety).

As can be seen from Figures 2.2 and 2.3, frauds concerning fats and oils have been quite common in recent years. In Figure 2.3 it can be observed that the majority of the frauds (59%) are due to mislabeling of the final product sold to the consumers. Still, a noteworthy percentage of the frauds consists of adulteration of the product (18%) by addition and/or replacement of the product with others of lower quality, unapproved treatment and or processes (5%) in order to improve the production yield and/or the organoleptic qualities of the product and, finally, alteration of origin documentation, composition and production method of the fat/oil transported and sold.

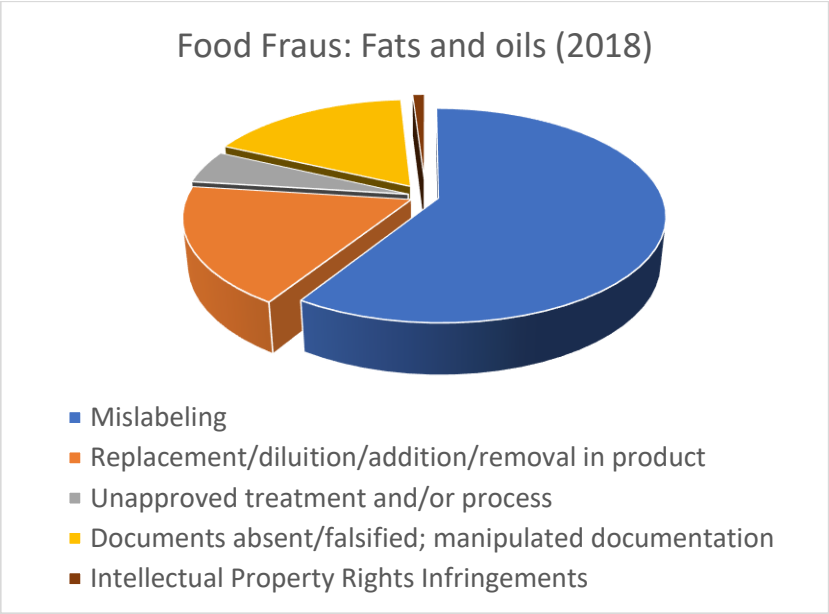

Figure 2.3 Types of suspected violations relating to fats and oils (data from "The EU Food Fraud Network and the System for Administrative Assistance - Food Fraud - Annual Report 2018.", European Commission for Health and Food Safety).

The rapid and reliable detection of such adulterations has been the object of numerous researches in recent years. Many innovative analytical procedures have been proposed, including not only sample preparation and analysis but also data processing and interpretation with chemometric techniques. As seen before, olive oil is a complex matrix, where the most abundant compounds (triglycerides and free fatty acids) are very similar both for composition and abundance to those present in other seed oils.

FT-NIR [24] and Raman scattering spectroscopy [25] techniques, implemented by chemometric data treatment, can be successfully employed to monitor the compositions and relative abundances of fatty acids, trans-fatty acids, and triacylglycerols.

NMR spectroscopy techniques (^{1}H, ^{13}C, and ^{31}P) have been extensively used in virgin oil adulteration control and two different approaches can be employed [26], [27]. In one case, NMR spectroscopy can be employed to perform quantitative analysis of olive oil triacylglycerols, fatty acids, and sterols, and anomalous compounds can be quickly individuated. In the other one, NMR can be employed to detect specific peaks

related to the "fingerprint" of low-quality seed oils typically used for adulteration, down to very low detection limits.

Mass spectrometry (both alone and coupled with LC technique) is probably one of the most common analytical techniques present in the literature regarding EVOO adulteration detection. Direct infusion of the oil sample in the Mass spectrometer leads to complex spectra revealing the fragments of all the present oil compounds. It has been demonstrated [28], [29] that, by processing the obtained spectra with chemometric tools, it is possible to discriminate between pure EVOOs and adultered oils. When combined with a separation technique (commonly HPLC), mass spectroscopy can be used to exactly determine all the components of the oil under examination. This methodology allows adulterant compounds to be detected at very low levels; if coupled with spectra databases, the methodology allows the geographical origin of the oil to be identified [30]–[32].

While these methods succeeded in identifying frauds, they have proved to be too expensive, time-consuming and difficult to apply to the large-scale analyses, routinely performed at custom offices on imported foods from Countries outside the EU. At the same time, with the removal of custom office at the border between different EU countries, it is increasingly difficult to identify adulterated olive oils marketed around the European Union.

2.2. Biosensors

To determine analytes of interest more and more sensitive and selective methods have been sought in the Analytical Chemistry field. At the same time, many attempts have been carried out to yield portable and straightforward systems for analyses on the field. All the methods involving biosensors hold these characteristics.

Numerous research groups deal with biosensor technology, driven by the great versatility of molecular recognition of receptors and because the single device allows the main analytical requirements to be satisfied: easy sampling and sample processing, quick processing data analysis, and interferences reduction.

A biosensor is defined as an analytical device capable of performing qualitatively and possibly quantitatively analyte determination employing the specific interaction between the analyte and bioactive component used. Due to this interaction, the variation of a physical or chemical property of the bioactive element is converted into a measurable signal, through the appropriate signal transducer [33]. The signal thus obtained, appropriately amplified and processed, will provide the qualitative or quantitative analytical information required. The purpose of a biosensor is, therefore, to convert a chemical parameter (concentration of an analyte or group of analytes) into a digital signal (Figure 2.4).

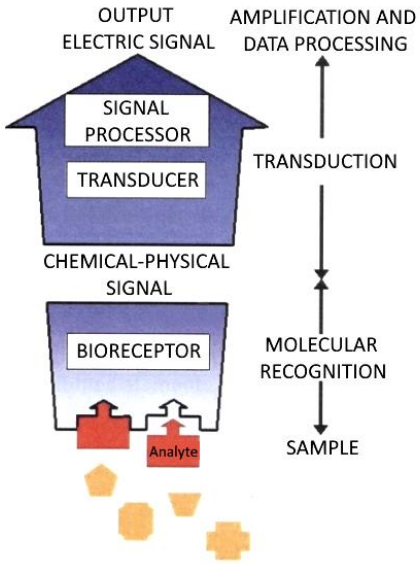

Figure 2.4 Scheme of a biosensor

Biosensors can be classified using different parameters:

- Analyte/bioactive element interaction kind: the measured signal derives from the concentration variation of a reagent or a product of the reaction catalyzed by the enzyme (biocatalysis) or from the variation of a chemical-physical property of the bioactive element (charge density; interaction with light; etc.), after its association with the analyte (bioaffinity) [34].
- Bioactive element type: the type of bioreceptor used varies widely depending on the searched analyte and the sensitivity and selectivity required. It is possible to use, as bioactive elements, single biomolecules (e.g., proteins, enzymes, antibodies, nucleic acid segments), entire microbial cells, parts of plant or animal tissues or small organisms (lichens, molds, etc).
- Transduction system: the transduction system employed in the biosensor strongly depends on the properties of the chosen bioactive component and the target analyte. The most common transduction systems are. [35]:
    - *Optical based*: measurement of the variation of intensity or frequency of electromagnetic radiation absorption or emission after the interaction between the analyte and bioactive component. [36].
    - *Acoustic based*: measurement of the vibration frequency variation of a piezoelectric crystal subjected to an alternating current after the interaction. [37]
    - *Calorimetric based*: measurement of the amount of heat produced or absorbed by the interaction (with known enthalpy). [38]
    - *Electrochemical based*: measurement of the variation of electrochemical parameters of the system:
        - Amperometric: measurement of current intensity produced in the measuring cell under a constant fixed potential. [39]
        - Potentiometric: measurement of the potential difference between the working electrode and reference electrode during the studied interaction [40]

- Conductometric: measurement of the conductivity variation in the measuring cell due to the studied interaction [41].

2.2.1. Enzymatic Biosensors

Among the numerous biological receptors useful to produce a biosensor, the most commonly used are enzymes. In the past years, many enzymes catalyzing a large number of analytical interest reactions have been discovered and characterized, especially for the food and environmental fields. Furthermore, enzymes are often highly specific for the substrates under examination, making them suitable for creating biosensors with high specificity.

In an enzymatic biosensor, the interaction between the substrate and the enzyme takes place in a specific region of the protein, the active site. Here the chemical reaction takes place, and then the reaction products leave the active site. After that, a new reaction cycle can begin [35]. Small amounts of enzyme, the catalyst, are needed to catalyze the desired reaction and thus miniaturized and reusable sensors can be assembled.

Enzymes show a drastic activity decrease if they work in non-physiological conditions or in the presence of inhibitors or product excess. These applicability limits of enzymes affect their use in biosensors in extreme conditions: very high/low temperatures, acidic/basic solutions, high ionic concentrations, presence of inhibitors, etc. It must be taken into account that some enzymes require cofactors to exploit their catalytic function; therefore, the reaction conditions for the cofactor must be considered too.

2.2.2. Electrochemical biosensors

Electrochemical biosensors have been the object of basic and applied research for more than fifty years. Leland C. Clark presented the first enzymatic electrode with

immobilized glucose oxidase during the Symposium at the New York Academy of Sciences in 1962 [42].

The most critical element of an electrochemical biosensor is the bioactive element which recognizes the target electroactive substance, producing the variation of an electrochemical property of the system transducted and recorded as a digital signal.

When enzymes-are used as bioactive components, the analyte acts as the enzymatic substrate; alternatively, the analyte can act as an inhibitor of a redox process involving the enzyme and another substrate. Furthermore, enzymes can be used to bind antibodies, antigens, or oligonucleotides with a specific sequence, creating mixed type sensors based on affinity. Common enzymes selected and studied to analyze clinical and food metabolites are alcohol dehydrogenase, glucose oxidase, glucose dehydrogenase, lactate dehydrogenase, and urease, etc. [43].

The most commonly used electrochemical biosensor is the amperometric one. Its operation is based on the measurement of the current produced by the oxidation or reduction of the analyte, at constant potential with respect to a reference electrode, in the presence of the counter electrode. The current thus produced is proportional to the concentration of the analyzed chemical species. The applied potential chosen depends on the oxidation/reduction potential of the analyte, on the reference electrode used and the presence of any electrochemical interferents.

The transfer of electrons between the enzyme and the electrode has been widely discussed along time.

Depending on the type of transfer, the amperometric biosensors can be divided into three generations (Figure 2.5):

- First generation biosensors: there is no electron transfer between enzyme and electrode. In this case, the concentration variation of the substrate or the product or a natural redox mediator (e.g.oxygen discharged at the working electrode) that gives rise to a redox reaction at the electrode, is measured.
- Second generation biosensors: the electron transfer between the enzyme and the electrode takes place through a mediator acting like a "shuttle system".

- Third generation biosensors: the direct electron transfer between the enzyme and electrode takes place (DET).

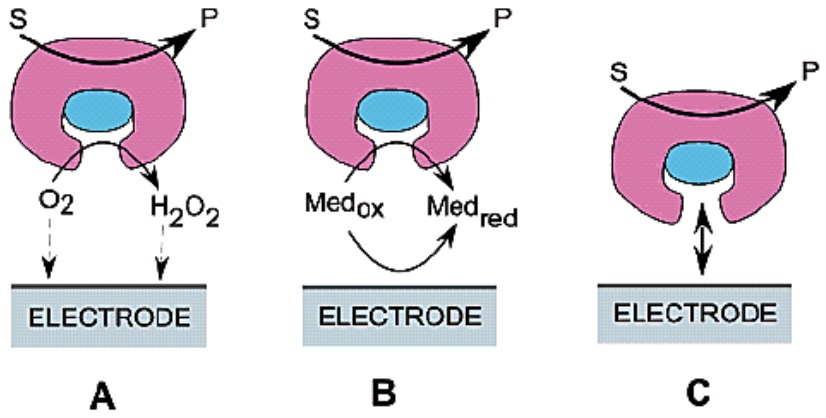

Figure 2.5 Amperometric biosensors: A) First generation; B) Second generation; C) Third generation (Antonelli M. L., et al., Edizione Nuova Cultura - Roma, 2015)

The first generation biosensors have obvious problems: the response is proportional not only to the substrate concentration but also to the secondary reagent concentration. The most common secondary reagent is oxygen, which causes further problems, mainly due to its high reduction potential (in absolute value) (-0.7 V).

In the second generation biosensors, problems have been overcome by replacing oxygen with a redox mediator. This kind of molecule can be oxidized and reduced reversibly by transporting electrons between the enzyme and the electrode. The mediator must have a low redox potential and a fast reaction to avoid interference by other electroactive substances.

The direct electron transfer (DET) that occurs in third-generation biosensors contributes to making the biosensor even more selective. The enzymatic reaction takes place directly on the working electrode, and the applied potential will-be the same as the enzyme. The absence of the mediator reduces the error sources. The principal disadvantage in the third generation biosensors development is the reduced number of redox enzymes that can give rise to the DET. Since the electron transfer channels of the enzyme must be near to the electrode and to the active site too, the structure and immobilization of the enzyme must be carefully studied.

Despite the previous issues, many third generation amperometric biosensors have been realized employing laccase, cytochrome c, peroxidase, glucose oxidase, alcohol dehydrogenase, etc. [44].

2.3. Nanomaterials

Recently the interest of the scientific community has been focused on “nanoscience” (formally defined by the National Nanotechnology Initiative in the USA), which deals with the study of the properties of nanometer-scale materials (1 to 100 nm). The idea to investigate the microscopic to make a change in scientific progress was set in 1959 by the American physicist Richard Feynman, considered the father of nanoscience, in a speech remembered as "There is plenty of room at the bottom" [45]. Since then, the interest in this sector began to develop, and it is continuing to increase.

Nanoscience represents a combination of different disciplines, ranging from physics to supramolecular chemistry, from material science to molecular biology. In general, nanotechnologies employ methods and knowledge specific to nanosciences and deal with the design, characterization, implementation, and application of structures, devices, and systems characterized by nanometric dimensions. Feynman's hypotheses proved to be well-founded in fact, nanomaterials were successfully employed in a large number of sectors, such as catalysis, optoelectronics, sensors, and drug delivery. The nanomaterials allow a broad spectrum of applications because the properties of materials (reactivity, mechanical strength, optical properties, magnetic properties, and electrical characteristics) strongly vary moving from the macroscopic to the nanoscale world. The properties of nanoparticles, therefore, differ both from those of massive substances, and from those of molecules and isolated atoms, being influenced by the presence of atoms that in this scale can be on the surface or in the bulk of the material (in nanoscale, electron-surface collisions cannot be neglected). Precisely because of this non-symmetry of the interface with the surrounding environment, there are considerable chemical-physical differences with bulk materials.

Nanomaterials can be classified based on the number of non-nanometric dimensions present in the system. At least one dimension must be in nanometric scale, i.e. <100 nm, so that, in these systems, at least one dimension shows quantum confinement effects (significant at size <10 nm):

- Nanocrystals, quantum dots, and atomic clusters: they are structures consisting of aggregates from tens to thousands of atoms, and present the three spatial dimensions in the nanometer scale. They are defined as 0D nanostructures.
- Nanotubes and Nanowires: they have one macroscopic dimension (the length), and two nanometric ones. Nanotubes, in particular, can be single or multiple coaxial structures. They are defined as 1D nanostructures.
- Nanostrates: they are thin surfaces or films, single or multiple, where the total stack thickness is in the nanoscale dimension. They are defined as 2D nanostructures.
- Nanostructures: they are materials having all the macroscopic dimensions but containing inside them 0D, 1D, 2D structures.

There are two general strategies for obtaining nanostructured materials: top-down and bottom-up. By the first method, nanomaterials are manufactured starting from macroscopic materials to reach nanoscale levels, through physical processes such as lithography, laser ablation, or irradiation of various types, etc.

The "bottom-up" method allows obtaining nanoparticles by chemical reactions starting from solutions, basing on the ability of specific atoms or molecules to self-assemble, through chemical bonds.

In both cases, the produced nanomaterials can be examined by various techniques to characterize their structure, and to find any defects:

- Scanning Electron Microscopy (SEM)
- Transmission Electron Microscopy (TEM)
- Scanning tunneling microscopy (STM)
- X-ray diffractometry

2.3.1. Multi-walled carbon nanotubes

Several research groups had already reported the discovery of structures similar to carbon nanotubes [46] dates back to the sixties, but it was only the article published by Ijima in 1991 [47] that carbon nanotubes became of interest in the scientific literature all over the world. Ijima first proposed a method for the synthesis of carbon nanotubes, without catalysts, similar to the fullerenes synthesis one [48]. Ijima discovered that nanometric tubular structures were formed by vaporizing graphite and each structure was constituted by coaxial tubes with a total diameter between 2 and 50 nm (single- or multiwalled nanotubes).

Carbon nanotubes are among the most resistant fibers known. They are chemically stable and are good conductors of electricity and heat. Trigonal carbon atoms covalently link each other forming a hexagonal network sheet, resulting in a structure that rolls up to form a single or a multi-tube. Each nanotube ends with a hemispherical structure similar to that of fullerene.

Carbon nanotubes have exceptional resistance to physical stress: subjected to axial stress, they bend over wide angles before deforming. Moreover, unlike what happens in some other polymers, these strains are elastic and disappear when the stress stops. There are three geometries in which the sheet can be rolled up to give rise to the nanotube: chair, zigzag, and chiral (Figure 2.6).

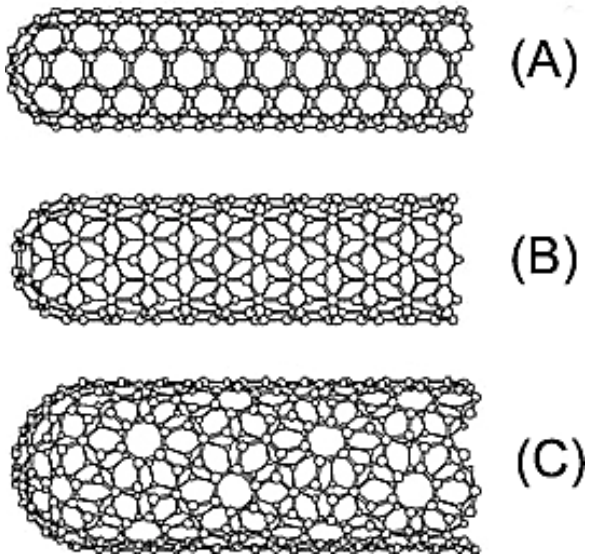

Figure 2.6 Nanotube structures: A) chair; B) zig-zag; C) chiral

The nanotube electrical conductivity depends on its structure: in chair conformation, it is similar to metals conductivity (106 S m^{-1}), while in zigzag and chiral conformations it tends to a semi-metallic behavior.

The high conductivity of carbon nanotubes is due to the quantum confinement of the electrons in the material. The only tube direction in which the electrons can disperse is the length: this derives from a characteristic of the starting material, graphene. By rolling the graphene to form a tube, boundary conditions are imposed on the carbon electrons. If the diameter of the nanotube becomes a multiple of the wavelength of an electron, the nanotube will be a conductor; otherwise, it will act as a semiconductor. A perfectly structured conductive nanotube will be a ballistic conductor, in which the resistance is not zero (as in the case of superconductors) but independent of the distance traveled by the electron in the tube (in contrast to Ohm's law).

From the chemical point of view, nanotubes are remarkably stable structures, almost inert, except for the fullerene-like ends. Precisely these ends can be "activated" by transforming them into functional groups (generally carboxylic functions) by treatment with oxidants, without altering the properties of the remaining structure. The functionalized ends can react with the target substances. This property is advantageous in the development of electrochemical biosensors.

2.3.2. Gold nanoparticles

Many materials radically change their properties in the transition from macro to nanostructures. This is particularly evident in the case of gold. In its massive state, gold is an almost inert element, which gives rise to oxides only in the presence of powerful oxidants. At the nanometric level, gold nanoclusters are more reactive and have a central role in numerous applications.

The strategy used for the production of gold nanoparticles is that discovered in 1994 by Brust and Schiffrin [49]: a solution of tetrachloric gold acid ($H[AuCl_4]$) is treated with sodium borohydride ($NaBH_4$), reducing Au^{III} to Au^{0}. To prevent the gold precipitation, a thiol (often alkylated) is added. Gold forms covalent bonds with thiols and the solutions thus prepared are stable for extended periods of time (Figure 2.7). The average size of gold clusters can be adjusted by varying the experimental conditions.

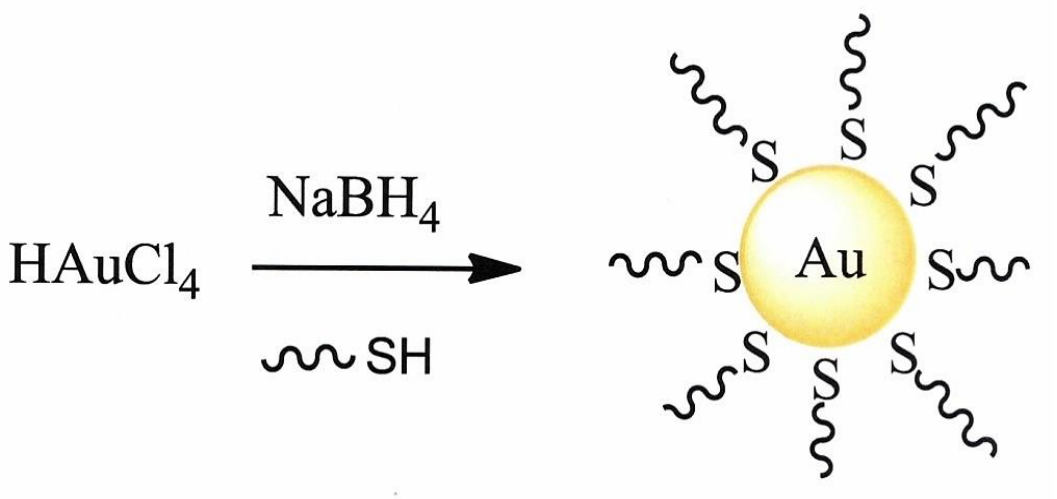

Figure 2.7 Functionalized gold nanoparticles: synthesis and structure

The alkyl groups of thiols can be further functionalized, allowing the gold nanoparticles to interact with molecules of biological origin without modifying their activity. These nanostructures may link bioactive elements to biosensors without polymeric immobilization, thus highly biocompatible systems can be prepared [50], [51].

2.3.3. Graphene

Graphene is a 2D nanostructured material, made entirely of sp^2 hybridized carbon atoms, arranged in a hexagonal network (Figure 2.8). The thickness of a graphene sheet is 0.345 nm.

Graphene was first observed in 1962 with an electronic scanning microscope in catalysis research. This material was rediscovered, isolated and characterized in 2004 [52] through an exfoliation procedure starting from graphite.

Three of the four valence electrons of carbons form covalent bonds with neighboring carbon atoms, the fourth valence electron of each atom gives rise to the π delocalization.

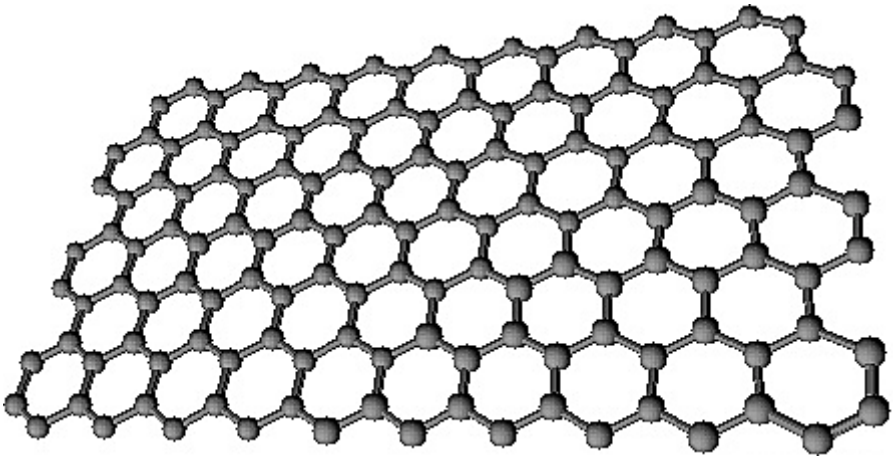

Figure 2.8 Graphene: planar monolayer of carbon atoms arranged in repeated hexagonal structures

These characteristics give to the graphene sheets a behavior similar to that of classical semiconductors: in its pure form it is not a good current conductor but, if adequately doped, it can reach an electrical conductivity comparable to that of excellent conductive metals such as gold and silver (GPH = 108 S m^{-1}, Au = 4.1 x 107 S m^{-1}, Ag = 6.30 x 107 S m^{-1}). The real limiting factor in the conductivity of graphene is the substrate on which it is deposited. The interactions between the π-graphene orbital and the substrate orbitals slow down the speed of movement of the electrons, significantly reducing the conductivity of graphene.

Graphene is used in numerous applications in the biosensor field, due to its smooth interaction with biomolecules or micro-organisms [53]. Since the immune defenses of micro-organisms cannot identify and destroy this nanomaterial, graphene-based biosensors allow performing *in vivo* measurements.

2.3.4. Titanium dioxide nanoparticles (TiO_2)

Titanium dioxide (IV), TiO_2, generally called titania, belongs to the family of transition metal oxides. The most famous polymorphs of titania existing in nature are five: rutile (tetragonal), anatase (tetragonal), brookite (orthorhombic), and two high-pressure polymorphs known as Akaogiite (monoclinic) and TiO_2 II (hexagonal α-PbO_2 like). Titania is prepared in the form of powders, crystals, thin films, nanotubes, nanorods, and nanoparticles. Liquid phase synthesis is one of the most convenient and conventional methods used in its chemical synthesis. This method offers the advantages of controlling the stoichiometry of the reaction, its products are homogeneous, and it allows the formation of complex shapes and the preparation of composite materials.

As a bulk material, rutile represents the most common phase; however, liquid phase preparation methods generally favor the anatase structure. When the particle size is rather small (less than 30 nm), the surface energy is an important part of the total energy, and it has been observed that the surface energy of the anatase is lower than that of the rutile and brookite [54].

Titania is a broadband semiconductor, as it has energy gaps at 3.2 eV, 3.02 eV, and 2.96 eV respectively for the anatase, rutile and brookite phases. Its properties are considered to be very similar to those of an ideal semiconductor for photocatalysis, due to its stability. Titania acts as a more performing photocatalyst when it is in nanoparticles form rather than in bulk. The increase in catalytic activity has been attributed to the particle size, which allows a greater surface area to be obtained per

unit of mass. Moreover, its low cost and its low dangerousness and toxicity towards man and the environment allow titania nanoparticles to be widely used.

When the diameter of the crystallites forming the semiconductor falls below the value of 10 nm, each charge behaves like a particle in the box. So, the energy gap increases and the boundaries of the band shift to higher potentials [55]. Currently, TiO_2 nanoparticles (TiO_2 NPs) are widely used for their high stability, anticorrosive and photocatalytic properties. TiO_2 NPs can be used in catalytic reactions, in the treatment of polluted water by hazardous industrial by-products, in nanocrystalline solar cells as photoactive material and in self-cleaning fabrics. In the nanomedicine sector, TiO_2 NPs are under study as useful tools in advanced imaging and nano-therapy. For example, TiO_2 NPs are evaluated as potential photosensitizers for use in photodynamic therapy (PDT). Furthermore, the unique physical properties make TiO_2 NPs ideal for use in various skincare products [56].

2.4. Room temperature ionic liquids (RTILs)

The term "ionic liquids" refers to chemical compounds consisting of different combinations of ions that are liquid at room temperature or in any cases below 100 °C. The ions used are generally of considerable size, with the cationic portion having low symmetry, these features prevent uniform packing of the ions. Generally, the cationic part is responsible for the physical properties while the anionic part is responsible for the chemical properties of the ionic liquid. One of the advantages, as a consequence of the chemical structure of ionic liquids, is that even a small change in the structure of the cation or anion can cause changes in properties such as viscosity, melting point, miscibility with water and density [57].

Ionic liquids can be divided into two families, aprotic (AIL) and protic (PIL). The difference consists in the presence of groups able to form hydrogen bonds, creating a network of bonds very similar to that of water.

The two most interesting properties of ionic liquids are:

- Liquid phase in wide range of temperature
- Negligible volatility due to extremely low vapor pressure (usable in high vacuum systems).

These properties, combined with the ability of ionic liquids to dissolve a large number of organic and inorganic species, have allowed the replacement of previously used organic solvents. With the introduction of "green" technologies, the search for substitutes for organic solvents has become of particular interest. Solvents are considered dangerous chemical compounds for simple reasons: they are used in large quantities; they are usually volatile liquids that are difficult to contain and discard, are frequently toxic to humans and harmful to the environment.

The first ionic liquids were obtained by Paul Walden in 1914 [58], but this class of compounds was not particularly interesting for researchers until the 1980s when Seddon used them as non-aqueous polar solvents. Therefore, the first ionic liquids used, defined as "first generation", are those described by Seddon [59], consisting of

an aromatic cation (e.g. N-butylpyrimidinium or 1-ethyl-3-methylimidazole) and an inorganic anion (e.g. chloraluminate). It is evident that these compounds, although not very volatile, presented toxicity problems, especially about the aromatic cation.

The ionic liquids subsequently studied were those having non-aromatic organic cations (e.g. Butylammonium + 3,4-dihydroxycinnamate). These compounds, defined as "second generation", had a limited diffusion despite their reduced toxicity, because only a few of the hundreds synthesized were liquids at room temperature [60].

Starting from the ionic liquids obtained, other systems were sought to make them compatible with the roles for which they were intended. Thus, task-specific ionic liquids (TSIL) were prepared in which the cation of a second generation ionic liquid was modified with different functional groups, thus giving new properties to the resulting compound. Many of these functionalized ionic liquids, defined as "third generation", were solid or extremely viscous at room temperature. This problem was partially worked out by solubilizing them in the non-functionalized ionic liquid, thus creating "task-specific" binary ionic liquids (BTSILs) [61].

Nowadays, to synthesize the "third generation" ionic liquids, the most commonly used salts are those having an alkylammonium, alkylphosphonium, N-alkylpyridinium or N, N-dialkylimidazolium cation (Figure 2.9). Despite their low volatility, considerable toxicity was observed for these ionic liquids due to the aromatic cation [62], [63].

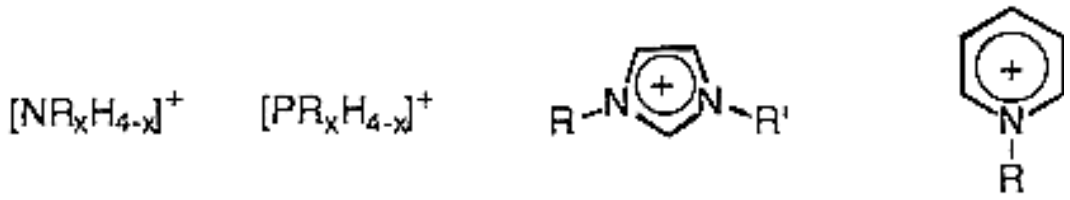

Figure 2.9 (a) Alkylammonium cation; (b) alkyl phosphonium cation; (c) N, N'-dialkylimidazolium cation; (d) N-alkylpyridinium cation.

There are two methods for the preparation of ionic liquids: metathesis of the halide salt (using silver, metals of the first group or ammonium salts of the desired anion), or acid-base neutralization reaction [64].

2.4.1. Non-toxic room temperature ionic liquids

The toxicity problem has long limited the use of ionic liquids, especially in the industrial field. Although less volatile than the common organic solvents, ionic liquids still required numerous precautions both for use and for disposal. It was also almost impossible to use them in a process or sensor employing biocomponents since the RTIL ions hindered the activity of numerous bioactive molecules, significantly reducing or completely blocking them. Since the toxicity of ionic liquids strongly depends on the chemical nature of the cation, researchers focused on creating ionic liquids with ions present in conventional biological systems. One of the best candidates for the role of the cation in the synthesis of highly biocompatible ionic liquids was choline, an essential micronutrient for all cells [65]. Considering the non-toxicity, biodegradability, and biocompatibility of amino acids, a widely available biomaterial, the twenty natural amino acids have been used as anions for the synthesis of ionic liquids. These choline-amino acid ionic liquids [Ch] [AA] are called "green" ionic liquids.

All the choline-amino acid ionic liquids have a very strong ionic couple, unlike the ionic liquids of previous generations in which the ionic pair was hampered by steric effects. Being [Ch] [AA] hydrophilic ionic liquids, their solubility in polar solvents is difficult. This peculiarity has been exploited for the development of miniaturized biosensors. These ionic liquids allow the bioactive components immobilization, on the working electrode (e.g. enzymes), without the problems of polymeric immobilization (enzyme inhibition, polymerization defects).

The knowledge of ionic liquids chemical and physical properties is critical to study the possibility of their applications in various fields of chemistry. The main chemical and physical properties investigated are viscosity, density, refractive index, and conductivity. The viscosity of all [Ch] [AA] ionic liquids is independent on the cutting speed, showing Newtonian behavior, and this feature is expected for all ionic liquids.

Viscosity covers a wide range, from the minimum value found for [Ch] [Ala] (0.72 Pa s) to the maximum obtained for [Ch] [Hys] (7063 Pa s).

It has been shown that the viscosity of ionic liquids depends on the molecular weight, structure, and symmetry both of the cation and the anion. The variability of the amino acids functional groups (R group) can give rise to many kinds of interactions (van der Waals, stacking, and hydrogen bond). Thus, when the chemical properties of amino acids are studied, it is possible to identify two groups relative to the structure of the functional R-group. One group may be constituted by amino acids with alkyl chains as R group, another with R group characterized by heteroatoms, capable of forming hydrogen bonds.

The density ranges, for the ionic liquids studied, from 1.05 g cm^{-3} to 1.20 g cm^{-3}. The density decreases with increasing molecular weight of the anion. There are two distinct trends for the two previously identified groups of [Ch] [AA]: RTILs formed by amino acids having heteroatoms in their R-group have an average density higher than those without. Furthermore, the presence of hydrogen bond can lead to an increase in density, while the substitution of a methyl group with a phenyl one, in the R-group chain, does not appear to produce any increase in density.

The refractive index of ionic liquids [Ch] [AA] decreases linearly with temperature. The refractive index values vary in the range from 1.48 to 1.54, the trend shows that the structure of the amino acid does not significantly influence the index. It should be however noted that the lowest values were observed for amino acids with the aliphatic R group, while the highest values were obtained for amino acids with an aromatic R group.

The conductivity of ionic liquids [Ch] [AA] measured at 25 ° C varies in the range from 0.12 μS cm^{-1} to 90.6 μS cm^{-1}. Conductivity is mainly dependent on the number and mobility of charge carriers. The relatively low conductivity of ionic liquids [Ch] [AA] is due to the low mobility of charge carriers. This, in turn, is caused by the size of the ions, the strength of the ion pair, and the formation of hydrogen bonds.

2.5. Deep Eutectic Solvents (DES)

The term Deep Eutectic Solvents (often shortened as DES) indicates a class of solvents formed by mixing two or more solids and resulting in an eutectic with a much lower melting point than each of its constituents. Similarly to RTILs, DES are liquid at room temperature. Unlike RTILs, which are constituted by ions with separated charges, DES are constituted by a mixture of Lewis or Brønsted acids and bases which act as hydrogen bond acceptors and hydrogen bond donors. In particular molar ratios, they create strong intermolecular interaction [66], [67] which help to drastically reduce the melting point of the formed mixture.

Their easy synthesis, lower toxicity, and ability to dissolve organic compounds (compared to traditional solvents or equivalent ionic liquids) have led DES to have special attention from the scientific community. DES present favorable physical properties such as low melting point, low volatility, high viscosity, high surface tension, and high thermal stability [68], [69]. Thanks to these properties, DES have found use in the last years in various fields such as organic synthesis [70], extraction [71], enzymatic reactions [72], electrodeposition [73], and chromatography [74].

All DES have a common formulation, with two constituents: one salt (inorganic or organic) and a Lewis/Brønsted acid-base couple species; the resulting structure can be expressed as Cat^+X^-zY, where $Cat^+$is a big cation (usually, but not only, ammonium, phosphonium or sulfonium cation), while X^- is a halide, acting as a small Lewis base, which interacts with a Lewis/Brønsted acid (Y).

Depending on the nature of the Lewis/Brønsted acid used, DES are categorized into four different types:

- *Type 1 DES*: the Lewis/Brønsted acid is a non-hydrated metal halide, such as Zinc [75], Gallium [76] or Indium [77].
- *Type 2 DES:* they use hydrated metal halides as Lewis/Brønsted acid and the cation from choline chloride. Some examples of metals used are Cobalt, Copper, or Chrome [78].

- *Type 3 DES*: this class of DES foregoes the use of metals using instead organic molecules as Lewis/Brønsted acids. Numerous classes of organic compounds have proved useful to create DES, such as amides, carboxylic acids, and alcohols. The DES thus produced are low cost, relatively biodegradable and, sometimes, even non-toxic. Since properties of the produced DES such as solvation selectivity depend on the Y element of the synthesized eutectic, this class results particularly versatile for application [79]–[81].
- *Type 4 DES*: these DES differ from those previously seen since they are synthesized using an inorganic cation. A commonly used cation in this type of DES is Aluminum chloride ($AlCl_3$), which forms DES when mixed with urea [82].

Similar to RTILs, DES often have potential windows in which they are electrochemically inert. Thanks to this, and the tunability of their other physiochemical properties, DES can be used to selectively extract compound from biological matrixes [83], [84] and directly analyze them with electrochemical methodologies without the need of further purification.

3. Experimental part

3.1. Materials

3.1.1. Reagents

All chemicals used in this work are of analytical grade. In particular potassium ferricyanide, potassium phthalate, potassium dihydrogen phosphate, and sodium monoacid phosphate are produced by Merck (Kenilworth, NJ, U.S.A.); potassium chloride, D-(+)- glucose monohydrate, potassium hydroxide, nitric acid and ethyl ether are produced by Carlo Erba (Cornaredo (MI), Italia); standard olive oil, lactic acid, caffeic acid, vanillic acid, p-cumaric acid, tyrosol, gallic acid, ethanol, multi-walled carbon nanotubes (MWCNT) (O.D.=(10±1) nm; I.D.= (4.5±0.5) nm; L=3-6 μm), choline hydroxide and all the amino acids used are produced by Sigma-Aldrich (Buchs, Switzerland). Titanium dioxide, anatase form with purity 99%, as nanoparticles with 5 nm diameter is produced by NanoAmor Nanostructured and Amorphous Materials Inc. (Houston, TX, USA)

Lipase enzyme from *Candida Rugosa* is a commercial product of Sigma-Aldrich (Buchs, Switzerland) stored at 4 °C.

Glucose oxidase from *Aspergillus Niger* and alcohol dehydrogenase from *Saccharomyces Cerevisiae* are produced by Sigma-Aldrich (Buchs, Switzerland) and stored at -18 °C.

All the solutions have been prepared using deionized water (R=18.2 MΩ/cm a 25 °C; TOC<10 μg L^{-1}) obtained using a Millipore Direct-Q UV3 (Millipore, Molsheim, France).

Ionic liquids are obtained by "liquid-solid" titration of a solution of choline hydroxide (liquid) with the amino acid of choice (solid) quantified by weighing, described in detail in section 3.2.6. Ionic liquids prepared and used in this work are Choline – Glycine ([Ch][Gly]); Choline – Serine ([Ch][Ser]) and Choline – Phenylalanine ([Ch][Phe]).

3.1.2. Preparation of solutions

The following solutions have been used:

- Nitric acid solution 2 mol L^{-1} used to activate (oxidize) MWCNT on the working electrode (DropSense ceramic electrodes) or the MWCNT used to functionalize GSI electrodes (method of functionalization is described in section 3.2.8);
- Solid mixtures of activated MWCNT and TiO_2 nanoparticles at different proportions (0:100, 30:70, 50:50, 60:40, 70:30, 80:20, 90:10 e 95:5). The solids were crushed in a ceramic mortar to obtain a finely mixed solid mixture.
- Phosphate buffer (I=0.05) made from potassium dihydrogen phosphate and sodium monoacid phosphate in suitable ratios to obtain pH=7.40, at which Lipase has its maximum activity and pH=8.00, at which Alcohol dehydrogenase has its maximum activity.
- Phthalate buffer (I=0.05) at pH 5,10, at which Glucose oxidase enzyme has its maximum activity.
- In order to analyze olive and seed oils two different techniques have been tested: in the first one, the Lipase enzyme was immobilized on the electrode (incubation on the electrode), while in the second one the Lipase was mixed with the oil sample before it was deposited on the electrode for analysis (external incubation).
    - For incubation on the electrode, an emulsion was prepared by mixing one of the oil samples with [Ch][Ser] RTIL and phosphate buffer pH=7.40, with a ratio of 40:40:20; 40 μL of this emulsion were deposited on the electrode. Lipase enzyme is already immobilized on the electrode together with nanomaterials and RTIL (as described in section 3.2.8). After 15 minutes (incubation time for the Lipase enzyme), the measurement was performed through cyclovoltammetry scans;
    - For external incubation, an emulsion was prepared by mixing one of the oil samples with [Ch][Ser] RTIL and phosphate buffer pH=7.40, with a ratio of 40:40:20, lyophilized Lipase enzyme was added to this emulsion

in order to obtain a total enzymatic activity of 103,68 U/μL. The vial containing the emulsion was put in a thermostated bath at 37 °C (temperature at which the Lipase used has its maximum activity) for 15 minutes (incubation time for the Lipase enzyme). After the incubation time, the emulsion was mixed again and 40 μL were deposited on the electrode (modified as described in section 3.2.8). The emulsion was analyzed through ciclovoltammetry scans.

3.1.3. Screen-printed electrodes (SPE)

The screen-printed electrodes (SPE) used in this work are prepared by employing Thick Film Technology (TFT). This technique is based on serigraphic printing and allows for sequential depositions, using different "masks", of thick film pastes (glassy carbon, silver, graphite) on a support made of isolating material. The supports used, which must provide both mechanical support and electrical insulation for the circuits, can be made of plastic (polyvinyl chloride, polycarbonate, polyester) or ceramic (Aluminum oxide, Magnesium oxide) material. The electrode array is printed on the support with a concentric geometry for the three electrodes: working electrode (graphite, glassy carbon or noble metals such as gold, platinum or silver), Counter electrode (graphite) and a reference electrode (silver) (Fig 3.1).

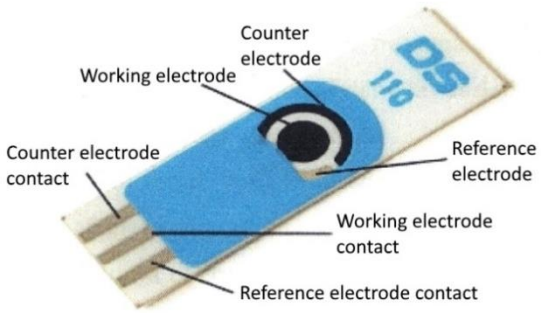

Fig 3.1: Screen-printed electrode printed on ceramic support by DropSens.

The circuits are then covered with a protective layer of dielectric material, leaving uncovered only the electrodes and the contacts to connect the potentiostat. In this work two types of screen-printed electrodes have been used, one of with ceramic material as substrate (Fig 3.1) produced by Dropsens, which will be referred further on as DS, the other printed on a plastic substrate by GSI Technologies (Fig. 3.2). In both cases, the working electrode had a diameter of 4 mm and a surface area of 12.56 mm^2. Electrodes printed on plastic had a much lower cost and, thanks to the versatility of the material used as substrate, both the geometry and the diameter of the working electrode can be personalized by the manufacturer to meet different needs (Fig 3.2).

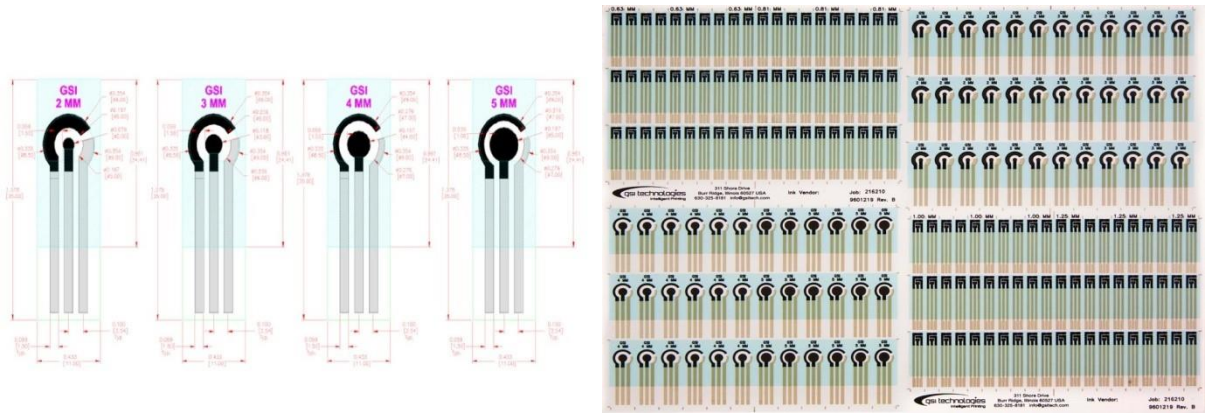

Fig 3.2: Screen-printed electrodes on plastic support, with different working electrode diameters, manufactured by GSI Technologies.

Both SPE types can be further modified by functionalizing the working electrode with nanomaterials, membranes, enzymes, or other sensing elements.

DS electrodes were bough both bare (Glassy Carbon working electrode) and already functionalized with different nanomaterials: Multi-Walled Carbon Nanotubes (MWCNT); Graphene (GPH) and Gold Nanoparticles (GNP). Both bare and nanomaterial-modified DS electrodes were characterized with SEM imaging to confirm the presence of the desired nanomaterial on the working electrode surface.

3.1.4. Olives sampling

Six Italian olives cultivar were studied: Frantoio (FRA), Leccino (LEC), Moraiolo (MOR), Nostrale (NOS), Canino (CAN), Itrana (ITR), produced in the center of Italy (Lazio region, Fig. 3.3).

During three harvest seasons (2016, 2017 and 2018), 42 olive samples of known cultivar and geographical origin were hand-picked and used to produce olive oils (Table 3.1). The monovarietal oils were laboratory-processed using a standardized method described in section 3.2.9. Samples were then stored in brown bottles at 4 °C. Within a few days from production, each oil sample was tested for free fatty acid content, peroxide value and polyphenols content using a CDR-FoodLab (CDR s.r.l - Ginestra Fiorentina - Firenze - ITALIA) instrument. The obtained values for all the produced oils fall inside the limits proposed by the EU for extra-virgin olive oils (acidity value< 0.8%, peroxides value < 20 meq O2/Kg oil).

Fig 3.3: Map of the EVOO samples territorial origin.

HARVEST		
2016	**2017**	**2018**
FRANTOIO_1/16	**FRANTOIO**_1/17	
LECCINO_2/16	**LECCINO**_2/17	**LECCINO**_2/18
LECCINO_3/16	**LECCINO**_3/17	**LECCINO**_3/18
LECCINO_4/16		
MORAIOLO_5/16	**MORAIOLO**_5/17	**MORAIOLO**_5/18
MORAIOLO_6/16	**MORAIOLO**_6/17	
NOSTRALE_7/16	**NOSTRALE**_7/17	**NOSTRALE**_7/18
	CANINO-8/17	
	FRANTOIO_9/17	
	FRANTOIO_10/17	
	FRANTOIO_11/17	
	FRANTOIO_12/17	
	FRANTOIO_13/17	
	FRANTOIO_14/17	
	FRANTOIO_15/17	
	ITRANA_16/17	
	LECCINO_17/17	**LECCINO**_17/18
	LECCINO_18/17	**LECCINO**_18/18
	MORAIOLO_19/17	
	NOSTRALE_20/17	
	NOSTRALE_21/17	
		NOSTRALE_22/18
		FRANTOIO_23/18
		FRANTOIO_24/18
		LECCINO_25/18
		LECCINO_26/18
		LECCINO_27/18

		MORAIOLO_28/18
		MORAIOLO_28/18
		FRANTOIO_30/18

Table 3.1 Monocultivar olive oil samples collected during 2016, 2017, and 2018 harvesting seasons. Samples bearing the same number have been collected from the same plant in different years.

3.2. Methods

3.2.1. Cyclic voltammetry

Cyclic voltammetry is a potentiodynamic electrochemistry technique: the current passing through an electrode in contact with the solution under test is measured with respect to the reference electrode. The potential applied to the working electrode varies through time, following a triangular wave function (Fig. 3.4). The current intensity measured will be proportional to the electrons exchanged in the redox processes at the working electrode, involving the analytes in solution [85].

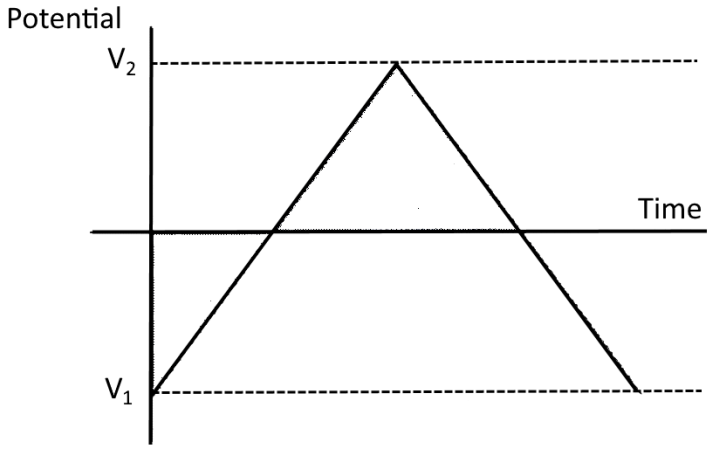

Fig. 3.4 Classical waveform for cyclic voltammetry

Applied potential is continuously and linearly varied over time. Potential variation in one unit of time is called scan rate.

If the potential applied to the working electrode is equal to the redox potential of one of the electroactive species in solution, an increase of the current flowing through the circuit will be recorded.

When the potential value reaches the maximum (or minimum) set, the scan will change direction and go back to the initial value. The current intensity measured is

reported in a diagram, according to the applied potential, called voltammogram (Fig. 3.5).

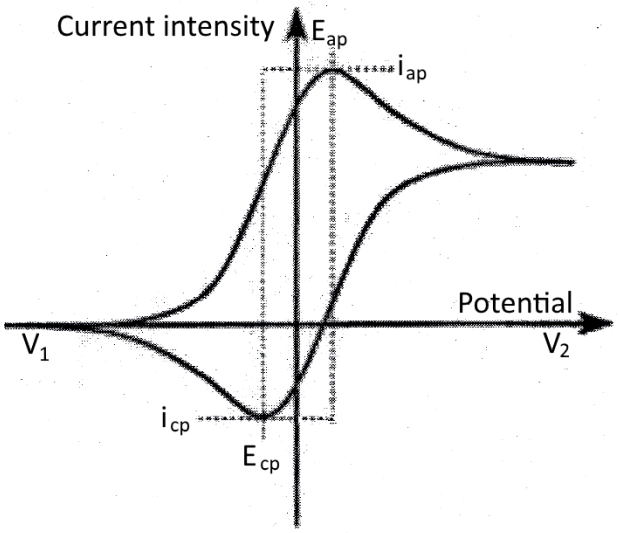

Fig. 3.5 Voltammogram of a reversible process

From a voltammogram is possible to define if the analyzed system is reversible (or quasi-reversible) or irreversible.

A reversible system has some important parameters:

- Oxidation (anodic) and reduction (cathodic) peaks are symmetric;
- The potential of the reversible redox couple (E^0) is centered between the anodic (E_{ap}) and cathodic (E_{cp}) peaks: $E^0 = \frac{E_{ap}+E_{cp}}{2}$;
- The difference in potential between E_{ap} and E_{cp} can be calculated from $\Delta E = {}^{59}/_{n}\, mV$ at 25°C, where n is the number of electrons implied in the redox process;
- Peak current intensity (anodic i_{ap} o cathodic i_{cp}) can be calculated with the Randles-Sevcik equation:

$$I_p = (2{,}99 \times 10^5) \times n^{3/2} \times A \times C \times D^{1/2} \times v^{1/2}$$

- Where:
- v is the scan rate (${}^{V}/_{s}$);

- n is the number of electrons implied in the redox process;
- A is the electrochemically active (cm^2);
- C is the concentration of the electroactive analyte in solution ($^{mol}/_{L}$);
- D is the diffusion coefficient for the electroactive analyte in solution ($^{cm^2}/_{s}$).

Thus, the current measured with each cycle results linearly proportional to the analyte concentrations and increases with the square root of the scan rate.

The previous part is not applicable for irreversible redox systems or if there are other chemical reactions coupled to the redox process under examination.

In the case of irreversible processes, due for example to a slow electronic exchange, the anodic and cathodic peaks are much more separate than expected by the theory, which will further increase with the increase of the scan speed. Furthermore, the peaks are less evident and asymmetric.

In redox systems coupled with other chemical reactions, the voltammogram obtained will differ from that of a theoretical redox pair based on how much the coupled reaction subtracts one of the two members of the redox pair from the balance.

3.2.2. Chronoamperometry

Chronoamperometry is an analytical technique in which, after applying a fixed potential to the working electrode, the current going through it is measured. The potential applied to the working electrode must be chosen so that only the desired redox reaction happens. During the measurement, the solution must be maintained in constant stirring so that no thermal, concentration, or viscosity gradients may form. By adding aliquots of an analyte at known concentration, a graph similar to the one reported in Figure 3.6 will be obtained, in which each current intensity variation can be correlated with a concentration variation of the analyte.

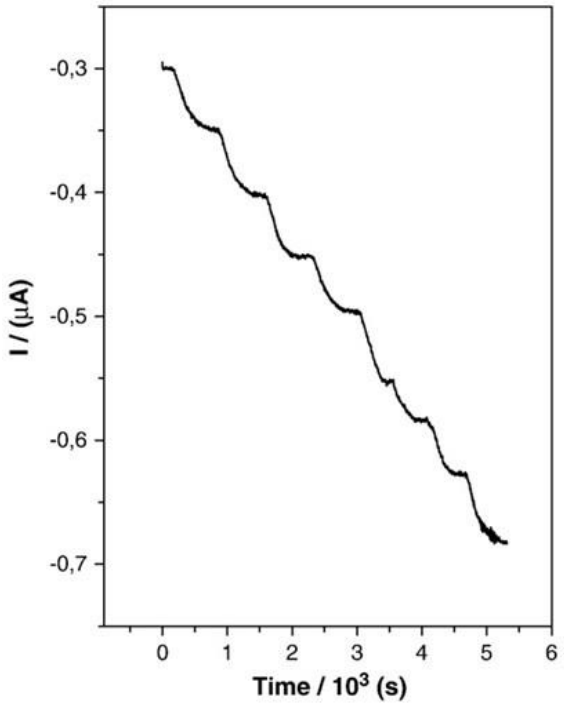

Fig. 3.6 Chronoamperometry: Variations in the intensity of measured current corresponding to analyte additions

It will then be possible to create a calibration curve (Fig. 3.7) for the analyte. The calibration curve can then be used to quantify the analyte in solutions of unknown concentration.

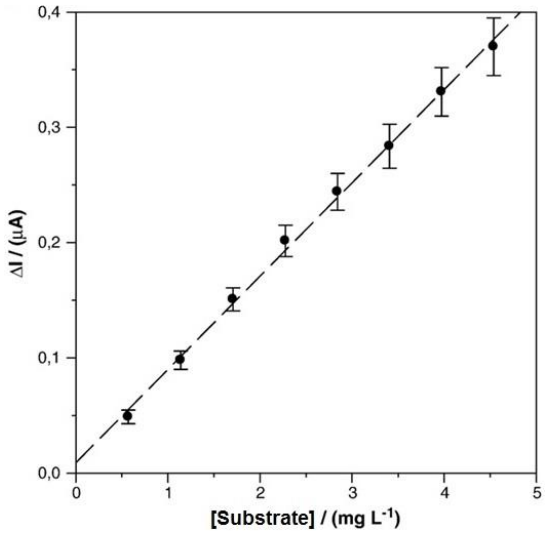

Fig. 3.7 Chronoamperometry: calibration curve

3.2.3. Electrochemically active area determination

The electrochemically active area is defined as the surface area of a working electrode able to perform the desired electrochemical reaction. It may differ from the geometrical area of the electrode depending on the modification and/or functionalization performed on the working electrode before the measure.

For all the electrochemically active area determination measures performed, a potassium ferricyanide solution 1 mM in KCl 0,1M was employed. These parameters were chosen because in these conditions the diffusion coefficient D (25 °C) is known.

The electrochemically active area can be calculated using the Randles-Sevcik equation:

$$I_p = (2{,}99 \times 10^5) \times n^{3/2} \times A \times C \times D^{1/2} \times v^{1/2}.$$

By performing cyclic voltammetries with the same electrode at different scan speeds, using the potassium ferricyanide solution above mentioned, it is possible to calculate the peak current intensities for each scan rate.

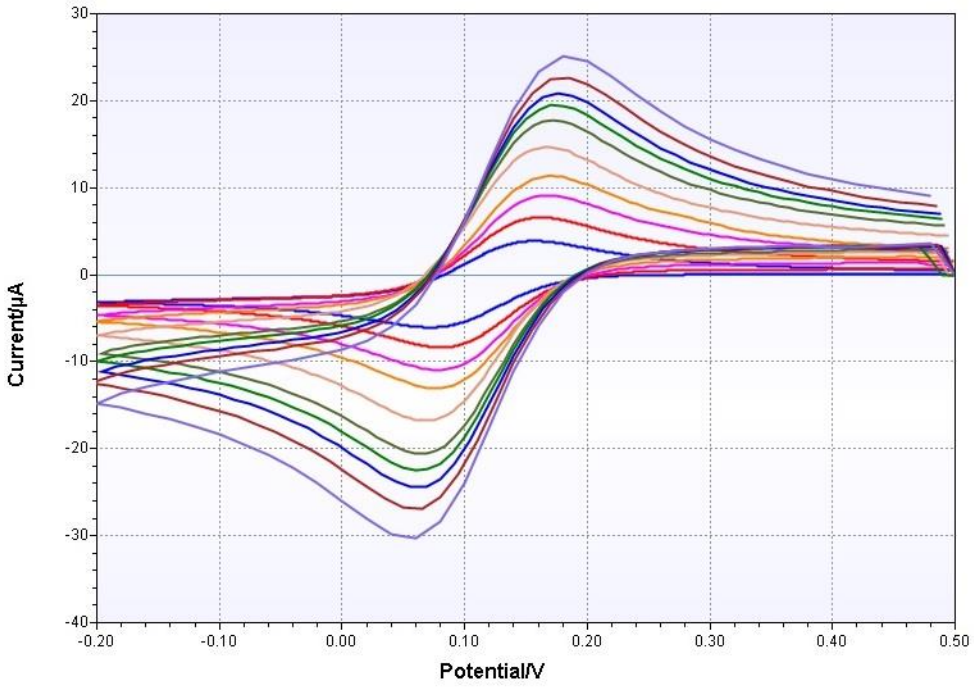

Fig. 3.8 Cyclic voltammetry scans performed at different scan speeds using potassium ferricyanide 1mM.

By plotting the peak current I_p versus the square root of scan speed $v^{1/2}$ the equation of a line I_p = m $v^{½}$. By calculating the angular coefficient m, it is possible to obtain the electrochemically active area, known the concentration of potassium ferricyanide in solution (1 mM) and its diffusion coefficient ($D = 7{,}6 \times 10^{-6}\ cm^2/_s$):

$$m = (2{,}99 \times 10^5) \times n^{3/2} \times \boldsymbol{A} \times C \times D^{1/2}.$$

Scan rate measurements were performed in a range of scan speeds from 5 mV s^{-1} up to 200 mV s^{-1}, for each speed three scans were performed, and the arithmetic mean of the peak intensities obtained for each tern was considered.

3.2.4. Energy-dispersive X-ray diffraction (EDXD)

The range of the electromagnetic spectrum with wavelengths between 0,01 and 20 nm is identified as the X-rays region. Due to their small wavelength, X-rays interact with the internal electrons of atoms, resulting in higher material penetration when compared to other electromagnetic spectrum regions. Therefore, they are the tool for studying the structure of materials. The structure of the material can be determined in terms of atoms, molecules or even larger structures and/or aggregates.

In this work, we use X-ray diffraction to investigate edible oil samples of different origin and composition. Due to the complexity of the oil matrix, it is impossible, employing X-ray diffraction, to determine the real oil composition; our aim is to search differences between edible oils based on significant structure organization differences.

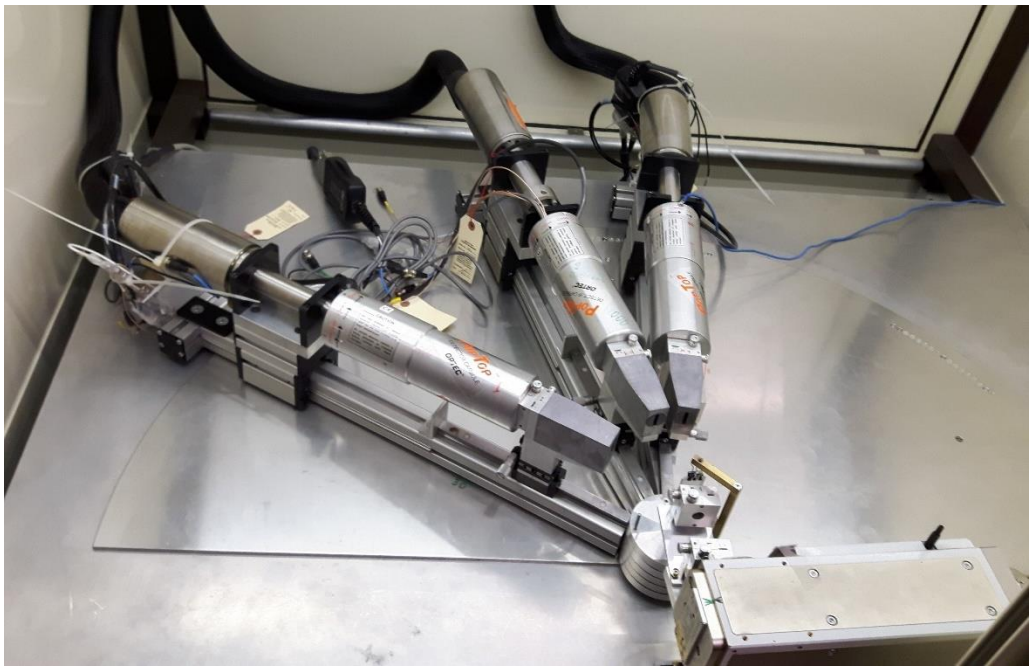

Figure 3.9 Energy Dispersive X-Ray Diffractometer used in this work. The three detectors allow collecting diffraction data simultaneously at three different angles.

Diffraction data are acquired by a custom-built energy-dispersive X-ray diffractometer, a modification of the first prototype [86]. The new instrument consists of a Seifert X-ray HV generator supplying a water-cooled Tungsten X-ray source with a maximum power of 3 KW. The Breemstralung component of X-Ray source was

used. Operating conditions are as follows: 50 kV high-voltage supply, 40 mA current intensity, 13.0-50.0 KeV energy range. The counting system consists of three Ge solid-state detector (SSD) connected via electronic chain to multi-channel analyzers. The diffractometer is fitted with collimating slits in front and behind the sample. The instrument operates in 0-2θ horizontal planar geometry (Figure 3.9). In this way an X-ray generator tube is fixed at 0 angle, while detectors are along a horizontal platform to different 2θ values. The three detectors are used simultaneously for data collection, all capable of being moved along the horizontal platform. The first detector (DET1) is positioned at high angle (2θ above 60°), covering the high **q** range (approximately 6-25 $Å^{-1}$ using 50 kV). A second detector (DET2) operates on low-to-middle scattering angles (2θ 6-20°), covering a low and intermediate-range of **q**. DET3 is placed in the central region (2θ 0-8°) in the "negative" half-plane

The sample holder is a Kapton tube with 2 mm in diameter.

3.2.5. Methods for determining the alcohol content in beverages

These methods are based on the determination of the density of mixtures consisting of water and ethyl alcohol in different proportions. The values obtained by these methods can then be used to determine the alcohol content of the drinks. Three types of alcohol can be distinguished:

- The actual alcohol content, which represents the number of ml of ethyl alcohol contained in 100 ml of wine, measured at 20 °C.
- The potential alcohol content, i.e. the ethyl alcohol obtainable from the complete fermentation of the sugars present. It is possible to calculate by multiplying the sugar grams contained in 100 mL of wine under test by 0.6 (yield factor in ethyl alcohol);
- the total alcohol content is the sum of the actual alcoholic content plus the potential one.

The determination of the actual alcohol content was usually carried out according to the densimetric and ebulliometric methods. The official E.E.C. method (Reg. N. 2676/90), in force until 2010, required double distillation, after alkalizing, and the measurement of the density of the distillate (always at 20 °C) with pycnometer or using a hydrostatic balance. The equipments used were: the pycnometer, the hydrostatic balance and, the Malligand ebulliometer for the ebullioscopic measurements.

For the determination of the alcoholic strength by pycnometer, the wine sample is distilled up to a volume equal to 2/3 of the initial volume. The hydroalcoholic solution obtained is poured into the pycnometer (previously calibrated) and diluted with distilled water up to the mark on the neck. The solution is stirred and the specific weight determined with an analytical balance. Through the consultation of specific tables (Reichard tables), the specific weight is converted to alcoholic content.

The method which employs the hydrostatic balance is based on the principle of Archimedes according to which an object introduced into a fluid receives a thrust

upwards equal to the mass of liquid displaced. The hydrostatic balance automatically provides the relative density with respect to distilled water at 20 °C. The value obtained from the balance, multiplied by the density of distilled water at a temperature of 20 °C, gives the absolute density value of the mixture under analysis. Through appropriate tables, or by means of a calibration line, it is possible to determine the alcohol content of the beverage under examination.

The determination of the alcoholic content through the Malligand ebulliometer represents a less rigorous but useful method for rapid and routine determinations in a laboratory. The method is based on the different boiling temperature of water (100 °C) and ethanol (78.3 °C), which together give a mixture that has an intermediate boiling point between that of the two substances. Wine is a hydro-alcoholic mixture and has a boiling point which decreases with an increase in the ethyl alcohol content. Thus, approximate ethanol concentration in a beverage can be calculated by comparing the boiling point of the beverage with a suitable calibration curve.

3.2.6. Room temperature ionic liquid preparation

The ionic liquids used in this work were prepared by potentiometric titration, as found in the literature [65]. A volume of choline hydroxide solution [Ch] [OH] (approximately 4 moles L^{-1}) was titrated by adding small amounts of solid amino acid under stirring at a temperature of 3 ° C. After each addition, a short period of time was allowed to pass in order to allow complete dissolution of the amino acid. Near the equivalent point, the amount of amino acid added has been reduced to around 1% of the stoichiometric quantity necessary for titration. After the equivalent point, an excess of 10-15% in moles of amino acid is added, and this quantity was subsequently back-titrated by adding a volume of a solution of [Ch] [OH] calculated with the following equation:

$$V_{[Ch][OH]bt} = \frac{V_{[Ch][OH]_{start}} * n_{AAexc}}{n_{AAeq}}$$

Where:

- $V_{[Ch][OH]bt}$ is the volume of choline hydroxide to be added in the back titration;
- $V_{[Ch][OH]_{start}}$ is the initial volume of choline hydroxide;
- n_{AAexc} are the moles of amino acid added in excess to the equivalence point;
- n_{AAeq} are the moles of amino acid added to reach the equivalence point.

As an example, the graph of the potentiometric titration between choline and phenylalanine is shown (Fig. 3.9).

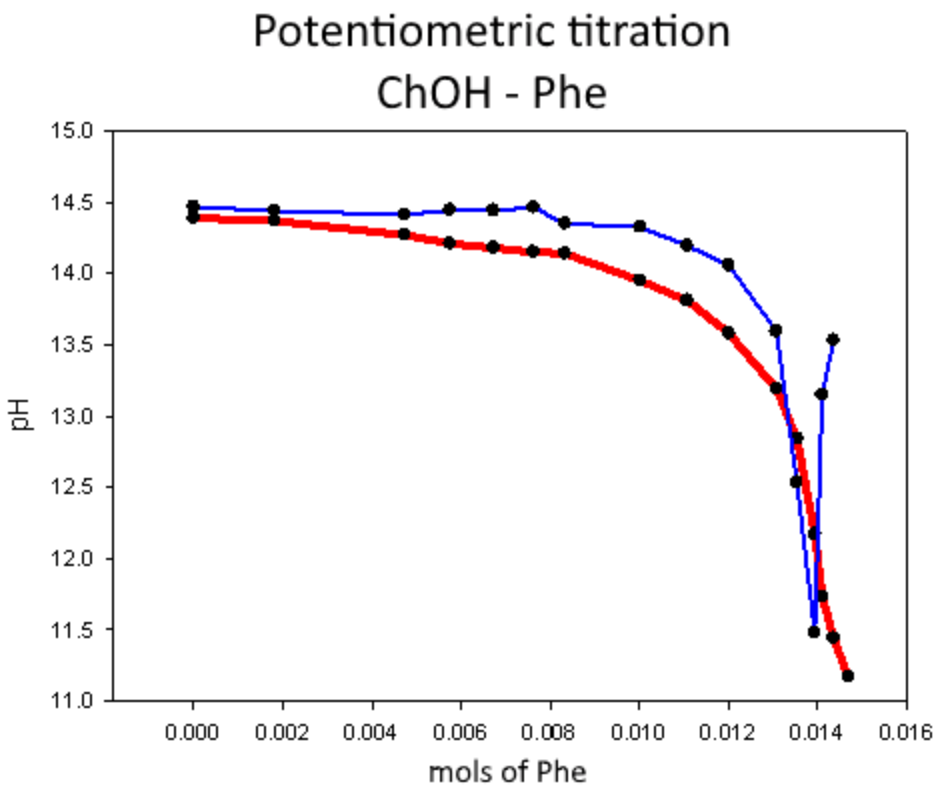

Fig 3.9: Potentiometric titration of [Ch] [OH] (46%; ϱ = 1.073 g cm^{-1}; about 4 moles L^{-1}) and [Phe] conducted at 3 ° C (red = measured values; blue = $\frac{\partial\, pH}{\partial\, mols\ of\ Phe}$).

The water was then removed at reduced pressure at 50 ° C and under continuous stirring. The product was subsequently brought to vacuum dry for 24 hours at 50 ° C under continuous stirring.

In this work, different ionic liquids were prepared, using glycine, serine, and phenylalanine as amino acids. The composition of the ionic liquids thus obtained was confirmed by NMR 1H spectroscopy. The NMR spectra of choline, phenylalanine and [Ch] [Phe] are shown below. (Fig. 3.10).

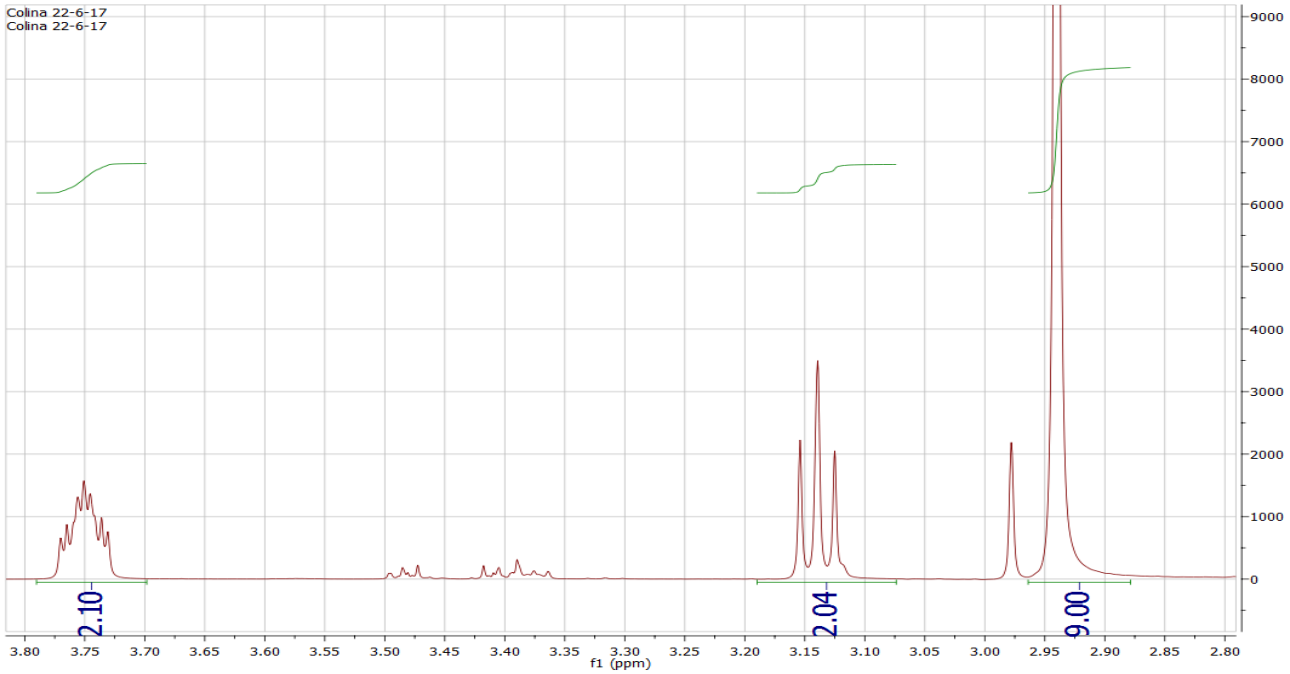
Colina 22-6-17
Colina 22-6-17
2.10
2.04
9.00
f1 (ppm)

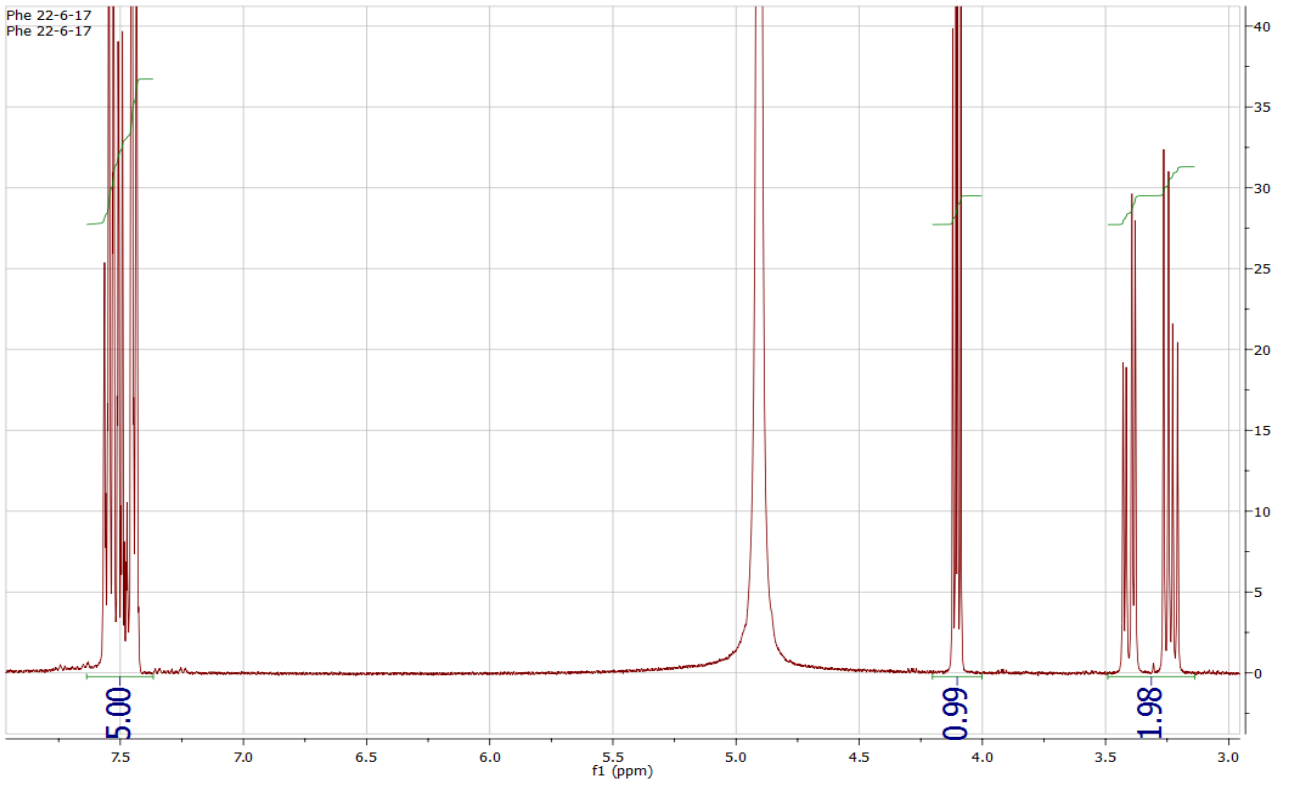
Phe 22-6-17
Phe 22-6-17
5.00
0.99
1.98
f1 (ppm)

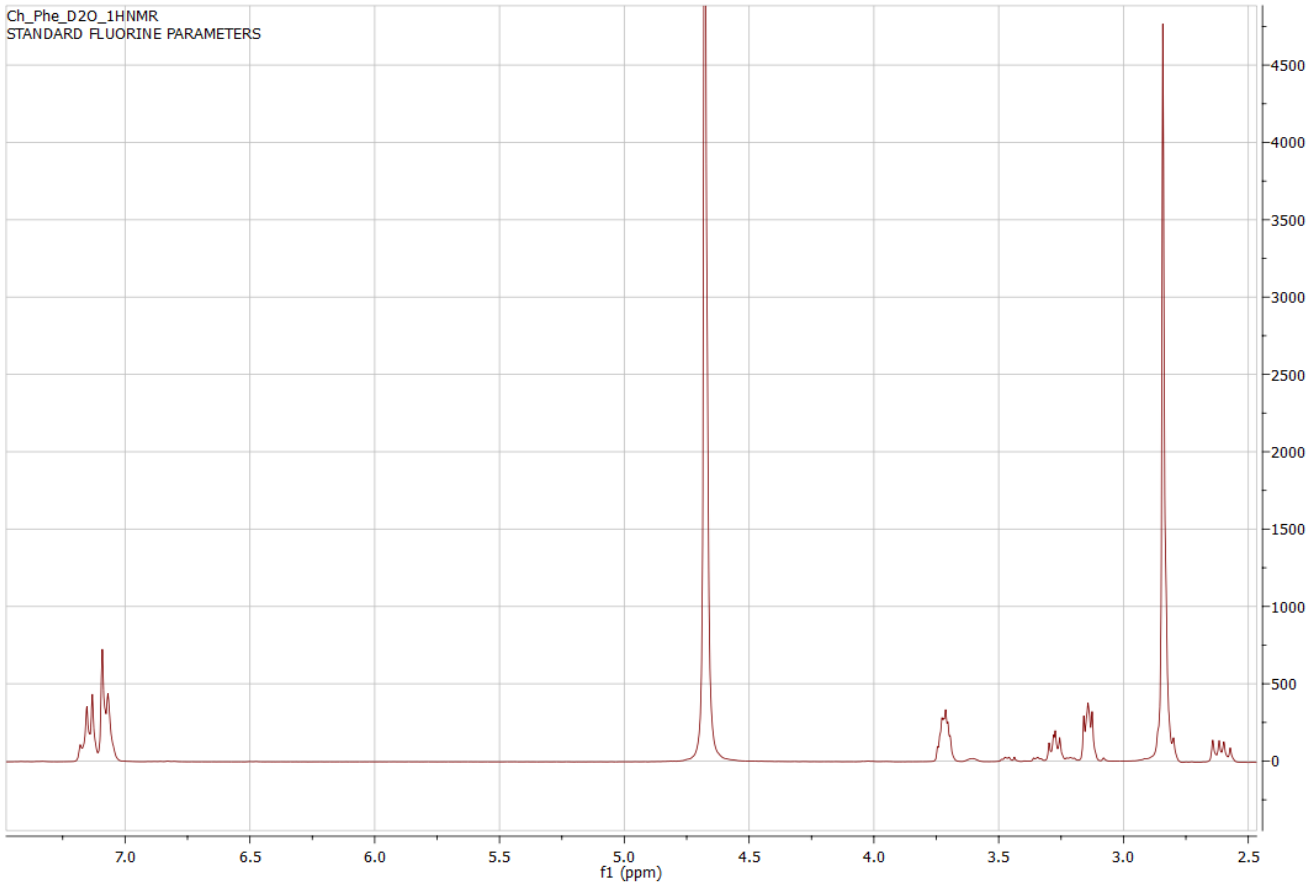

Fig. 3.10: ^{1}H NMR spectra of choline hydroxide (top), phenylalanine (center) and ionic liquid [Ch] [Phe] (bottom).

3.2.7. Deep eutectic solvent preparation

DES have been prepared according to the literature [87], [88], with some modifications to reduce viscosity [89]: Lactic acid, glucose, and water have been mixed in a 6:1:6 proportion. The mixture was stirred for 90 minutes at 50°C until no solid residue could be seen, and the solution became clear. The prepared DES was stored at 4°C.

3.2.8. Electrodes Functionalization

Two different functionalization drop-casting strategies have been employed.

For electrodes already modified with nanomaterials (DS electrodes), 20 μL of a solution prepared by mixing the chosen [Ch][AA] RTIL and a 0.1 M KCl solution (in a 2:3 ratio) were deposited on the working electrode. The electrode was then put in a desiccator and left to dry at a controlled temperature (25 °C) overnight. Electrodes modified with MWCNT were activated before the functionalization as follows: 20 μL of nitric acid 2 mol L^{-1} were deposited on the working electrode. After 30 minutes, the acid was removed, the electrode thoroughly washed, rinsed and then functionalized as above described.

- Ceramic electrodes modified with MWCNT (DS) used to create the calibration curve for glucose: these electrodes were activated before the functionalization as described above. After the activation, 20 μL of a RTIL [Ch][Phe]/phthalate buffer solution (pH=5.10) containing Glucose Oxidase enzyme (total activity 0.50 IU μL^{-1}) were deposited on the working electrode. The SPE was then put in a desiccator and dried overnight at 25 °C.
- Ceramic electrodes modified with MWCNT (DS) used to create the calibration curve for ethanol: these electrodes were activated before the functionalization as described above. After the activation, 20 μL of a RTIL [Ch][Phe]/ phosphate buffer (pH=8.00) solution containing Alcohol Dehydrogenase enzyme (total activity 2.00 IU μL^{-1}) were deposited on the working electrode. The SPE was then put in a desiccator and dried overnight at 25 °C.
- Measures on oils using ceramic electrodes modified with MWCNT (DS): these electrodes were activated before the functionalization as described above. After the activation, 20 μL of a RTIL [Ch][Phe]/phosphate buffer solution (pH=7.40) containing Lipase enzyme (total activity 103.68 IU μL^{-1}) were deposited on the working electrode. The SPE was then put in a desiccator and dried overnight at 25 °C.

Electrode without nanomaterials modification have been subjected to different functionalization, depending on the intended use. The MWCNT used in all the subsequent functionalization were activated by suspending them in nitric acid 2 mol L^{-1} for 30 minutes. The suspension was then filtered, washed with distilled water and dried in an oven at 60 °C.

- Electrochemically active area optimization: Different weighed amounts of MWCNT (1.0 mg, 1.3 mg, 1.6 mg) were suspended in solutions of RTIL [Ch][Phe]/distilled water with ratios of 40:60, 30:70 and 20:80 for a total volume of 100 μL.
- Electrochemically active area optimization with solid mixtures of MWCNT and TiO_2: 100 μL of RTIL [Ch][Phe]/distilled water solutions (30:70 ratio) were added to suspensions of 1.3 mg solid mixtures of MWCNT and TiO_2, (with ratios 0:100, 30:70, 50:50, 60:40, 70:30, 80:20, 90:10 e 95:5). 20 μL of the obtained suspension were deposited on the working electrode of the SPE and left to dry overnight in a desiccator at 25 °C. (Fig. 3.11).

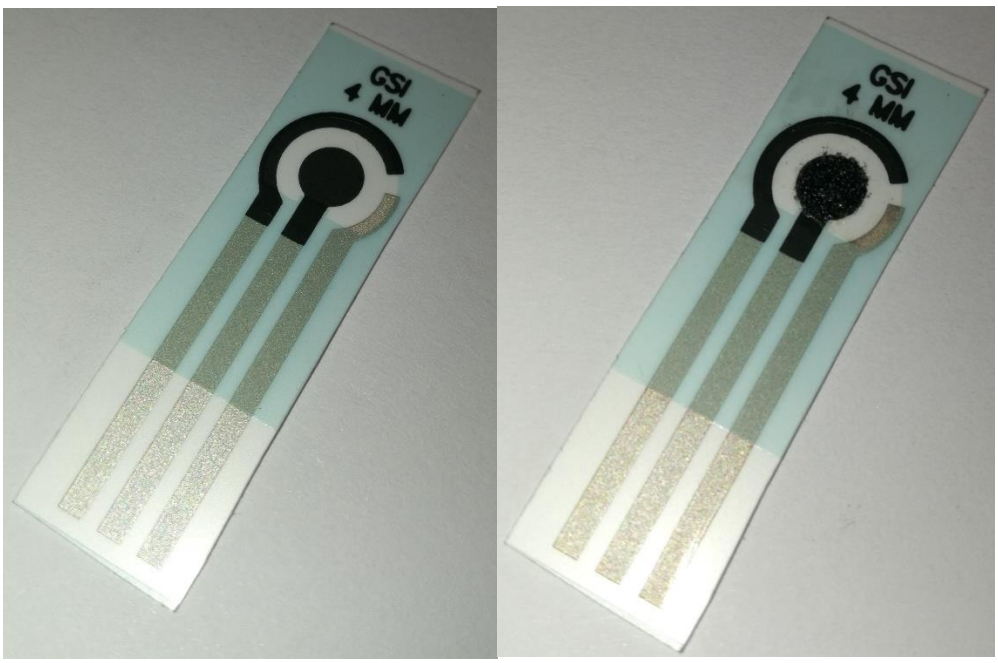

Fig 3.11: GSI electrodes functionalized with TiO_2 and MWCNT (ratio 5:95), [Ch][Phe] and distilled water (ratio 30:70). On the left, bare electrode; on the right, modified working electrode after drying for 12 hours at 25 ° C.

- Electrodes used to create the calibration curve for ethanol analysis and the quantification measures in real samples were prepared as follows: a weighed quantity of Alcohol dehydrogenase enzyme was mixed with the solid mixture of MWCNT and TiO_2 (95:5 ratio), this solid was suspended in a [Ch][Phe]/phosphate buffer (pH=8.00, 30:70 ratio) solution in order to have a final enzymatic activity of 2 IU μL^{-1}. 20 μL of the obtained suspension were deposited on the working electrode of the SPE and left to dry overnight in a desiccator at 25 °C.
- Electrodes used for polyphenol quantification in DES extract: a certain amount of MWCNT blended with TiO_2 was mixed with an optimized percentage of Nafion perfluorinated ion-exchange resin, the prepared suspension was kept on ultrasonic bath for 1 hour. 8 μL of this suspension were dropped on the working electrode and then dried at 36 °C for thirty minutes.
- Electrodes used to perform the measures on oils were functionalized using two different methods, depending on the chosen analysis:
    - *Measurements using internal incubation*: a weighed quantity of Lipase was mixed with the MWCNT/TiO_2 mixture (95:5 ratio), then suspended in a volume of RTIL [Ch][Phe]/phosphate buffer solution (pH=7.40) in order to obtain a total activity of the enzyme of 103.68 IU μL^{-1}. 20 μL of the obtained suspension were deposited on the working electrode of the SPE and left to dry overnight in a desiccator at 25 °C.
    - *Measurements after external incubation*: in these measures, the Lipase enzyme is added to the oil/[Ch][Ser] emulsion described in section 3.1.2. Thus, the electrodes used were prepared, depending on the experiment, by suspending 1.3 mg of MWCNT/TiO_2 solid mixture (95:5 ratio) or 1.3 mg of MWCNT in 100 μL [Ch][Phe]/phosphate buffer solution (pH=7.40, 30:70 ratio). 20 μL of the obtained suspension were deposited on the working electrode of the SPE and left to dry overnight in a desiccator at 25 °C.

3.2.9. Olive oil extraction: mechanical process

Considering that most of the commercial oils are produced in a continuous cycle method, our olive oil extraction method tries to simulate industrial production, in the best way and with standardized process stages.

The olive samples, of known cultivar and geographical origin, were pretreated by washing with abundant running water and subsequently dried. The olives were then ground with a Retsch GM 300 shredder machine at 900 rpm for five minutes (this method does not allow the kernels to break and therefore remain intact), after which the kneading was performed at 500 rpm for thirty minutes. The olive paste obtained is then centrifuged for twenty minutes at 4000 rpm. The centrifuged paste looks like a stratified mass in which the oil is the supernatant while in the lower part there is the vegetation water of the olives and the pomace with the kernels (Fig. 3.12). The extracted oil is stored in dark glass bottles at 4 ° C. Within a few days from production, each oil sample was tested for free fatty acid content, peroxide value and polyphenols content using a CDR-FoodLab (CDR s.r.l - Ginestra Fiorentina - Firenze - ITALIA) instrument. The obtained values for all the produced oils fall inside the limits proposed by the EU for extra-virgin olive oils (acidity value< 0.8%, peroxides value < 20 meq O_2/Kg oil) [15], [16].

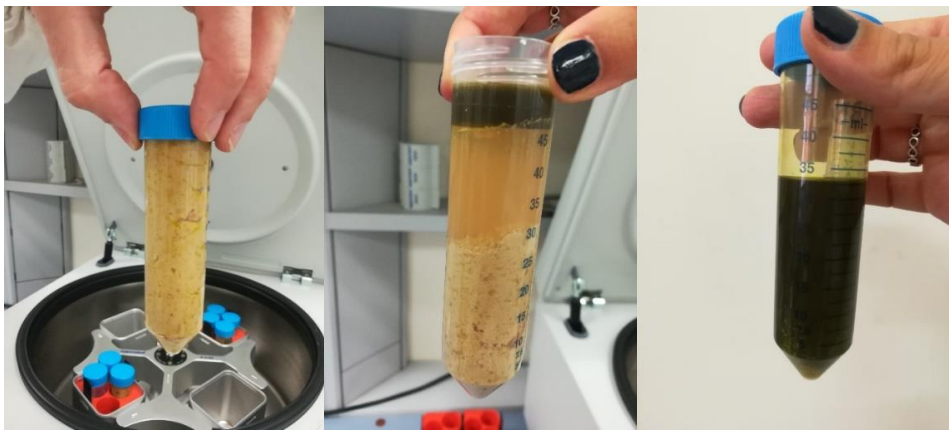

Fig. 3.12: Stages of oil extraction from olives. Left image, the olive paste is poured into the Falcon to be inserted in the centrifuge. Central image, we note the stratification obtained after centrifugation, oil as supernatant, vegetation water in the middle, pomace and hazels in the bottom. Right image, the supernatant oil of the various extractions of the same olive sample is collected in a Falcon.

3.2.10. Chemometric data processing

Chemometrics is the application of mathematical-statistical methods for solving chemical problems. It contains various methods such as experimental design, modeling, classification, linear, and non-linear calibration. The peculiarity of chemometrics is the possibility of simultaneously studying the effect of numerous variables on the process under examination. This allows obtaining the maximum information from any data set, regardless of the level of complexity, providing valid answers in a shorter time, with a considerable saving of time and resources.

Among the various chemometric techniques, the experimental design was used in this work.

The experimental design (ED) is used for the optimization of products and processes, as it efficiently determines the set of conditions necessary to obtain optimal responses. It is therefore convenient to design a series of experiments using experimental planning techniques, which allow defining the minimum number of measures to be carried out in order to obtain, according to the number and type of responses to be optimized, the best description of the relations between phenomenon and variables studied. These tests are appropriately designed to be able to obtain the maximum information from the system in question, investigating the response surfaces. The response surface is the graphic representation of the response of a system, depending on the variations of the factors acting on it.

To carry out experimental design, it is necessary first of all to define the objective of the experiments, that is the response (or the responses) that must be optimized. At this point it is necessary to identify all the factors that could affect the response; then proceeding to the planning of the experiments choosing in a reasonable manner the experimental domain, defined as the set of levels (values) that the factors to be investigated can take. Once the experiments are performed, the data obtained are analyzed and transformed into information. This information makes it possible to elaborate models that approximate the experimental situation more or less well. If the

approximation obtained is not satisfactory, new measures to be carried out on the system are planned to improve the quality of the model. Conversely, if the model approaches the system studied well, the optimal conditions of ED are sought and, therefore, the values of the factors that determine the best characteristics of the product or process.

3.3. Instrumentation

Instrumentation employed in this work:

- ZX3 Vortex Mixer (Velp Scientifica, Usmate (MB) Italia);
- Analytical scale Crystal (Gibertini, Novate Milanese (MI) Italia);
- Millipore Direct-Q UV3 (Millipore, Molsheim, France);
- Sonicator (Labospital, Roma, Italia)

PH measurements were made using a potentiostat Gibertini (Novate Milanese (MI) Italia) with a combined electrode INGOLD U402 – M6 – S7/100 (Urdorf, Switzerland) All electrochemical measurements were performed with SPE electrodes interfaced with a PalmSens Electrochemical Sensor Interface produced by PalmSens BV (Utrecht, Netherlands) equipped with potentiostatic control and capable of performing various voltammetric techniques and a type III μ-Autolab potentiostat, interfaced with a GPES control program (EcoChemie, Utrecht, The Netherlands).

Free fatty acid content, peroxide value, and polyphenols content quantifications in oil samples were performed using a CDR-FoodLab instrument (CDR s.r.l - Ginestra Fiorentina - Firenze - ITALIA).

3.4. Enzymes

3.4.1. Lipase

Lipases (Triacylglycerol Lipases; EC 3.1.1.3) are a class of enzymes that catalyze the hydrolysis of ester bonds in triglycerides or the formation of esters from glycerol and fatty acids depending on the chemical conditions of the reaction environment.

Lipase was discovered for the first time in 1848 by Claude Bernard who, studying the emulsions of water and fatty substances, noticed that the pancreatic secretions of animals allowed to stabilize the solutions and saponify the fatty substances. He attributed these reactions to an enzyme, later named "Pancreatic Lipase" [90].

Lipases are enzymes that are extremely widespread in nature, from bacteria to humans, and play a fundamental role in the digestion of fatty substances.

Most of the Lipases characterized and marketed are of fungal origin and extracted from species such as *Rhizopus Oryzae*, *Candida Rugosa*, *Aspergillus Niger*, *Thermomyces Lanuginosus* and *Rhizomucor Miehei*. However, Lipases from almost all living domains are studied and marketed, from bacteria (Lipase from *Pseudomonas Cepacia*) to animals (Lipase from *Porcine pancreas*).

Although the catalyzed reaction is always the same, the reaction products may be different depending on the number of hydrolyzed ester bonds. This depends on the biological role of the organism that produces the enzyme. Generally, Lipases of microbial origin tend to break all the three glycerol ester bonds, and therefore the reaction products are free fatty acids and glycerol. On the contrary, Lipases of animal origin (for example pancreatic) preferably break the ester bonds in the 1 and 3 positions; consequently, among the reaction products monoglycerides can also be found [91], [92].

In prokaryotes and fungi, Lipases are produced to facilitate the absorption of nutrients from the external medium, in particular pathogenic microorganisms often produce them to facilitate their entry into the host organism. Almost all the higher animals

instead of synthesizing Lipases in pancreas to digest the triglycerides, introduce them with the diet.

Despite the enormous difference in both origin and biological purpose, most of the Lipases are monomeric proteins of about 50 kDa molecular weight with similar structures, characterized by two molecular domains.

They are usually membrane enzymes, which carry out their catalytic activity at the water-lipid interface.

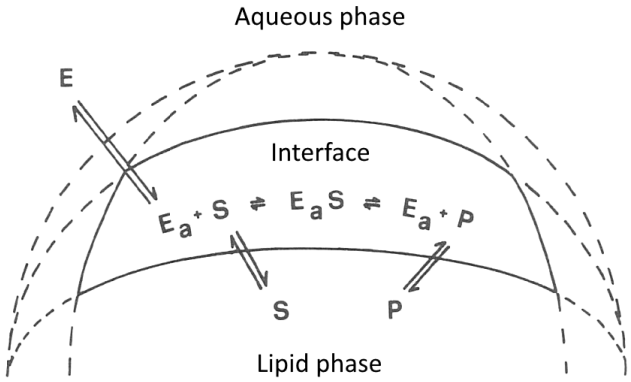

Fig. 3.13 Mechanism of action of Lipase at the water-lipid interface

The Lipase used in this work, from *Candida Rugosa*, is non-site-specific and therefore hydrolyzes all the three ester bonds, giving glycerol and three fatty acids as final products.

An important characteristic of Lipases is that the aforementioned reactions are catalyzed only at a bi-phasic oil-water interface. In these circumstances the enzyme undergoes an activation called "interfacial activation", in which a secondary structure that normally occludes the active site, rearranges in the presence of an apolar phase, allowing the substrate to reach the active site.

The choice of the buffer system is particularly important since numerous cations inactivate Lipases enzymes (i.e. Hg^{2+}, Fe^{2+}, Ca^{2+}, Mg^{2+}, Cu^{2+}, Co^{2+} ions inactivate the Lipase from *Candida Rugosa*).

From the above, it appears that the processes catalyzed by Lipases are not redox, since they do not involve exchanges of electrons between the substrate and the environment. This does not limit their use in biosensors as it is possible to measure both the pH variations caused by the production of free fatty acids [93] and the oxidation-reduction reactions of other electroactive compounds released during the hydrolysis (eg vitamins, polyphenols) [94]. These properties make Lipases an interesting class of enzymes for the study of complex systems such as for example, edible vegetable oils.

3.4.2. Glucose oxidase

Glucose oxidase (D-glucose-1-oxidase; EC 1.1.3.4) (GOx) is an enzyme of the oxidoreductase family, which catalyzes the oxidation of D-glucose to D-gluconolactone in presence of oxygen, producing hydrogen peroxide as a secondary product (Fig. 3.15).

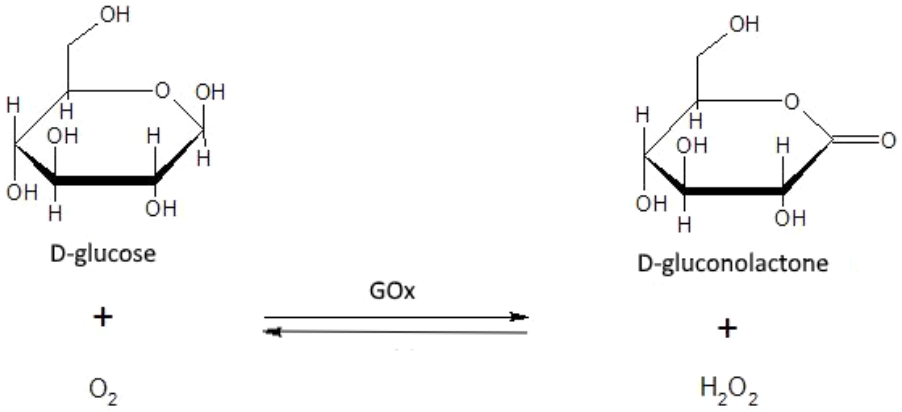

Fig. 3.15 Oxidation of glucose to gluconolactone with hydrogen peroxide formation, catalyzed by glucose oxidase

The enzyme was discovered in 1928 by Muller in the colonies of *Aspergillus Niger* and *Penicillium Glaucum*. It was subsequently identified in numerous species of fungi and insects, since the hydrogen peroxide produced by the reaction inhibits the growth of bacteria and fungi, especially those species lacking an enzyme for the elimination of radicals [95], [96], facilitating hence the growth of the organism producing the GOx enzyme.

Glucose oxidase is a homo-dimeric enzyme, i.e. consisting of two identical molecules, each weighing 80 kDa. Between the two molecules of the enzyme, there are two coenzyme FAD molecules that act as an electron transporter during catalysis. It is a highly specific enzyme for D-glucose, other monosaccharides are negligibly oxidized (activity <2% compared to that with D-glucose) [97].

The reaction catalyzed by Glucose oxidase occurs in two stages: in the first one, glucose is oxidized to gluconolactone while the coenzyme FAD is reduced to $FADH_2$.

The gluconolactone thus produced undergoes non-enzymatic hydrolysis producing gluconic acid unbinding the enzyme active site. In the second stage, oxygen oxidizes the $FADH_2$ to FAD, producing hydrogen peroxide and returning the enzyme to the initial state.

This last reaction was exploited in glucose oxidase first-generation biosensors: the concentration variation of hydrogen peroxide was measured with a platinum electrode in a glucose solution to which the enzyme was added. There were some problems in the application of this configuration: first, the relatively high potential applied to the platinum electrode (+0.6 V vs Ag / AgCl) could lead to the discharge of numerous compounds normally present in biological fluids, such as ascorbic and uric acids. It must also be considered that the concentration of oxygen in biological fluids is generally of an order of magnitude lower than the physiological concentration of glucose (oxygen is the limiting reagent in redox), this can lead to a lower quantity of hydrogen peroxide produced by the reaction independent from the actual concentration of glucose. A solution to these problems was found by replacing the oxygen with a synthetic electrochemical mediator able to transport electrons from the enzymatic active site to the surface of the electrode. Various mediators were tested, substituted ferrocene compounds (a Fe^{2+} atom bound with the π electrons of two cyclopentadienyl rings) or conducting salts (planar molecules having extended π electron systems capable of stacking together) were the best ones [98].

Another solution was to bind the enzyme to the electrode with modified polymers. The proximity of the enzyme to the electrode, obtained for example with immobilization, is not enough to obtain direct electronic transfer since the redox centers of the enzyme, i.e. the FAD groups, are covered by a thick protein layer which acts as an insulator. Polymers functionalized with lysine on top and a system of functionalized osmium atoms bound along the whole polymer chain were therefore used to penetrate the FAD-covering protein layer. The system created allows fast electron transfer from the enzyme active site to the electrode with minimum

overvoltage, thus strongly improving the sensitivity and selectivity of the biosensor [99].

The development of nanomaterials made possible to further improve Glucose oxidase-based biosensors: various studies [100], [101] show the possibility of directly connecting the redox sites of the enzyme to the electrode by exploiting the extremely reduced section of carbon nanotubes. These nanostructures, in fact, manage to pass between the meshes of the protein layer covering the FAD centers, without any loss in conductivity.

3.4.3. Alcohol Dehydrogenase

Alcohol dehydrogenases (Aldehyde reductase; EC 1.1.1.1) are a class of enzymes that catalyze the interconversion between alcohol and aldehydes or ketones with the participation of NAD^+/ NADH coenzyme. The enzyme was purified for the first time in 1937 from the microorganism *Saccharomyces cerevisiae*.

The Alcohol dehydrogenase enzyme plays two opposite roles depending on the source organism: in eukaryotic bacteria, fungi and plants the Alcohol dehydrogenase transforms acetaldehyde, obtained from pyruvate by the elimination of carbon dioxide, into ethyl alcohol by transforming the NADH in NAD^+, the latter essential for performing glycolysis.

In higher animals, including humans, Alcohol dehydrogenase catalyzes the opposite reaction, from ethyl alcohol to acetaldehyde, the latter is then excreted by the kidneys (Fig. 3.16)

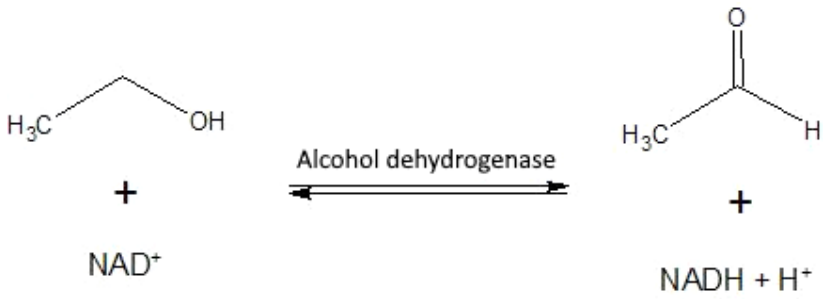

Fig. 3.16 Alcohol dehydrogenase: reaction mechanism

All the Alcohol dehydrogenase enzymes have a similar structure: a homo-dimer weighing 80 kDa; the active site contains two zinc atoms. These zinc atoms have a role both in maintaining the enzyme quaternary structure and in carrying out the reaction: one of the reaction intermediates involves the formation of a highly unstable alcoholate ion (RO^-). In this phase, zinc plays an electron-attractor role, stabilizing the alcoholic ion and allowing the reaction ending [102].

Alcohol dehydrogenase has always played a key role in many human activities. It is, in fact, the enzyme that allows the dough leavening and the fermentation of alcoholic beverages (both performed by the yeast Saccharomyces Cerevisiae).

In more recent times, Alcohol dehydrogenase has been applied in the production of high purity alcohol, its great specificity towards its substrate ensures a very small number of secondary reaction products [103].

In the field of biosensors, Alcohol dehydrogenase is widely used in industrial analyses of food products, thanks to the possibility of having direct electron transfer between the enzyme and the electrode. It is, therefore, possible to develop sensors with a rapid and extremely sensitive response, allowing prompt intervention on the industrial production line [104].

A particular interest is addressed to develop miniaturized biosensors for measurements of alcohol levels in biological systems outside the analysis laboratories. An example is the amperometric biosensors based on Alcohol dehydrogenase employed to measure the alcohol concentration in human breath [105].

4. Results and discussion

The production of a biosensing platform with the best performances, from an electrochemical point of view, was the first goal to be reached. To this end, the behavior of electrodes modified with different nanomaterials in the presence of the various RTILs chosen were studied. Once the best combination was identified and its applicability for the development of biosensors tested, we went on to optimize the electrode modification procedure with a chemometric system to obtain the best electrochemical performances.

4.1. Study of the interactions between ionic liquids and nanomaterials

To evaluate how the different ionic liquids chosen for this study could be used to improve the electrochemical performance of screen-printed electrodes, water mixtures of different ionic liquids were used to modify DS electrode, both bare and already functionalized with nanomaterials, as described in section 3.1.3.

Cyclic voltammetry measurements have been performed on nanomaterials-containing electrodes, not functionalized with ionic liquids, to create a reference system for comparison.

Nanomaterial functionalization of WE	Elettroattive area (E_a) mm^2 ± *SD*
None (Bare GC electrode)	2,72 ± *0.03*
GC + Graphene	6,85 ± *0.48*
GC + Multi-Walled Carbon Nanotubes	8,10 ± *0.13*
GC + Gold nanoparticles	4,20 ± *0.09*

Table 4.1: Comparison of electro-active areas of SPE electrodes functionalized with different nanomaterials. The reported values are obtained from the average of three replicated measurements

From Table 4.1, it can be seen how the electrodes modified with nanomaterials have larger electro-active areas than the classical GC electrodes. In particular, electrodes

modified with carbon nanotubes appeared to have the largest electroactive area among all the considered electrodes. This increase in electroactive area is attributed to the deposited nanostructures, creating a three-dimensional rough surface, as can be seen from the SEM images, that was able to perform higher electronic exchanges (Figure 4.1)

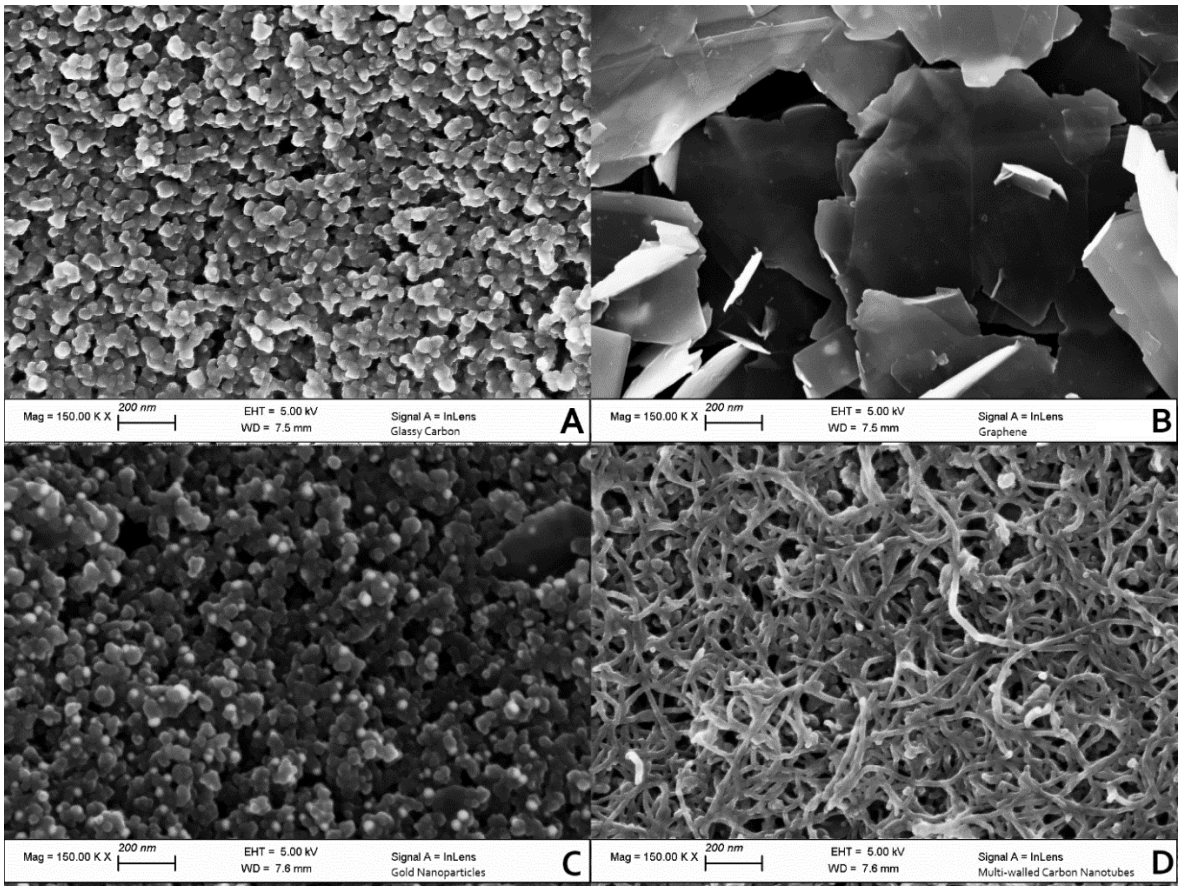

Figure 4.1: SEM images at 150,000 magnifications of GC electrodes (A) and with different nanomaterials B: GPH, C: GNP, D: MWCNT

The study continued by analyzing how different RTILs deposited on the nanomaterials-containing electrodes influenced the electroactive surface.

Electrode material	[Ch] [Gly] (E_a mm²) ± *SD*	[Ch] [Ser] (E_a mm²) ± *SD*	[Ch] [Phe] (E_a mm²) ± *SD*
GC + GPH	6,23 ± *0.16*	7,13 ± *0.09*	5,32 ± *0.62*
GC + MWCNT	4,39 ± *0.07*	4,99 ± *0.01*	9,94 ± *0.04*
GC + GNP	6,97 ± *0.05*	4,85 ± *0.33*	3,14 ± *0.33*

Table 4.2: Comparison of the electroactive areas of GC electrodes with different nanomaterials and functionalized with RTILs (GPH = Graphene, MWCNT = Multi-walled carbon nanotubes, GNP = gold nanoparticles). The reported values are obtained from the average of three replicated measurements.

From the data reported in Table 4.2, it can be noted that the use of different ionic liquids leaded to significant variability of the measured electroactive areas. This can be explained considering the wide range of interactions that can be established between RTILs and nanomaterials.

All the nanomaterials/RTILs combinations lead to similar values of E_a , unless in the case of MWCNTs in the presence of [Ch] [Phe] RTIL; this behavior could be explained with the higher viscosity of the [Ch] [Phe] ionic liquid which allows a higher local concentration of electroactive substances in the proximity of the electrode.

The data obtained for the electrodes modified with MWCNT differ significantly from those seen above, when modified with the [Ch][Phe] RTIL showing a sharp increase in the measured electroactive area (Fig. 4.2).

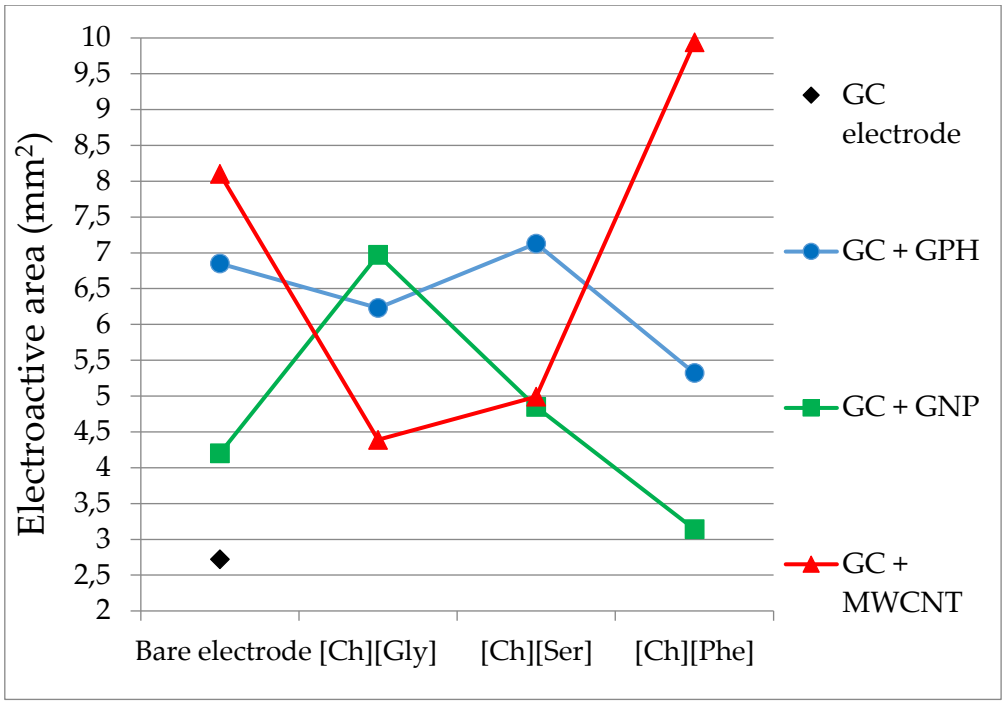

Figure 4.2 Comparison of electroactive areas measured for nanomaterials-containing electrodes in the absence and presence of the studied ionic liquids

To understand the reasons for this anomaly, it is necessary to analyze in detail the interactions between ionic liquids and the structure of carbon nanotubes. Multi-walled carbon nanotubes are concentric cylindrical structures with high conductivity. Electrons flow inside the cylindrical structure, consequently only the ends of the nanotubes can participate in redox processes. These ends have a hemispherical shape, with carbon atoms organized in alternating pentagons and hexagons. The oxidation process wherein the MWCNTs are subjected prior to their functionalization with RTILs partially oxidizes these fullerene-like structures, thus forming carboxyl groups. It is possible to suppose that the presence of the Phenylalanine aromatic ring should be responsible for the marked differences in the observed E_a as this RTIL interacts with the MWCNT structure.

4.1.1. Modified electrode test: Glucose oxidase

In order to test the modified electrode performances, an electrochemical biosensor has been assembled. Glucose oxidase enzyme (GOx) was chosen, being able to easily transfer electrons from glucose to the electrode through its active site. The reaction catalyzed by Glucose oxidase is the oxidation of glucose to D-glucono-δ-lactone with the production of hydrogen peroxide. To be sure of the catalytic activity of GOx after its immobilization on GC-MWCNT by means of ionic liquid [Ch] [Phe], cyclic voltammetry measurements in presence of glucose were performed (Fig. 4.3 A). The reaction occurs even in the absence of the enzyme, but the amperometric response is much lower (Fig. 4.3 B).

Subsequently, an investigation of the influence of different immobilization methods on the GOx catalytic efficiency was carried out. The methods used were: immobilization with a 0,1% (v/v) Nafion solution; a two-step immobilization using glutaraldehyde 2,5% (v/v) to create a suitable base on the WE, followed by immobilization of the enzyme using Nafion 0,1% [39]; a 30% solution (v/v) of [Ch][Phe] RTIL in pH 5.1 buffer solution. The results obtained using the three immobilization systems are presented in Table 4.3.

Immobilization used for GOx	**Potential (V)** ± *SD*	**Oxidation peak intensity (μA)** ± *SD*
NAFION 0,1% (v/v)	0,027 ± 0,005	0,805 ±0,152
Glutaraldehyde 2,5% + NAFION 0,1% (v/v)	0,027 ± 0,004	1,134 ± 0,226
RTIL [Ch][Phe] 30% (v/v)	0,076 ± 0,002	4,605 ±0,100

Table 4.3: Comparison of different immobilization systems for glucose oxidase enzyme in presence of 0.01 mol L^{-1} glucose in phthalate buffer. The reported values are obtained from the average of three replicated measurements

The best results in terms of intensity were obtained using [Ch][Phe] RTIL. The difference in the oxidation intensities could have various explanations.

The polymer structure probably influence the availability of the enzyme active site

after the immobilization process. Moreover the polymers employed are unable to transfer electrons, whereas the [Ch] [Phe] RTIL helps electron transfer in conjunction with CNT, by increasing the WE electrochemically active area.

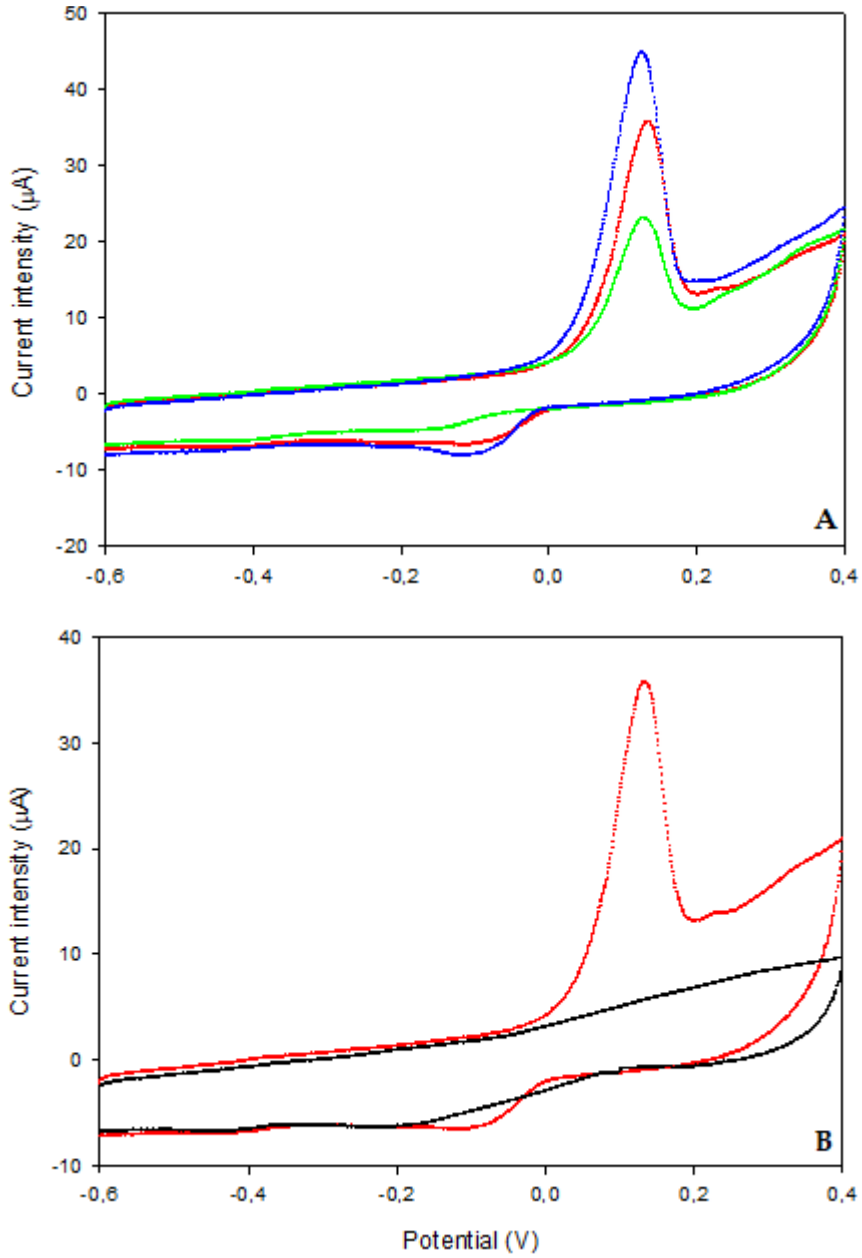

Figure 4.3: **A)** Cyclic voltammograms of the glassy carbon - multi-walled carbon nanotubes + [Choline][Phenylalanine] + glucose oxidase electrode in presence of different glucose concentrations: 0,001 mol L^{-1} (green line), 0,005 mol L^{-1} (red line), 0,010 mol L^{-1} (blue line);
B) Cyclovoltammetry scans performed for a 0,005 mol L^{-1} glucose solution in the absence (black line) and in the presence (red line) of glucose oxidase enzyme immobilized on the MWCNT electrode.

After several chrono-amperometric measurements, optimal experimental conditions have been reached and the calibration curve was calculated.

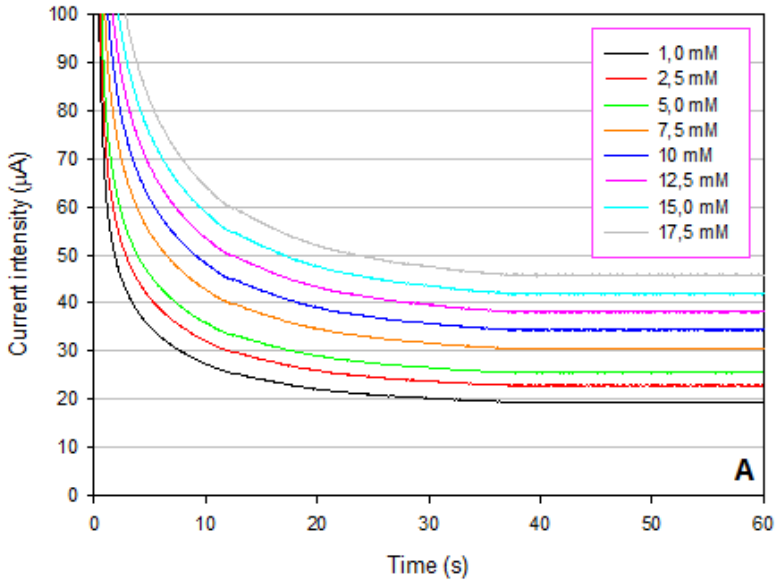

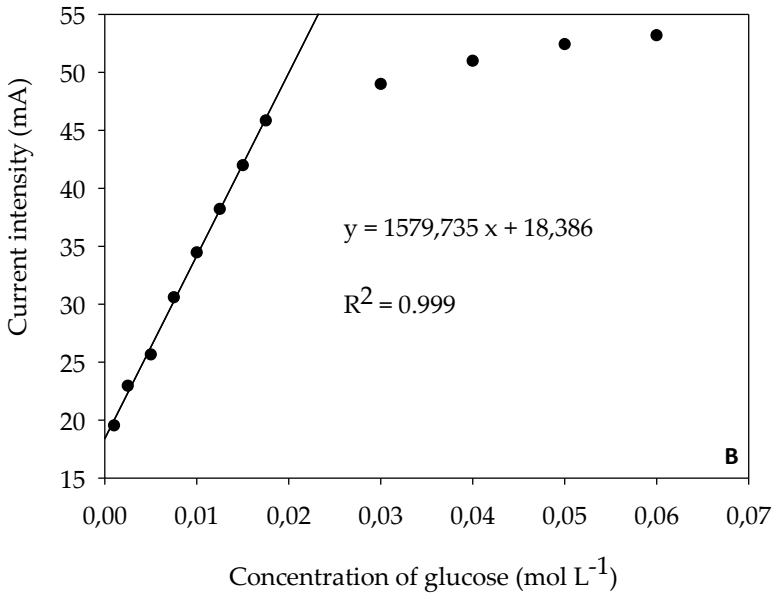

Figure 4.4 A) Chronoamperograms obtained with GC/MWCNT/[Ch][Phe]/GOx biosensor, for solutions ranging from 1 (lowest), to 17.5 mM (highest) glucose; potential applied for measurement is +0.130 V. **B)** Calibration curve for glucose analysis with the glucose oxidase biosensor. The reported values are obtained from the average of three replicated measurements.

As shown in Figure 4.4, the modified electrode presents a good linear range (0.001-0.0175 mol L^{-1}), and an optimum correlation coefficient (R^2=0.995), indexes of reliability of the proposed apparatus.

The modified electrode has been tested by performing glucose analysis on a commercial energy drink. 1 mL of the energy drink was diluted up to 100 mL using pH 5.1 buffer solution in order to have the proper pH value for the analysis and a glucose concentration fitting the range of biosensor calibration curve. The measured glucose concentration was 0.79 ± 0.07 mol L^{-1}, in good agreement with the labeled value. Our results were compared with a standard titration method based on the reaction between hydrogen peroxide, produced by the GOx action on glucose, and potassium permanganate [106]. The energy drink was first treated with activated carbon in order to bleach it. 40 mL of the clear solution were put in a titration flask together with 60 mL of pH 5.1 buffer and 5 mg of GOx. The titration flask was then corked and put in a thermostated bath at 25 °C for 30 minutes to allow the enzymatic reaction to proceed. Once the reaction time expired, 100 mL of diluted (10%) sulfuric acid were added to the solution which was then titrated with KMnO4 0,5 mol L-1, stopping when a faint pink color appeared. Applying this method to the same sample of energy drink, we obtained a glucose concentration of 0.70 ± 0.06 mol L^{-1}. The relatively small difference in the results obtained with the two methods could be attributed to the spontaneous decomposition of small quantities of hydrogen peroxide during the titration process.

4.1.2. Modified electrode test: Alcohol Dehydrogenase

A second test of the modified electrode was performed using the enzyme Alcohol dehydrogenase. Alcohol dehydrogenase enzymes catalyze the dehydrogenation of primary alcohols to aldehydes. The enzymatic reaction involves the transfer of two electrons to NAD^+ coenzyme, which is reduced to NADH. Since there is a 1:1 proportion between ethanol transformed in acetaldehyde and NADH produced, the latter can be oxidized in an electrochemical biosensor to measure the concentration of ethanol. The Alcohol dehydrogenase (ADH) enzyme was immobilized by ionic liquid [Ch][Phe] on the surface of GC/MWCNT screen-printed electrode. The biosensor was characterized using linear sweeps scans in the presence of ethyl alcohol at different concentrations.

An anodic peak at 0.206 V was observed, with intensity proportional to the concentration of alcohol in solution. To verify the linear dependence between anodic peak intensity measured and ethyl alcohol concentration, chrono-amperometric measurements have been carried out.

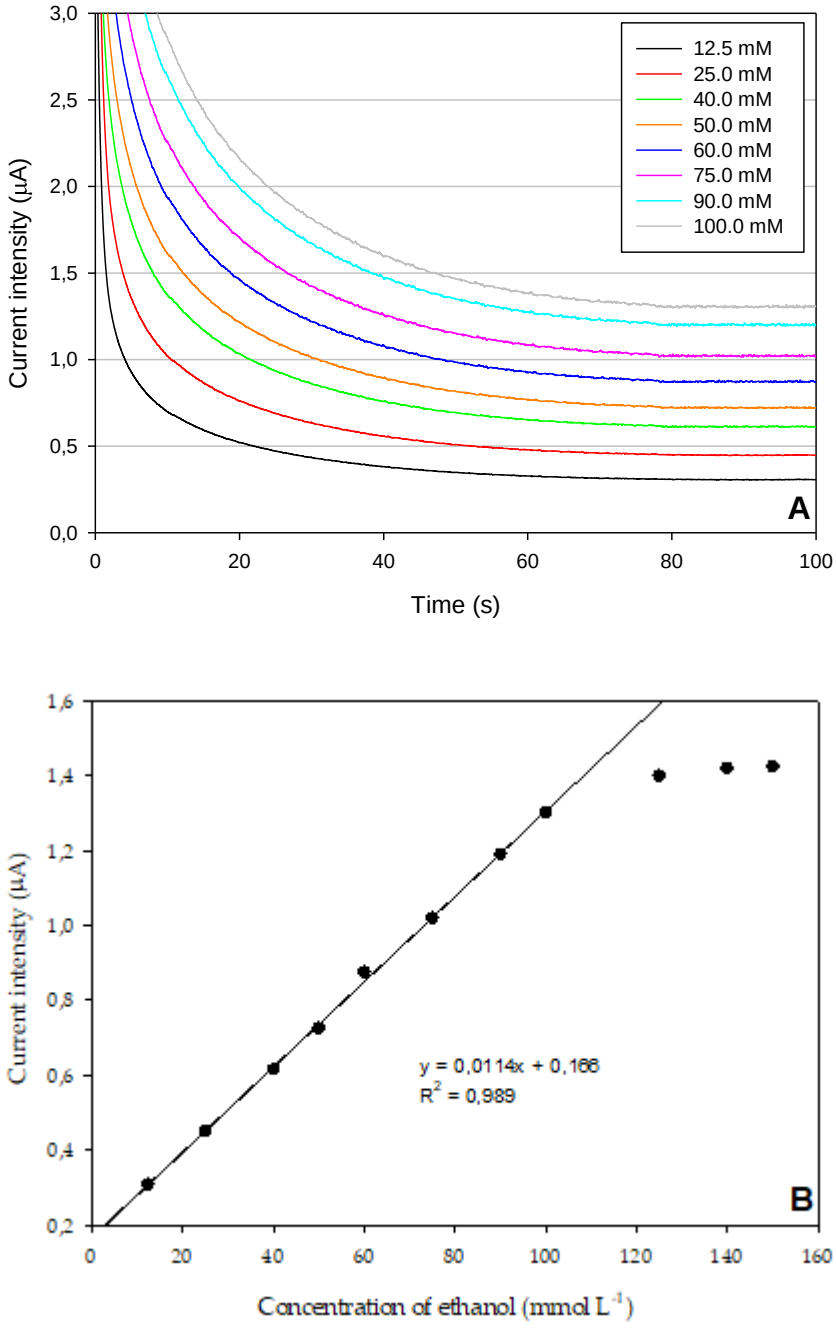

Figure 4.5 A) Chronoamperograms obtained with GC/MWCNT/[Ch][Phe]/ADH biosensor, for solutions ranging from 12.5 (lowest), to 100 mM (highest) ethyl alcohol; potential applied for measurement is +0.206 V. **B)** Calibration curve for ethyl alcohol analysis with the alcohol dehydrogenase (ADH) modified electrode. The reported values are obtained from the average of three replicated measurements.

As can be seen in Figure 4.5, the ADH biosensor shows a wide linear range (12.5 –100 mmol L^{-1}) and a good correlation coefficient (R =0.989). Once again, to demonstrate the increase in performances due to the proposed assay, a comparison against electrodes prepared without RTIL or MWCNT respectively is reported in Table 4.4.

Working electrode modification	Slope of the calibration curve	R^2	Limit of Detection (mmol L^{-1})	Limit of Quantification (mol L^{-1})
GC-MWCNT+ADH	0,00060	0,92212	0,0241	0,0731
GC+[Ch][Phe]+ADH	0,0013	0,96704	0,0073	0,0222
GC-MWCNT+[Ch][Phe]+ADH	0,0114	0,98900	0,0037	0,0110

Table 4.4 Comparison of the performances for different modifications of the working electrode, using Alcohol dehydrogenase enzyme. (R^2, LOD and LOQ)

An essential feature of the ADH enzyme from *Saccharomyces cerevisiae* is its high selectivity towards ethyl alcohol. To confirm whether this selectivity was maintained after its immobilization on the electrode, measurements were carried out using three similar alcohols: ethanol, methanol, and isopropanol. These two lasts have been chosen because they are very toxic to humans. Methyl alcohol is metabolized to formic acid, which has a minimal lethal dose in humans of 1 g/kg of body weight in people not having simultaneously consumed ethanol [107].

Substrate	Concentration (mmol L^{-1})	Anodic peak current intensity (μA) ± *SD*
Ethanol	25,0	0,450 ± 0,002
Methanol	25,0	0,029 ± 0,001
Isopropanol	25,0	Not detected

Table 4.5 Selectivity of Alcohol dehydrogenase modified electrode with respect to different short-chain alcohols as substrates.

As can be seen in Table 4.5, the proposed electrode modified with ADH maintains the high selectivity towards ethanol, characteristic of the enzyme. This suggests that the developed immobilization procedure does not negatively influence either the structure or the active site of the enzyme.

4.2. Electrode modification: optimizing electrochemical performances

In order to best exploit the electrochemical properties of multi-walled carbon nanotubes (MWCNT), the deposition method was studied with respect to different ratios between MWCNT / [Ch][Phe] dispersion and [Ch] [Phe] / distilled water solution. In this way, the best proportion of these three components, that would provide an electro-active area higher than the one recorded using DS MWCNT electrodes, was found. The development of the sensor platform was carried out on GSI electrodes (screen-printed electrodes, with a glassy carbon working electrode). Since they are printed on plastic support, they provide different advantages such as lower cost per electrode, simple disposal and great surface uniformity of different electrodes. The chemometric approach of the experimental design (ED) was used to efficiently determine the set of experimental conditions to apply in order to obtain optimal responses. The experiments were planned by choosing the experimental domain, that is, the set of levels that the studied factors can assume. In particular, three levels were chosen for the [Ch] [Phe] / water ratio (40:60, 30:70 and 20:80 respectively) and as many levels for the MWCNT amount (1.0, 1.3 and 1.6 mg per 100 μL of mixture), giving so a symmetrical design at three levels. The electrodes were prepared using the method described in paragraph 3.2.8 and were subsequently characterized using cyclic voltammetry measurements, dropping 40 μL of potassium ferricyanide solution 1 mmol L^{-1} in KCl 0.1 mol L^{-1} on the electrode. The CV scans were performed at increasing speeds, from 5 mV s^{-1} up to 80 mV s^{-1}. For each speed three scans were performed, and the arithmetic mean of the relative peak intensities obtained was considered. The results of the performed experiments are shown in Table 4.6 and Figure 4.6.

	Electroactive area ± *SD* (mm²)		
mg MWCNT / **% [Ch][Phe]**	1.0	1.3	1.6
20	63.9 ± 0.2	70.9 ± 0.7	70.1 ± 0.4
30	47.1 ± 0.9	84.3 ± 0.6	69.1 ± 0.3
40	6.4 ± 0.2	47 ± 0.2	12.9 ± 0.2

Table 4.6 Comparison of electroactive areas between GSI electrodes functionalized with MWCNT quantities (1.0 mg, 1.3 mg and 1.6 mg) dispersed in solutions of [Ch] [Phe] / bidistilled water in a ratio of 20:80, 30:70 and 40:60. The values shown are obtained from the average of three measurements.

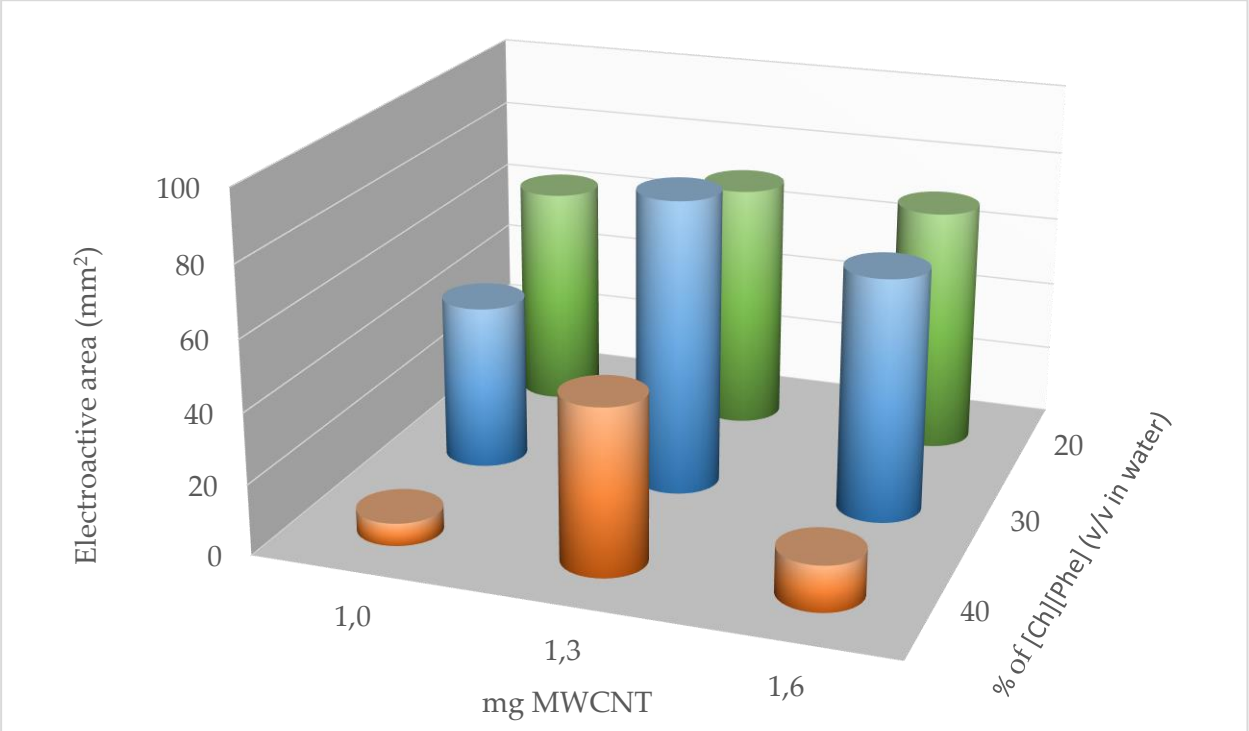

Figure 4.6 Comparison of electroactive areas between GSI electrodes functionalized with quantities of MWCNT dispersed in solutions of [Ch] [Phe] / bidistilled water in different ratios.

From the results of Table 4.6, it can be seen that the electroactive area of the modified GC electrodes is influenced by the amount of MWCNT and [Ch] [Phe] / water proportions. In particular, it is possible to note that high proportions of [Ch] [Phe] (in orange) do not lead to an increase in the electroactive area. The two main ionic liquid

properties, conductivity and viscosity, play contrasting roles during the electron transfer process.

The lowest [Ch] [Phe] / water ratio (in green) allows obtaining fairly high electroactive areas. On the other hand, the deposition turns out to be more difficult since MWCNTs, in presence of small quantities of RTIL, do not create a homogeneous dispersion, instead forming clots.

From the obtained data, the best operative conditions appear to be [Ch] [Phe] / water ratio = 30:70 with a MWCNT amount of 1.3 mg per 100 μL of suspension. The experimental data were processed with MATLAB, a numerical calculation and statistical analysis software, to obtain the graphical plot of the system behavior as a function of the examined parameters (Fig. 4.7).

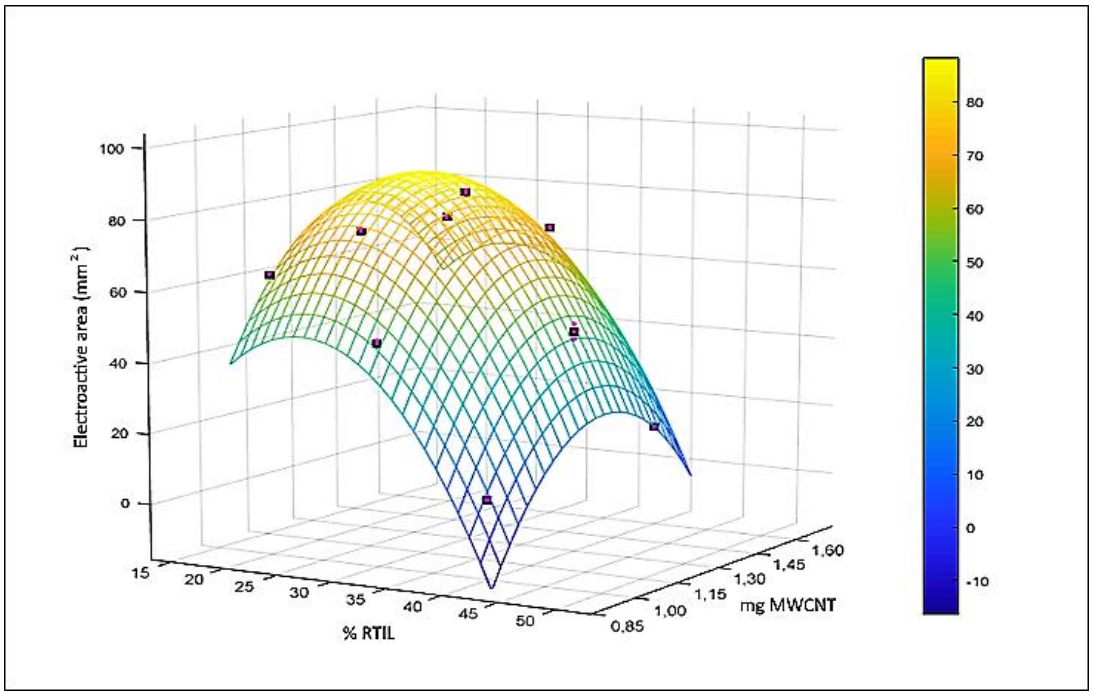

Figure 4.7 Obtained by MATLAB analysis of the results of the experiments performed (points correspond to experimental data).

From this model, it appears that the best MWCNT amount is 1.3 mg per 100 μL of suspension, as found in the experimental results. Regarding the [Ch] [Phe] / water ratio, the model suggests an optimal proportion equal to 25:75, but experimentally resulted that the deposition is more complicated and less reproducible for ratios lower than 30%. Since the difference between the predicted response (25:75) and the

experimental one (30:70) is extremely small, the electrodes used in the subsequent measurements have been prepared using the latter proportion.

To test the stability over time, electrodes were modified with mixtures having [Ch] [Phe] / bidistilled water ratios of 30:70 and 20:80 (1.3 mg of MWCNT). These proportion have been chosen since they gave rise to the largest measured electroactive area. After depositing the mixture, the electrode was dried for 12 hours in a dryer at 25 ° C. The time when the electrodes were taken out from the dryer is set as time = 0 for the stability tests, conducted for a total of 144 hours. The electrodes stability over time is shown in Figure 4.8.

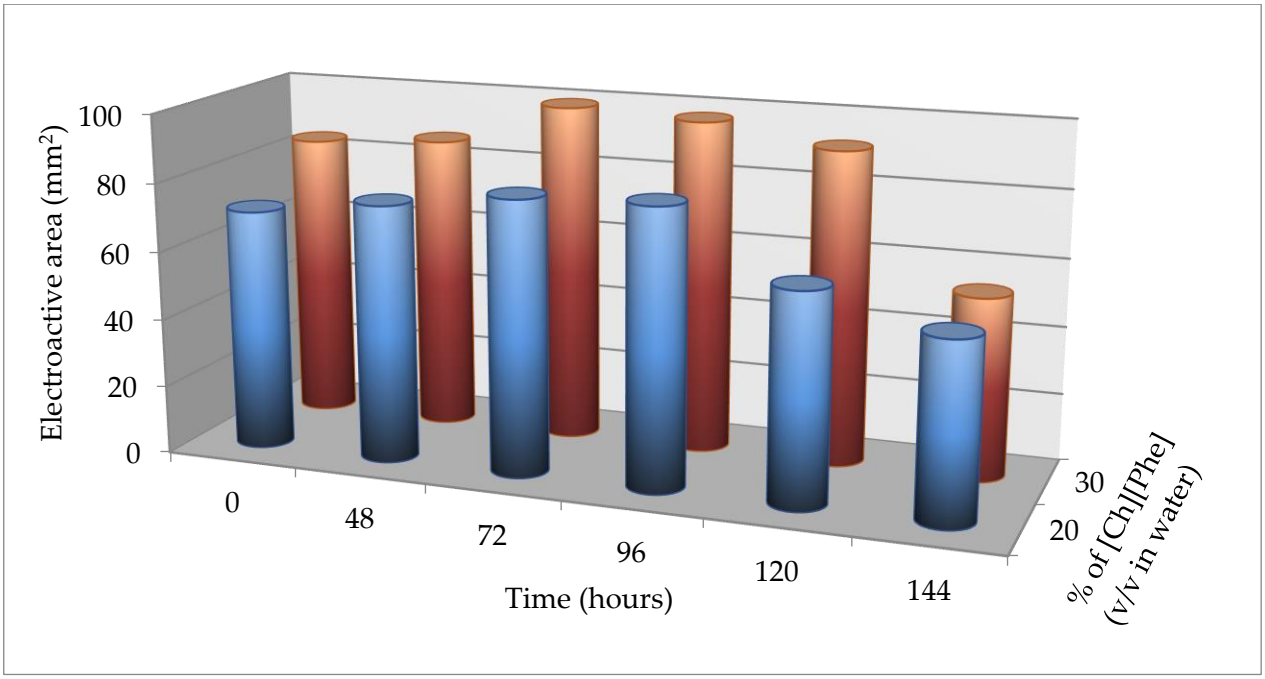

Figure 4.8 Stability over time of GC / MWCNT (1.3 mg) / [Ch] [Phe] electrodes / GSI bidistilled water in a ratio of 20:80 and 30:70

The data obtained confirm that the electrode functionalized using the [Ch] [Phe] / bidistilled water (ratio 30:70) is the most performing in terms of stability over time.

Up to 96 hours, the electroactive area undergoes an almost constant increase and then decreases for times exceeding 100 hours. To better understand this behavior over time, measurements carried out on the just modified electrodes (wet electrodes), after 24 hours and after 96-hours. The results show that 90% of the deposited water evaporates in the first 24 hours, while 10% is retained by the solid mixture. This behavior may be

indicative of a rearrangement of water molecules during the drying, favoring the electronic transfer towards the surface of the working electrode.

The GSI electrodes modified with the optimized mixture (1.3 mg of MWCNTper 100 μL; 30:70 [Ch][Phe]/water ratio) are indicated with the abbreviation GC / MWCNT / [Ch] [Phe] / water (GSI).

In order to obtain even more performing electrodes, titanium dioxide nanoparticles (TiO_2) integrated in the modification process above described. In the literature, numerous works studying the performance of mixtures of MWCNT and titanium dioxide nanoparticles report increased electrochemical performances following the addition of TiO_2 [108], [109].

Different ratios of MWCNT and TiO_2 nanoparticles were evaluated in terms of the electroactive area extension. The MWCNT:TiO_2 ratios examined were: 0: 100, 30:70, 50:50, 60:40, 70:30, 80:20, 90:10 and 95: 5. An amount of 1.3 mg of each dispersion was suspended in 100 μL of the [Ch] [Phe] / water solution (30:70 ratio). 20 μL of this dispersion were deposited on the working electrode. The so modified electrodes were dried in a desiccator at a temperature of 25 ° C for 12 hours and subsequently characterized by cyclic voltammetry measurements. The results of the experiments are reported in Table 4.7 and Figure 4.9.

% TiO_2	**5 %**	**10 %**	**20 %**	**30 %**	**40 %**	**50 %**	**70 %**	**100 %**
E_a (mm^2) ± *SD*	96.90 ± 0.03	60.82 ± 0.03	35.00 ± 0.02	33.00 ± 0.01	3.90 ± 0.90	3.20 ± 0.02	2.00 ± 0.60	1.50 ± 0.20

Table 4.7 Electroactive areas (Ea) determined with modified electrodes GC / MWCNT / TiO_2 / [Ch] [Phe] / bidistilled water in a ratio of 30:70. The TiO_2% refers to the TiO_2 / MWCNT ratio on a total nanomaterial weight of 1.3 mg. The values shown are obtained from the average of three measurements.

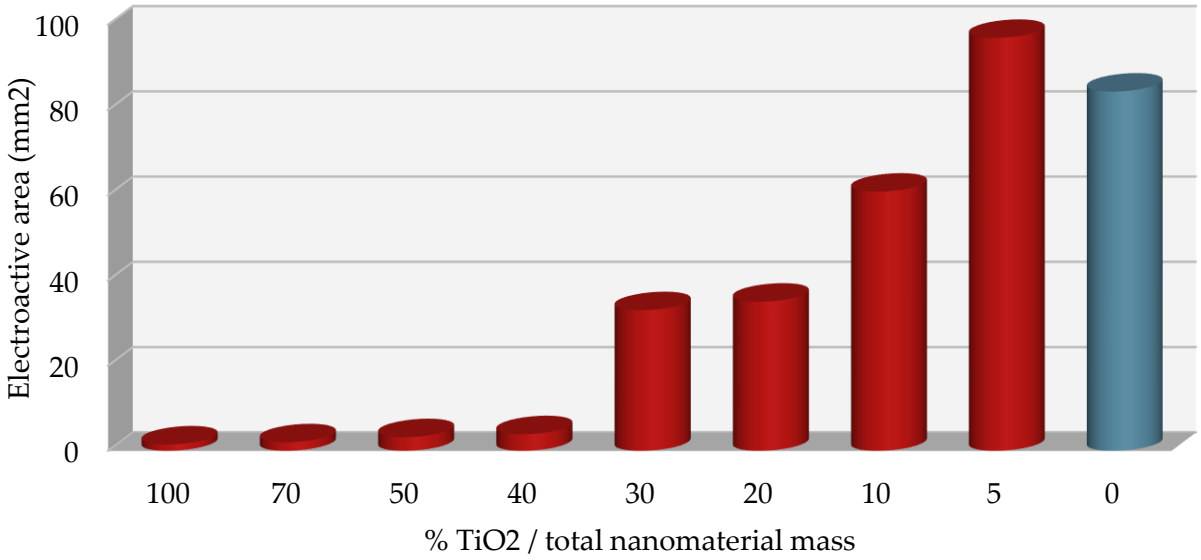

Figure 4.9 Electroactive areas determined with modified GC / MWCNT / TiO_2 / [Ch] [Phe] electrodes / bidistilled water in a ratio of 30:70. The proportions of TiO_2 / MWCNT are 100: 0, 70:30, 50:50, 40:60, 30:70, 20:80, 10:90, 5:95 (in red) and 0: 100 (in blue) on a total nanomaterial weight of 1.3 mg.

From the results obtained it is possible to notice that small additions of titanium dioxide nanoparticles lead to an increase in the electroactive area of the working electrode. In particular, an addition of 5% (w/w) of titanium dioxide nanoparticles to the modification mixture leads to an increase in the electroactive area of about 15 %. It can be assumed that structures similar to those reported in the work of Kang S. et al. [109] appear by varying the percentages of TiO_2 nanoparticles (Figure 4.10 A,B). the structure reported in Figure 4.10A can be proposed for high percentages of TiO_2 nanoparticles, whereas, at low TiO_2 percentages, the self-assembly process should result in a greater functionalization of the TiO_2 nanoparticle by the carbon nanotubes (Figure 4.10 B) and, consequently, the electroactive area can be much higher.

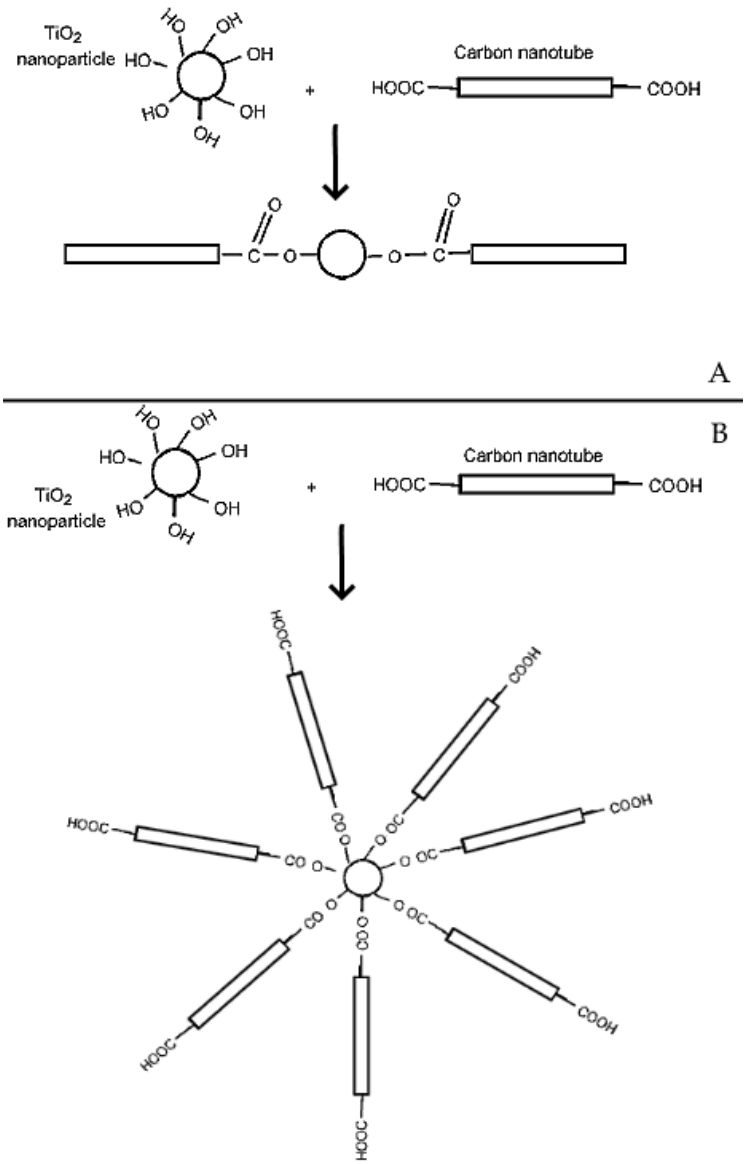

Figure 4.10 Mechanism of interaction between titanium dioxide nanoparticles and carbon nanotubes in suspension: in Figure A in presence of a high percentage of titanium dioxide nanoparticles; in Figure B in presence of a low percentage of titanium dioxide nanoparticles.

The best performances in terms of electroactive area are found for the electrodes prepared using the TiO_2 / MWCNT 5:95 ratio. The electrodes prepared with this method are indicated with the abbreviation GC / MWCNT (95%) / TiO_2 (5%) / [Ch] [Phe] / water (30:70) GSI.

The performance of GC / MWCNT (95%) / TiO_2 (5%) / [Ch] [Phe] / water (30:70) GSI electrodes were compared with those of electrodes without TiO_2 for stability over time. The tests were conducted as before for 30 days. The results are shown in Figure 4.11.

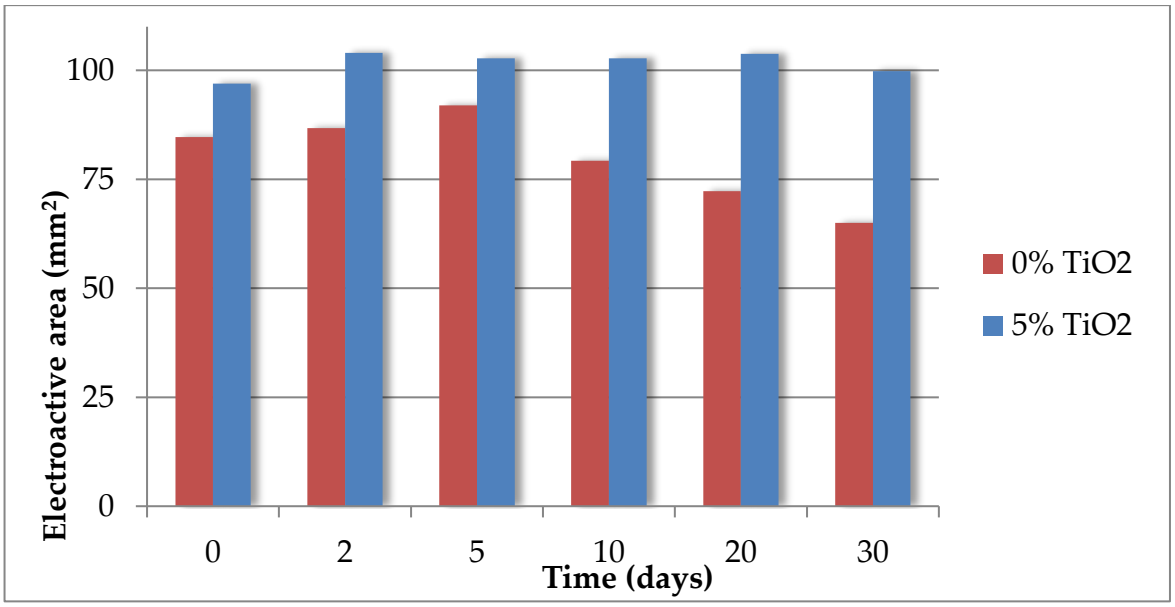

Figure 4.11 Stability over time of electrodes modified with [Ch] [Phe] and nanomaterials. (MWCNT / TiO_2 (blue) mixture =95:5; total weight= 1.3 mg per 100 µL of suspension.

The stability tests confirm that the TiO_2 / MWCNT mixture (95:5 ratio) shows the best performances in terms of stability. In particular, after a small increase 48 hours after the deposition, the electroactive area is stable up to 30 days. These results confirm the suitability of the GC / MWCNT (95%) / TiO_2 (5%) / [Ch] [Phe] / water (30:70 ratio) electrode as a good modification for the development of sensors and biosensors.

4.2.1. New MWCNT / TiO_2 electrode test: Alcohol Dehydrogenase biosensor

It is known in literature [110] that various nanomaterials can interact with enzymes, both in the active site and in other sensitive areas, resulting in a reduction of the catalytic activity of the enzyme or even in a total inhibition. An Alcohol dehydrogenase biosensor was assembled using the new platform to test the analytical performances and to compare them with those of the previously developed ADH biosensor.

Cyclic voltammetry measurements were conducted in the presence of ethyl alcohol as a substrate. Two peaks were observed: an anodic one at 0.055 V and a cathodic one at -0.060 V, with very similar current intensities, showing that the redox system is reversible. Once the oxidation potential of the reaction catalyzed by NADH was identified for the assembled system, linear voltammetry measurements were performed to construct a calibration curve useful for ethyl alcohol determination in solution. The standard solutions of ethyl alcohol have been prepared in phosphate buffer at pH = 8.00 to respect the optimal working conditions of the enzyme.

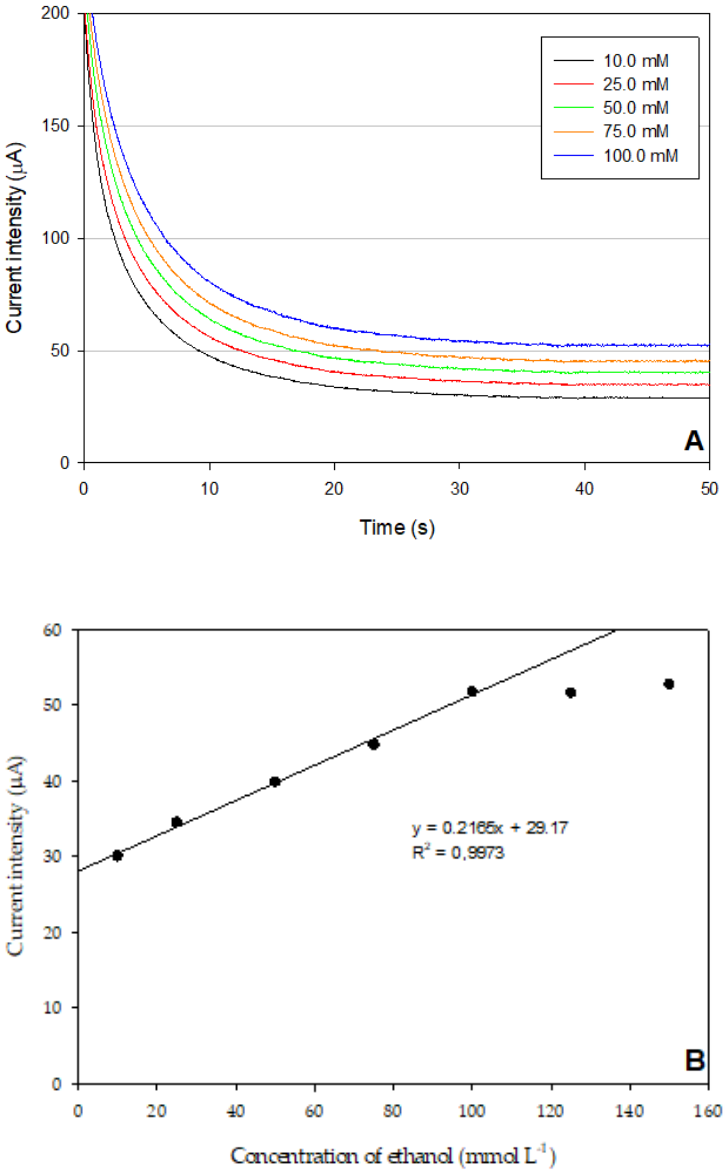

Figure 4.12 A) Chronoamperograms obtained with GC / MWCNT / TiO_2 / [Ch] [Phe] /ADH biosensor, for solutions ranging from 10.0 (lowest), to 100 mM (highest) ethyl alcohol; potential applied for measurement is +0.055 V. **B)** Calibration curve ethyl alcohol determination (concentration range: 0.01-0.150 moles L^{-1}), ADH 40 IU. The reported values are obtained from the average of three replicated measurements.

As shown in Figure 4.12, the biosensor has a good linearity range (10.0-100.0 mmol L^{-1}), and a good correlation coefficient (R^2 = 0.9973). The analytical parameters characterizing the biosensor are compared in Table 4.8 with those obtained with the previous electrode modification.

Electrode modification	Slope	R^2	LOD (Limit of detection)	LOQ (Limit of quantification)	Linearity range
GC_GSI /MWCNT/TiO_2 (95: 5)/[Ch][Phe]/ pH = 8.00 buffer/ADH	0,2165	0.9973	0,7 mmol L^{-1}	2,1 mmol L^{-1}	10,0 –100 mmol L^{-1}
GC_DS /MWCNT/[Ch][Phe]/pH = 8.00 buffer/ADH	0,0114	0,9890	3,7 mmol L^{-1}	11,1 mmol L^{-1}	12.5 –100 mmol L^{-1}

Table 4.8 Parameters characterizing the performance of the enzymatic biosensor developed on GSI electrode (GC_GSI / MWCNT / TiO_2 (95: 5) / [Ch] [Phe] / pH = 8.00 buffer / ADH) and comparison with the parameters of the biosensor previously developed on Dropsens electrode (GC_DS / MWCNT / [Ch] [Phe] / pH = 8.00 buffer / ADH)

As can be seen from the results in Table 4.8, the biosensors developed using the GSI modified electrode are better than the DS electrode ones. In particular, both the LOD and LOQ values are almost five times lower with the [Ch][Phe]/CNT/TiO_2 platform. The two platforms show the same upper limit of the linearity range. It can be supposed that this limit does not depend on the electrode modification but on the turnover frequency of the enzyme.

The biosensor developed was tested on real samples, using it to determine the alcohol content of a brandy and a commercial red wine. The results obtained with the biosensor were compared with those obtained using the reference method described in regulation [111]. The official method to quantify the alcoholic content of a beverage is the densimetric method, after appropriate distillation of the alcoholic beverage. Since the density of the ethyl alcohol/water mixture does not vary in a linear way by varying the relative ratios, a specific calibration curve has been constructed for the hydrostatic balance. Before measurements with the biosensor, the real samples were diluted to fit the alcohol concentration inside the linearity range. To this end the brandy sample was diluted 1: 133 while the red wine sample was diluted 1: 6.85.

Beverage	Declared alcohol content ($\%_{v,v}$)	Alcohol content measured with the hydrostatic balance ($\%_{v,v}$) ± *SD*	Alcohol content measured with the biosensor ($\%_{v,v}$) ± *SD*
Brandy	50.0	49,03 ± 0,11	51,10 ± 0,10
Red wine	11,5	11,46 ± 0,03	11,76 ± 0,01

Table 4.9 Comparison of the results obtained with the biosensor and those obtained with the hydrostatic balance method on real samples.

Table 4.9 shows the results obtained with the biosensor and the official quantification method. There is a good agreement between the results obtained with the biosensor and those obtained with the reference method, both for the brandy and the red wine.

4.3. New platform application: extra-virgin olive oils classification system

As reported in detail in section 3.4.1, Lipases are a class of enzymes that catalyzes the reaction of hydrolysis of the ester bonds in triglycerides. The products of this reaction are fatty acids and glycerol. It is therefore evident that Lipase cannot be considered a redox enzyme since in the reaction described above there is no change in the oxidation state of the molecules involved. This factor would seem to make Lipase enzymes unsuitable for the development of amperometric biosensors. From the literature [94] it is however known that, during the enzymatic hydrolysis reaction, in addition to fatty acids, numerous compounds known with the generic name of antioxidants become available for oxidation.

The idea behind the development of this biosensor is to classify olive oils according to the geographical origin or to the cultivar. Olive oils produced from olives of known origin and cultivar (Location and cultivar of the plants described in section 3.1.4) were obtained using the method described in section 3.2.9.

As stated in section 3.2.9, before the analysis with the electrode platform, all oils were tested for acidity, peroxide content and total phenolic content to verify they were within the values proposed by EU regulation [15], [16] for extra-virgin olive oil. The results obtained are shown in Figure 4.13.

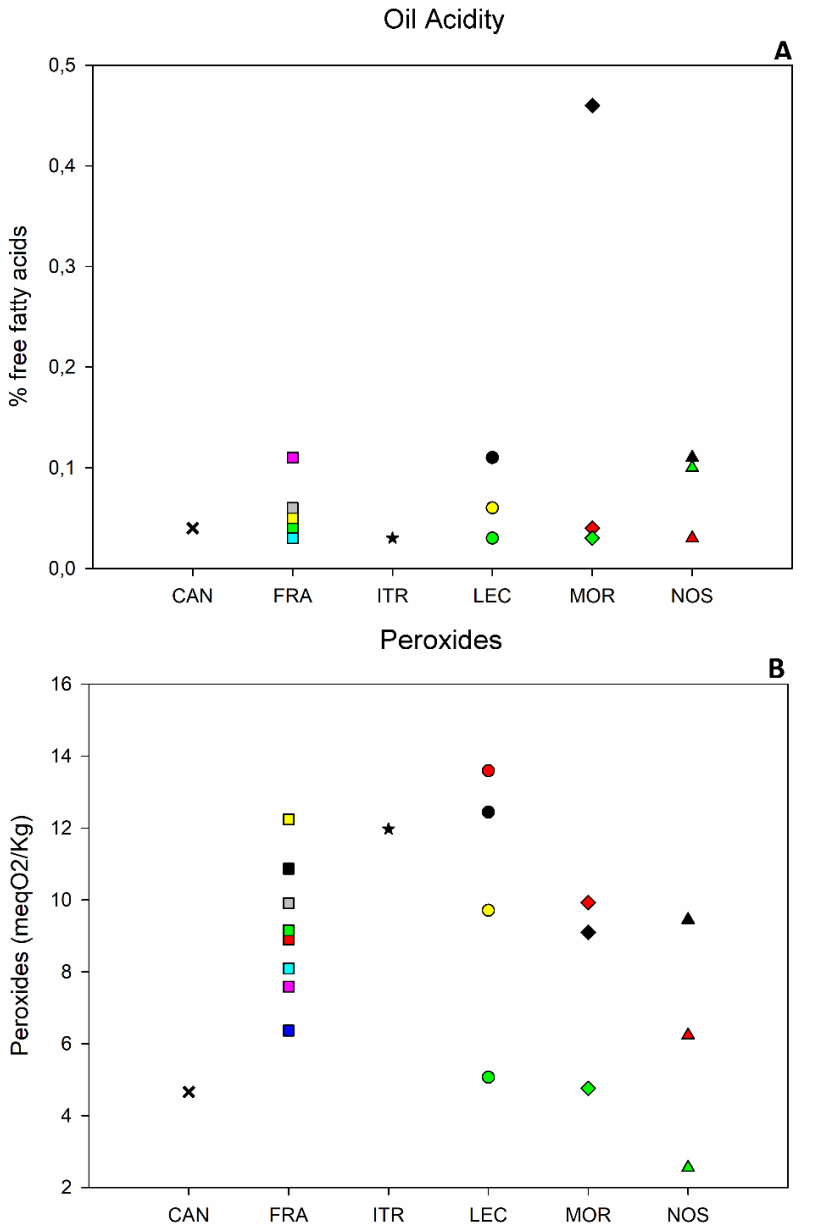

Figure 4.13 Acidity determination (A) and Peroxides quantification (B) on olive oil samples. Different colors refer to different olive oil samples.

The acidity values (in terms of free fatty acids percentage) are similar for all the examined oils, except for an outsider: a Moraiolo cultivar oil (which is still within the limits set to be considered an EVOO).

As far as the peroxide content is concerned the values seem to be quite dispersed. Peroxide content can vary for oils of the same cultivar and also for oils of different cultivar. Therefore, the classification or discrimination of the oil variety based on these parameters remains not possible.

4.3.1. Optimization of olive oil analysis

Olive oil is a complex matrix, ranging from macro components such as triglycerides and free fatty acids down to micro components such as antioxidants and other substances in trace concentrations coming from the plant treatment and olive processing.

The first system used was based on the CNT-DS electrode with immobilized Lipase (GC/[Ch][Phe]/MWCNT/Lipase) described in section 3.2.8. Since the enzyme was already immobilized on the electrode, the oil emulsion was prepared according to section 3.1.2 - Incubation on the electrode: oil sample, [Ch][Ser] RTIL and phosphate buffer pH=7.40 are mixed in 40:40:20 ratio; 40 μL of this emulsion are deposited on the electrode. After 15 minutes (incubation time for the Lipase catalysis), the measurement is performed by means of cyclovoltammetry scans. The results obtained are reported in Table 4.10 and Figure 4.14.

Geographical origin	**Cultivar**	**Oxidation peak potential (V ± *SD*)**	**Oxidation peak intensity (μA ± *SD*)**
Fiano Romano	Leccino (3)	0,252 ± 0,003	24,18 ± 0,03
Fiano Romano	Frantoio	0,258 ± 0,007	14,46 ± 0,09
Fiano Romano	Nostrale	0,233 ± 0,008	19,17 ± 0,07
Arpino	Moraiolo	0,243 ± 0,008	15,29 ± 0,06
Isola del Liri	Leccino (4)	0,255 ± 0,006	23,75 ± 0,03
Arpino	Leccino (1)	0,246 ± 0,006	23,75 ± 0,07
Bracciano	Leccino (2)	0,251 ± 0,007	22,71 ± 0,02

Table 4.10 Potential and current intensity of oxidation peaks for the various oils tested on DS GC / MWCNT / [Ch] [Phe] / buffer / Lipase electrodes. The values shown are obtained from the average of three measurements.

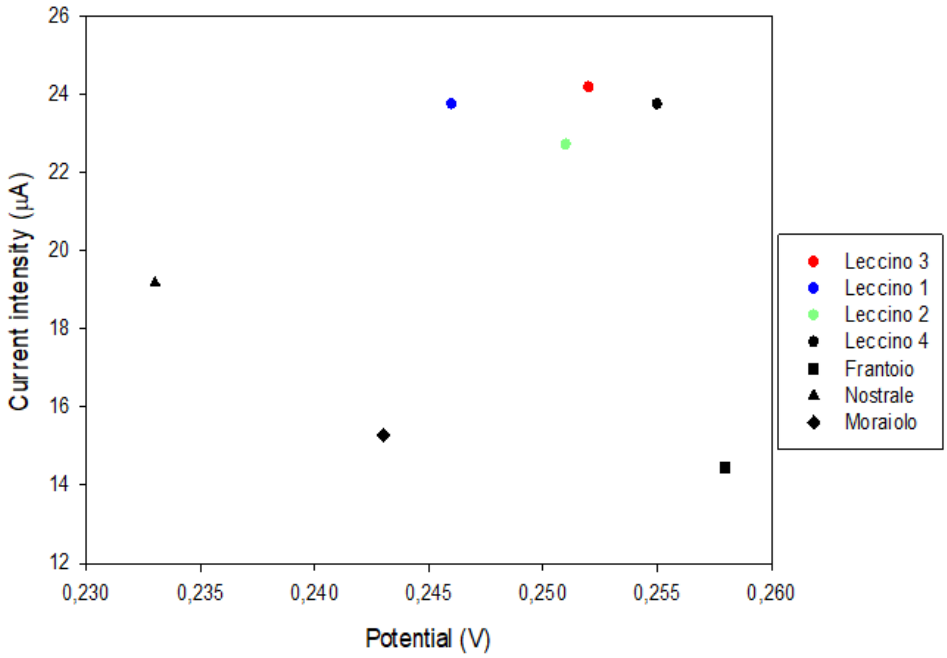

Figure 4.14 Potential and current intensity of oxidation peaks for the various oils tested on DS GC / MWCNT / [Ch] [Phe] / buffer / Lipase electrodes. Different colors correspond to different geographical origin (see Table 4.10)

The results show an oil grouping according to the cultivar of the olives. Points of different color refer to Leccino cultivar samples of different geographical origin.

Since the GSI electrodes are much cheaper than the DS ones, the same oil samples were analyzed employing the GC / MWCNT / [Ch] [Phe] / water / Lipase GSI electrodes (incubation on the electrode). The results obtained are shown in Table 4.11 and Figure 4.15.

Geographical origin	Cultivar	Oxidation peak potential (V ± *SD*)	Oxidation peak intensity (μA ± *SD*)
Fiano Romano	Leccino (3)	0,248 ± 0,003	22,50 ± 0,10
Fiano Romano	Frantoio	0,272 ± 0,009	12,30 ± 0,05
Fiano Romano	Nostrale	0,239 ± 0,008	17,60 ± 0,09
Arpino	Moraiolo	0,247 ± 0,006	15,80 ± 0,03
Isola del Liri	Leccino (4)	0,255 ± 0,005	18,30 ± 0,02
Arpino	Leccino (1)	0,244 ± 0,009	23,90 ± 0,03
Bracciano	Leccino (2)	0,249 ± 0,008	22,90 ± 0,04

Table 4.11 Potential and current intensity of anodic peaks for the various oils examined with the modified GSI electrode-based biosensor (Lipase from Candida Rugosa 103.68 IU μL^{-1}). The values shown are obtained from the average of three measurements.

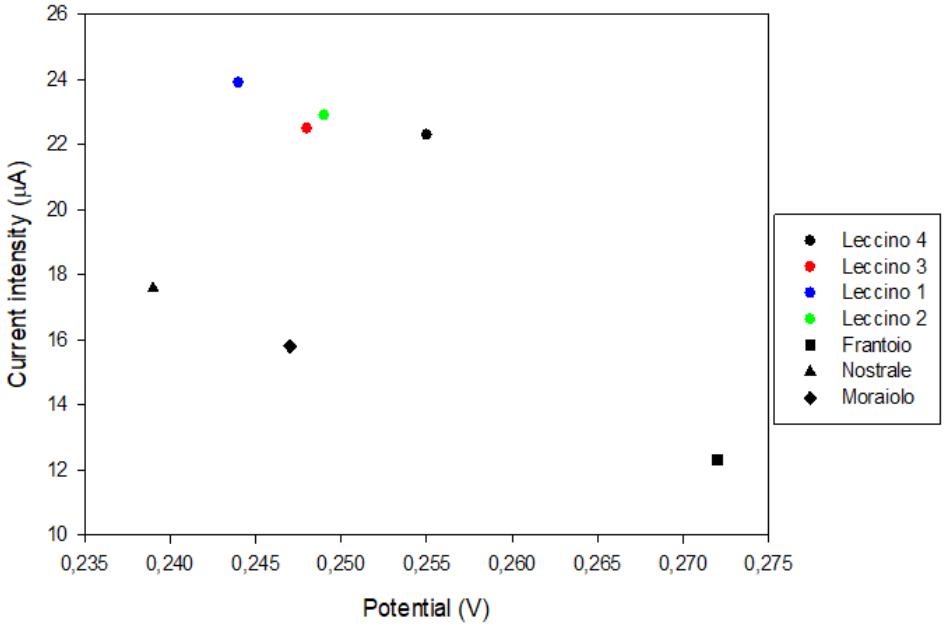

Figure 4.15 Potential and current intensity of anodic peaks for the various oils examined with the modified GSI electrode-based biosensor (Lipase from Candida Rugosa 103.68 IU μL^{-1}). Different colors correspond to different geographical origin (see Table 4.11)

Comparing the graphs shown in Figures 4.14 and 4.15, a strong similarity is observed, and thus the possible correlation between cultivar and content/type of antioxidants in the oil samples is confirmed. For all the following measures the less expensive GSI modified electrodes were used

One crucial detail of Lipases is that they work at the oil-water. It was thus decided to develop a different method of enzyme/substrate incubation, which could improve the catalytic action of the enzyme. To this end, enzyme-substrate incubation was carried out, no longer on the electrode but in a vial, placed in a water bath thermostated at 37 ° C for 15 minutes. The enzymatic activity in the vial (mixture described in section 3.1.2) was maintained the same as that of the previous incubation method (immobilization on the electrode). After incubation, the emulsion was deposited on the electrode and immediately analyzed in the same operative conditions as before. The results are shown below (Table 4.12 and Figure 4.16).

Geographical origin	**Cultivar**	**Oxidation peak potential (V ± *SD*)**	**Oxidation peak intensity (μA ± *SD*)**
Fiano Romano	Leccino (3)	0,209 ± 0,006	43,51 ± 0,08
Fiano Romano	Frantoio	0,227 ± 0,005	49,56 ± 0,07
Fiano Romano	Nostrale	0,169 ± 0,004	81,61 ± 0,05
Arpino	Moraiolo	0,172 ± 0,006	51,30 ± 0,06
Isola del Liri	Leccino (4)	0,241 ± 0,008	32,23 ± 0,05
Arpino	Leccino (1)	0,237 ± 0,005	20,99 ± 0,04
Bracciano	Leccino (2)	0,209 ± 0,005	27,36 ± 0,05

Table 4.12 Potentials and current intensities of the anodic peaks for the various oils examined with external incubation method (modified GSI electrode, Lipase from Candida Rugosa 103.68 IU μL^{-1}). The values shown are obtained from the average of three measurements.

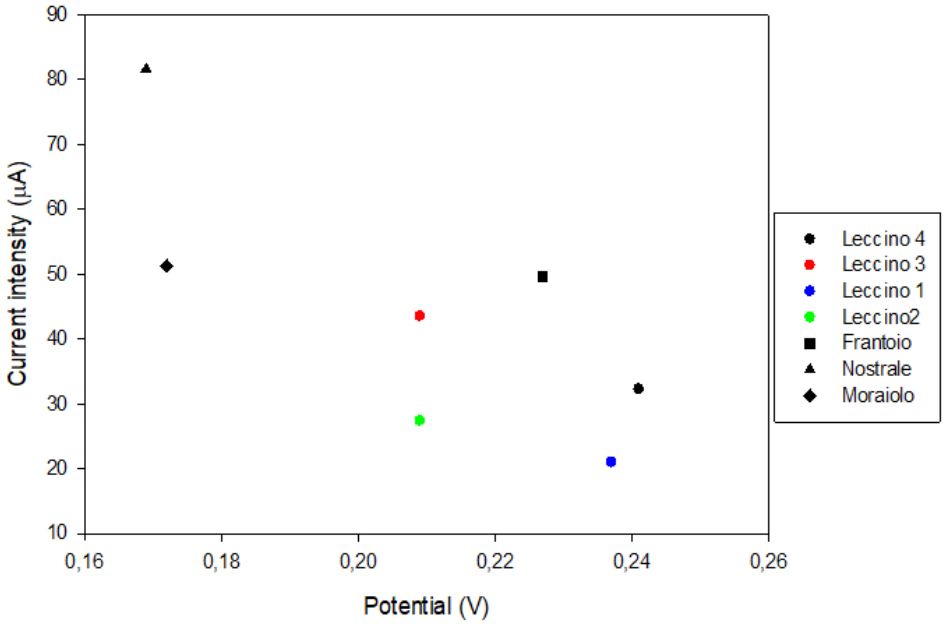

Figure 4.16 Potentials and current intensities of the anodic peaks for the various oils examined with external incubation method (modified GSI electrode, Lipase from Candida Rugosa 103.68 IU μL^{-1}). Different colors correspond to different geographical origin (see Table 4.12)

The introduction of the external incubation methodology allows Lipase to better act on the oil. The results show a considerable increase in terms of anodic current intensity; at the same time, there is a general reduction in the potential of anodic discharge peaks and a greater dispersion of the data points.

Since the addition of titanium dioxide to the nanomaterial mixture on the electrode surface significantly increased its electrochemical performance (section 4.2), the GSI GC / MWCNT / TiO_2 / [Ch] [Phe] / buffer electrode was coupled with the external incubation methodology to analyze the same oils in order to choose the best analytical methodology.

Table 4.13 and Figure 4.17 show the results obtained.

Geographical origin	Cultivar	Oxidation peak potential (V ± *SD*)	Oxidation peak intensity (μA ± *SD*)
Fiano Romano	Leccino (3)	0,250 ± 0,001	35,369 ± 0,005
Fiano Romano	Frantoio	0,239 ± 0,001	23,620 ± 0,003
Fiano Romano	Nostrale	0,224 ± 0,001	35,298 ± 0,003
Arpino	Moraiolo	0,207 ± 0,002	25,034 ± 0,001
Isola del Liri	Leccino (4)	0,248 ± 0,003	33,304 ± 0,002
Arpino	Leccino (1)	0,263 ± 0,002	29,279 ± 0,003
Bracciano	Leccino (2)	0,252 ± 0,002	26,706 ± 0,003

Table 4.13 Potentials and current intensities of the anodic peaks for the various oils examined with an external incubation method on a biosensor based on a modified GSI electrode with multiple-wall carbon nanotubes and titania nanoparticles (Lipase from Candida Rugosa 103.68 IU μL^{-1}). The values shown are obtained from the average of three measurements.

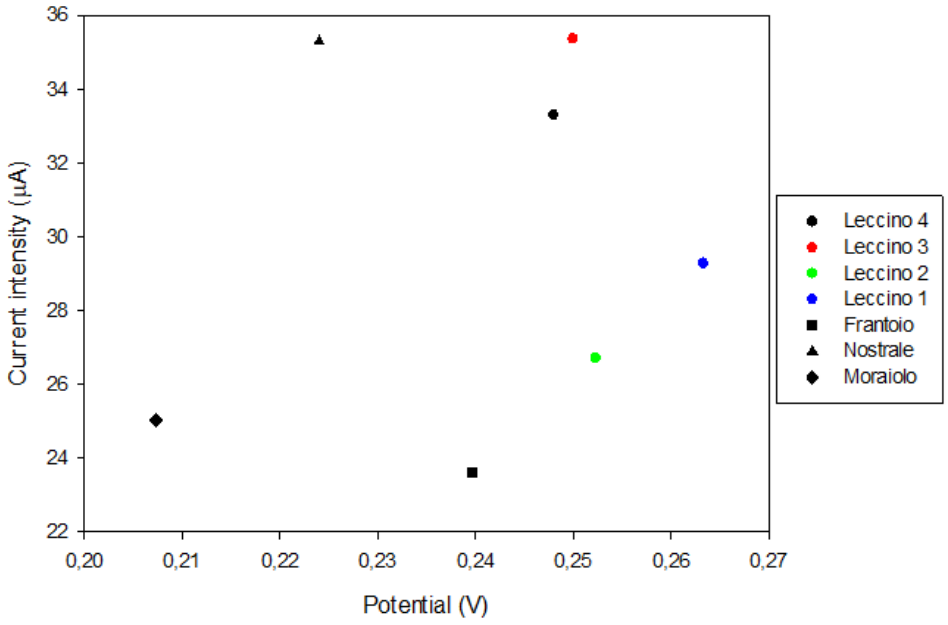

Figure 4.17 Potentials and current intensities of the anodic peaks for the various oils examined with the external incubation method on a modified GSI electrode with multi-walled carbon nanotubes and titania nanoparticles (Lipase from Candida Rugosa 103.68 IU μL^{-1}). Different colors correspond to different geographical origin (see Table 4.13)

The results obtained with the GC/MWCNT/TiO_2/[Ch][Phe] platform show a good aggregation of results for the Leccino cultivar samples. The results regarding the other cultivars are quite far from the Leccino grouping, which makes possible a

classification for olive oils based on their cultivar. Moreover, from Table 4.12 and 4.13, it clearly comes out that the platform using MWCNT and TiO_2 has much higher reproducibility (SD) both for the oxidation peak potential and intensity. Finally, as shown in section 4.2, the electrode modified with MWCNT/TiO_2 shows much higher stability over time when compared to the electrodes modified without TiO_2. Thus, the GSI electrode GC / MWCNT / TiO_2 / [Ch] [Phe] / buffer, with external incubation methodology has been selected for all following analyses on extra-virgin olive oils.

4.3.2. Analysis and classification of extra-virgin olive oils with the optimized analytical method.

The proposed sensing method does not employ a specific electrocatalysis process to quantify the amounts of specific antioxidants. Instead, it allows wide-spectrum oxidation of the antioxidant compounds that are naturally present in EVOOs, which are released from the oil matrix upon hydrolytic action of Lipase enzyme on triglycerides.

Three independent treatments were performed on each oil sample (see 3.1.2); each resulting emulsion was analyzed with a different single-use modified electrode. For each triad of measurements, the standard deviation values of both potential and current intensity were calculated. For potential measurements, the standard deviations ranged from 0.0006 to 0.001 V; for current intensity measurements they ranged from 0.181 to 0.982 μA.

The result average values of oils produced during 2016, 2017, and 2018 harvest seasons, expressed in terms of potential and current intensity of the anodic peak, are reported in Figure 4.18.

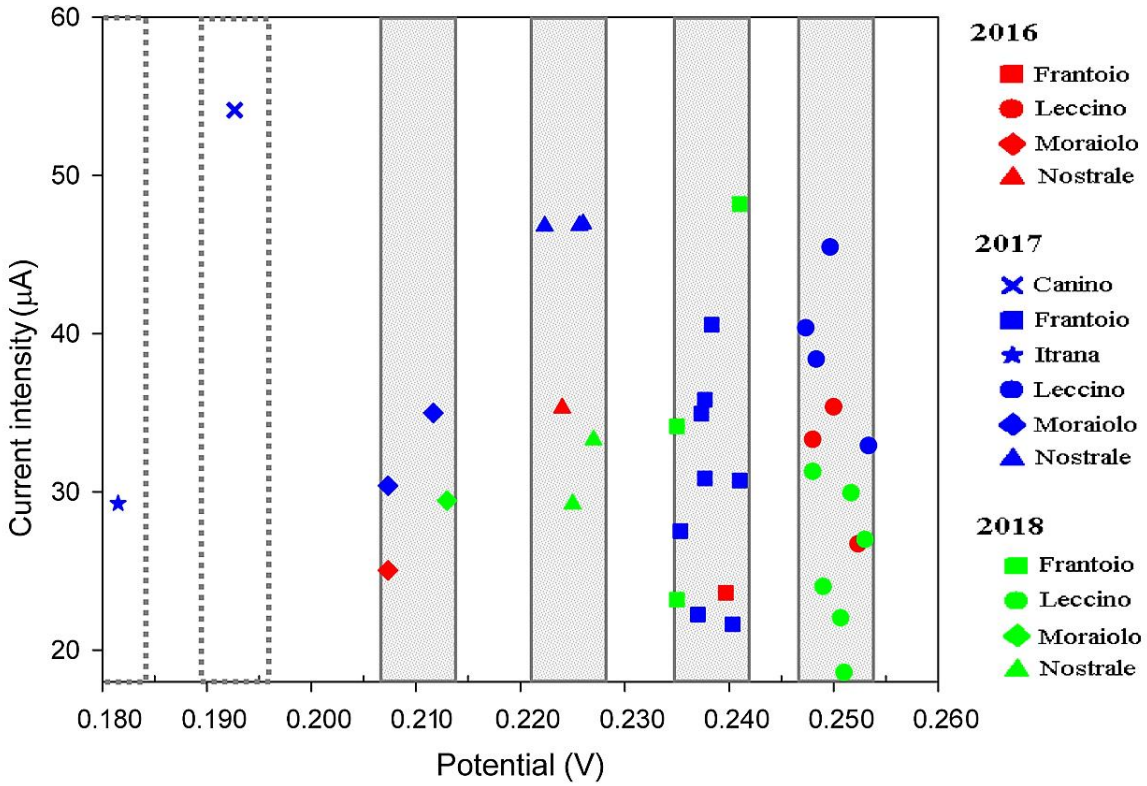

Figure 4.18 Results obtained for each oil sample produced from olives harvested in 2016 (red symbols), 2017 (blue symbols) and 2018 (green symbols). Different symbol shapes indicate different olives cultivar.

As can be seen, a categorization of the oils based on cultivar can be easily performed. The potential values of the anodic peak appear to be the most correlated variable with the olive's cultivar. This suggests that the differences in the relative abundance of antioxidants in the oils of different olive cultivar constitute the basis of the proposed classification process. Furthermore, the potential values seem to undergo only small variations for oils obtained from the same plant across different production years. These findings strengthen the thesis that the only significant variable which influences the antioxidant relative abundance in oil is the cultivar of the olives; thus confirming the validity of the present approach for the definition of criteria to categorize extra-virgin olive oils.

In Table 4.14 the average potential found for each cultivar has been reported.

Moreover, for each cultivar a "potential window" has been determined: a potential interval into which all the samples belonging to a specific cultivar have their oxidation peak maximum.

Cultivar	Potential window (V)
CANINO	0.193
FRANTOIO	0.235 – 0.241
ITRANA	0.182
LECCINO	0.247 - 0.253
MORAIOLO	0.207 - 0.213
NOSTRALE	0.223 - 0.227

Table 4.14 Average potential and the potential window for each examined cultivar.

The various cultivars produce oils presenting a potentiometric response quite specific for each. Indeed, the ranges of potential values for each cultivar are well separated and do not present overlap with near categories. This property minimizes the risks of assigning the wrong category to an oil sample with unknown cultivar.

On the other hand, the current intensities of the anodic peaks show no correlation with the oil cultivar: it is supposed that, while the measured oxidation potential depends mostly on the nature of the antioxidant species that vary from one cultivar to another, the corresponding current intensity is determined by the total antioxidant content of the oil.

The results show that the platform allows the classification of EVOOs from different mono-cultivar based on the oxidation potential of the antioxidant compounds, made available by the enzymatic hydrolysis. Since no enzyme is immobilized on the electrode, there is no risk of performance reduction after long storage periods. Furthermore, since no concentration of specific analytes has been measured, there is no need to calibrate the platform response with respect to different antioxidants before use. The final result is a cost-effective sensor able to identify the olive cultivar in a quick and reliable way, and usable by untrained personnel.

4.4. Polar antioxidants quantification in olive oils through electrochemical analysis of DES extract

4.4.1. Electrode modification optimization

One common kind of fraud regarding olive oils is the production of a mixture of EVOO with oils of lower quality (mainly virgin olive oil, but also *lampante* oil and various seed oils) which is then sold as EVOO. Sometimes seed oils are added with green-yellow additive (mainly chlorophyll and carotenoids) and sold as olive oils.
Official analytical techniques [112]–[114] can identify this kind of frauds but are too expensive and time-consuming to be performed on the field.
The main difference between extra-virgin olive oils and seed oils is that in the latter polar phenolic compounds are almost absent since the industrial extraction procedure involves the use of high-temperature water steam for extraction. The seed oil is then extracted from the emulsion using apolar organic solvents. It could then be useful to develop a sensor platform able to quantify the amount of polar phenolic compounds in an oil sample.
Traditionally, polar phenolic compounds are extracted from olive oil using different organic solvents, mainly hexane, acetonitrile, and methanol [115]. In this work, in order to minimize the method environmental impact, Deep Eutectic Solvent composed of glucose and lactic acid is used. In literature it has been proved that this DES can selectively extract polar phenolic compound from EVOO [87]–[89]
It was observed that the previously used GC / MWCNT / TiO_2 / [Ch] [Phe] / buffer modified electrode reacted to the DES, blocking further redox reactions. Thus, in order to have a sensitive sensor for phenolic compounds, a glassy carbon electrode was modified with the mixture of MWCNT and TiO_2 described in section 4.2, suspended in Nafion perfluorinated ion-exchange resin.

The working electrode surface was analyzed before and after modification using Scanning Electron Microscopy. SEM images (Figure 4.19) show that the modification with MWCNT, TiO_2, and Nafion was successful.

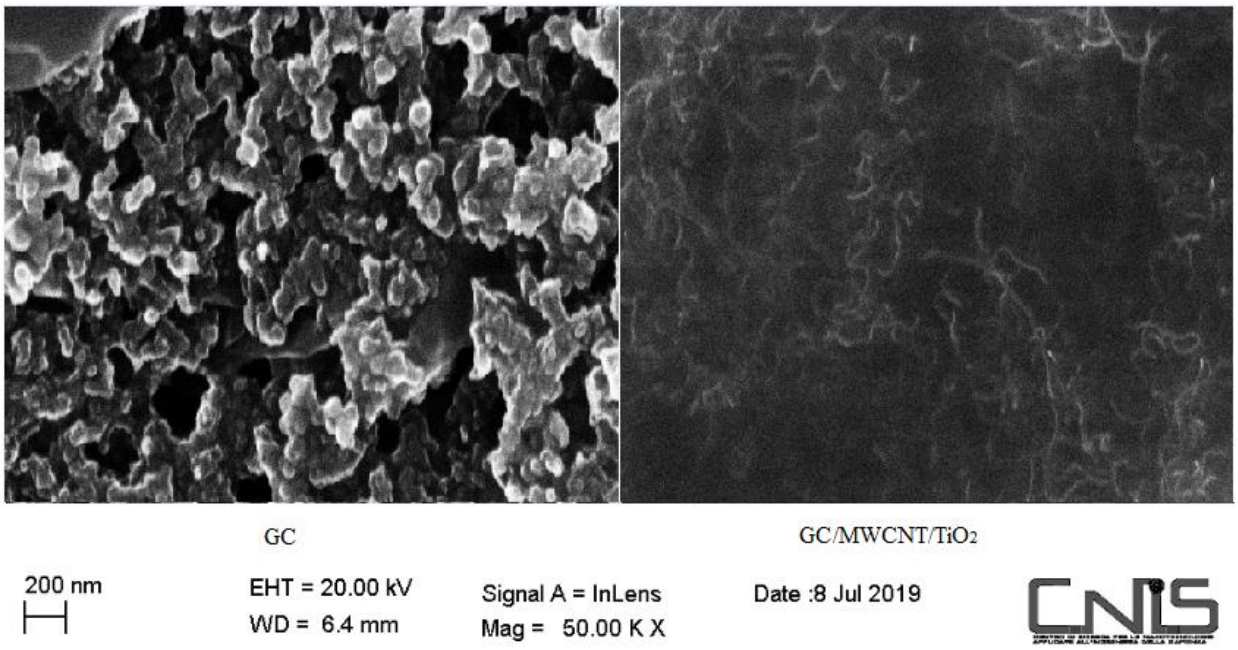

Figure 4.19 SEM images of A) glassy carbon electrode and B) GC modified with (MWCNT/TiO_2)/Nafion

The conditions of the electrode modification were optimized by measuring the electrochemical response of two pure phenolic compounds present in EVOO, which were dissolved in DES and analyzed through cyclic voltammetry.

In Table 4.15 are reported the peak intensities related to caffeic acid (CA) and vanillic acid (VA) depending on the quantities of the MWCNT / TiO_2 blend suspended in different suspensions of Nafion (different % w/w Nafion in alcoholic solution).

%w/w Nafion →	0.5		2		5	
CMWCNT/TiO_2 (mg mL^{-1})↓	I_{CA} (μA) ± *SD*	I_{VA} (μA) ± *SD*	I_{CA} (μA) ± *SD*	I_{VA} (μA) ± *SD*	I_{CA} (μA) ± *SD*	I_{VA} (μA) ± *SD*
0.5	7.897 ± 0.003	1.075 ±0.002	12.707 ± 0.001	1.897 ± 0.001	3.507 ± 0.007	1.445 ± 0.008
2	1.838 ± 0.002	0.347 ± 0.005	4.613 ± 0.003	1.103 ± 0.006	2.625 ± 0.006	0.581 ± 0.007
3	0.992 ± 0.004	0.313 ± 0.004	2.227 ± 0.007	0.776 ± 0.002	1.141 ± 0.009	0.276 ± 0.004

Table 4.15 Oxidation peaks intensities of the caffeic acid and vanillic acid by varying the nanomaterials blend and Nafion percentage in alcoholic solution.

The modified electrode surface appears more uniform when low quantities of the MWCNT / TiO_2 blend are used. The modified electrode response with respect to phenolic compounds seems to be directly correlated with the increasing percentage of Nafion, up to 2 %. Higher concentrations of Nafion cause the electrochemical response decreasing. Based on these results the electrode was modified with 0.5mg mL^{-1} of MWCNT / TiO_2 solid blend, dispersed in Nafion 2% solution.

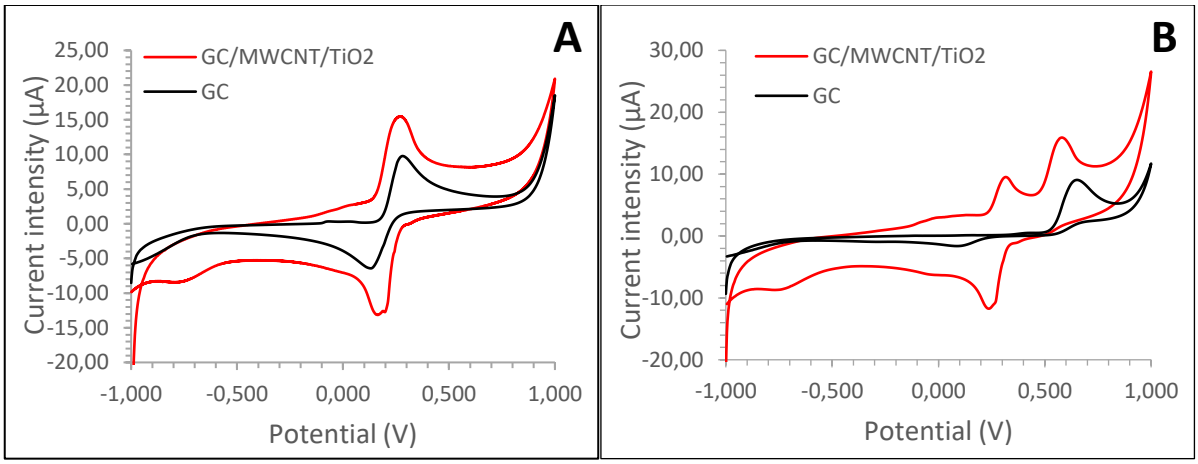

Figure 4.20 Cyclic voltammograms of A) caffeic acid (1.1 mmol L^{-1}) and B) vanillic acid (1.1 mmol L^{-1}) obtained using bare glassy carbon electrode (GC) and modified electrode. Caffeic acid and vanillic acid dissolved in DES. Scan rate: 20mV s^{-1}.

4.4.2. Extraction of total phenolic compounds with DES

The reported method of extraction of phenolic compounds by DES [89] uses oil-hexane solution (1 mL of oil sample and 2 mL of hexane shaken with 5 mL of DES). In order to develop a method environmentally friendly, it was tried to extract the polar phenolic compounds from olive oils without hexane. In this extraction method, the volume of the hexane was substituted by an equivalent volume of DES (1 mL of oil sample shaken with 7 mL of DES).

In Figure 4.21 the comparison of the square wave voltammetry (SWV) results relative to the phenolic compounds present in the two DES extracts (with and without hexane) by using the GC/MWCNT/TiO_2 electrodic platform are reported. It can be seen that the extraction without hexane gave higher current intensities.

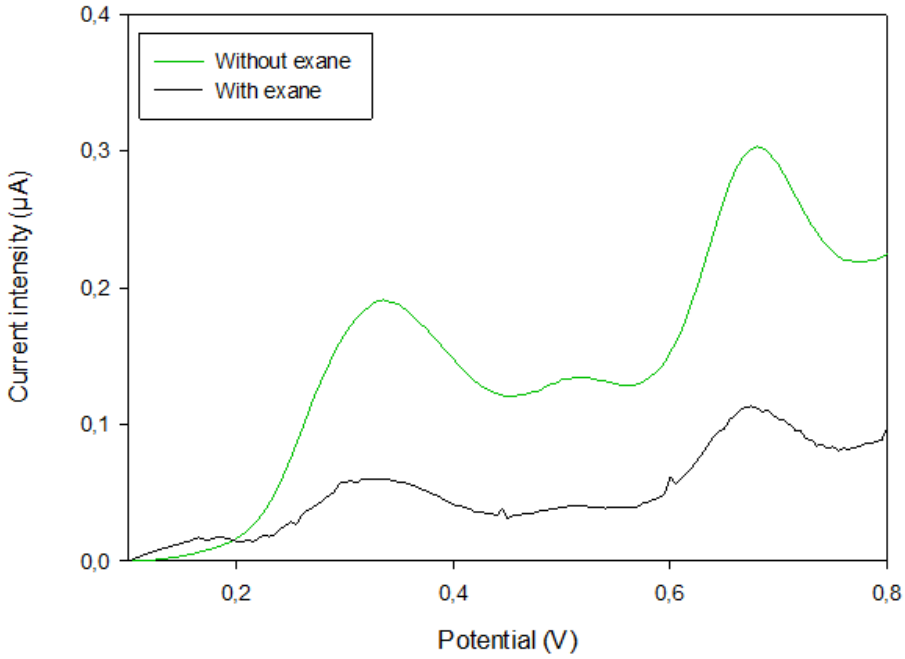

Figure 4.21 Comparison of square wave voltammograms relative to phenolic compounds extracted with DES, present in the EVOO sample and in the EVOO-hexane sample.

Measurements to determine the best oil:DES proportions for the antioxidants extraction were carried out by adding a fixed quantity of vanillic acid (VA) or caffeic

acid (CA) to one EVOO sample (antioxidant concentration added in the sample =0.1 mmol L^{-1}).

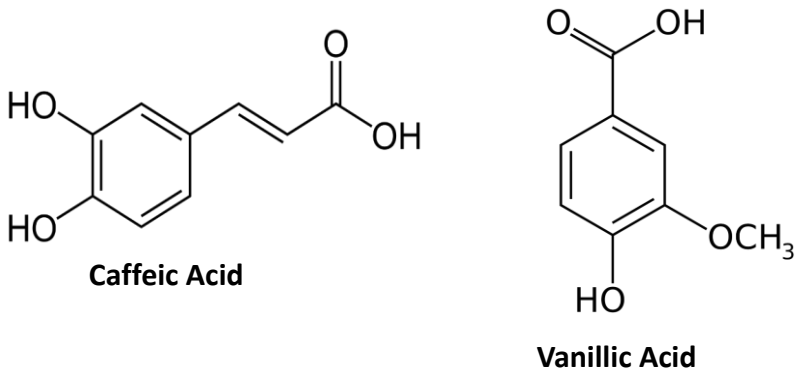

Figure 4.22: Antioxidants used in the optimization of the extraction process: caffeic acid (left) and vanillic acid (right).

At first, the electrochemical responses of the DES extracts obtained from pure oil and oils strengthened with CA or VA were analyzed using the proportions previously reported (oil:DES = 1:7). In Figure 4.23, the relative voltammograms are reported.

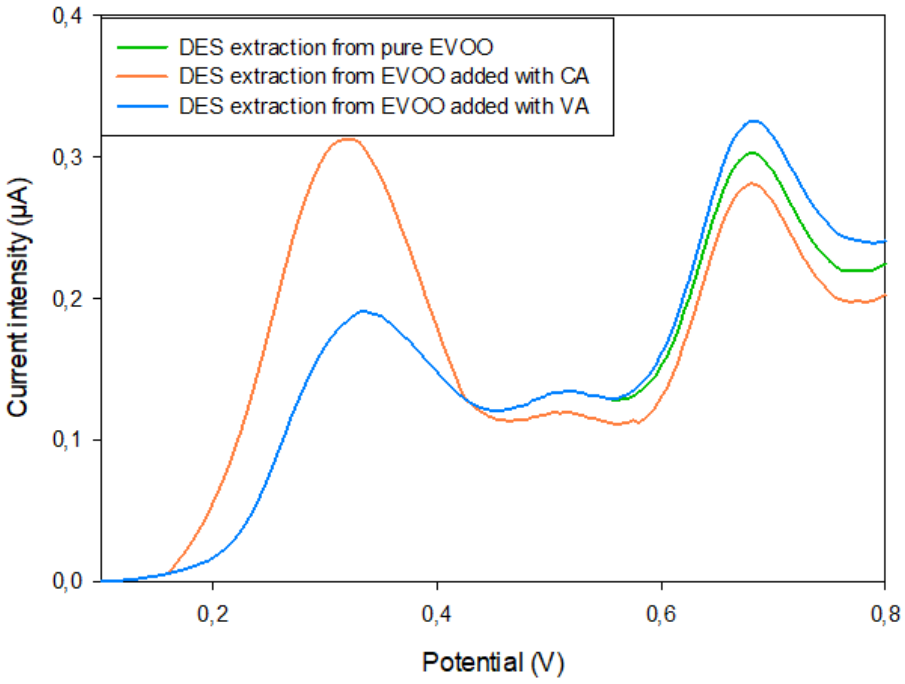

Figure 4.23 Comparison of the SWV results relative to pure oil and oil samples strengthened with caffeic acid and vanillic acid; CA and VA concentrations 1 mmol L-1: oil:DES = 1:7.

As it can be seen caffeic acid shows the oxidation peak at about 0.32 V and the vanillic acid peak appears at 0,68 V

Then measurements were carried out on the strengthened samples by varying the amounts of DES. The peak intensities for each antioxidant compound were obtained by the subtraction of the pure oil values from those of the strengthened samples (Figure 4.24).

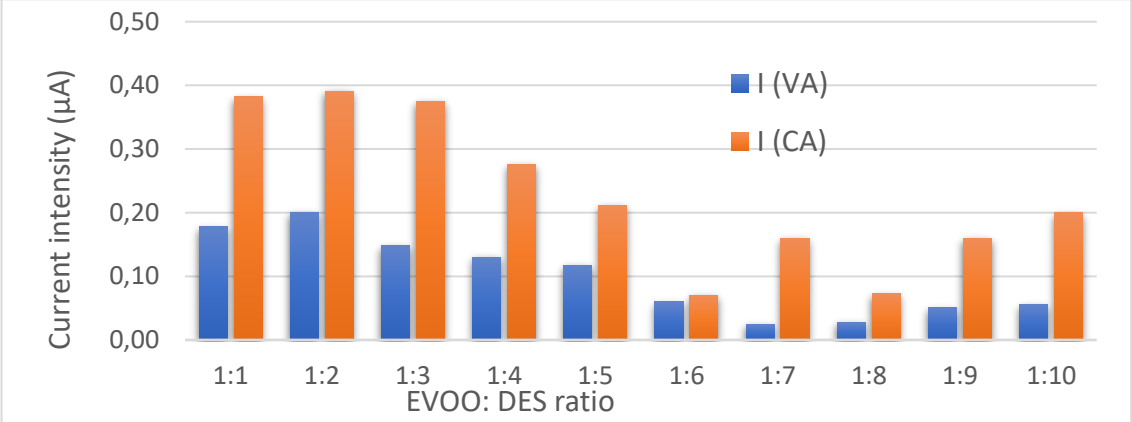

Figure 4.24 Effect of EVOO:DES ratios on antioxidant peak intensity responses relative to CA and VA strengthened oils respectively.

The ratio EVOO:DES=1:2 gave rise to the best results for both antioxidants.

Ultrasound techniques are known to be an efficient non-thermal extraction method [116], thus the sonication effect on the extraction efficiency of phenolic compounds from EVOO has been studied. These tests have been done by varying the sonication time, from 2 to 20 minutes. The optimal sonication time resulted 10 min. The CA and VA intensity signals are quit doubled compared with those obtained without sonication (Figure 4.25).

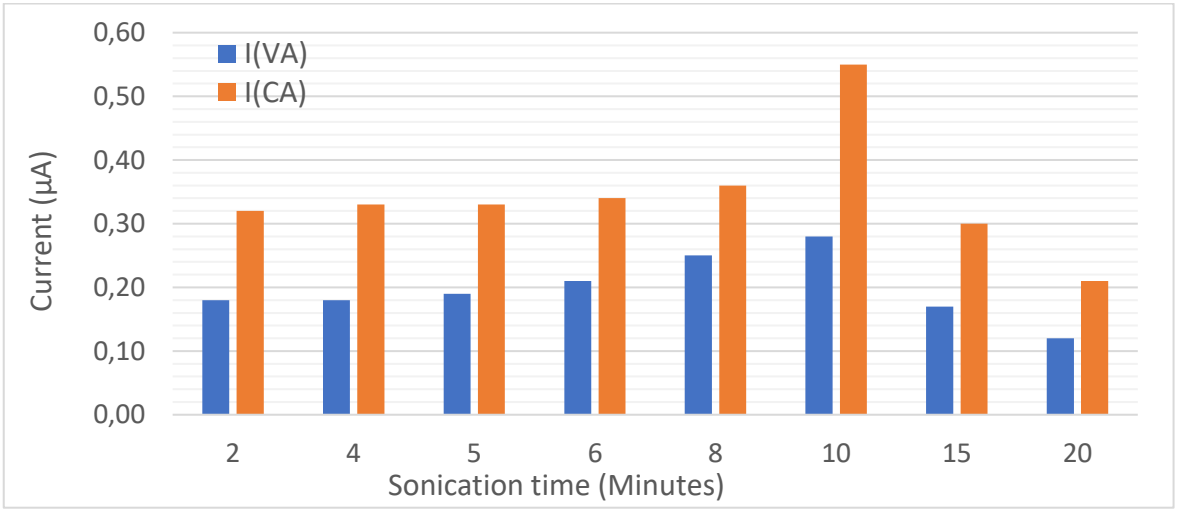

Figure 4.25 Effect of ultrasonication time on the current intensity of CA and VA peaks.

Another technique useful to further improve the efficiency of the extraction process was centrifugation. Therefore, this technique was also used by testing its efficiency on the extraction of phenolic compounds from EVOO/DES samples. Three different rotation speeds and different times of centrifugation have been examined. The results obtained are shown in Figure 4.26.

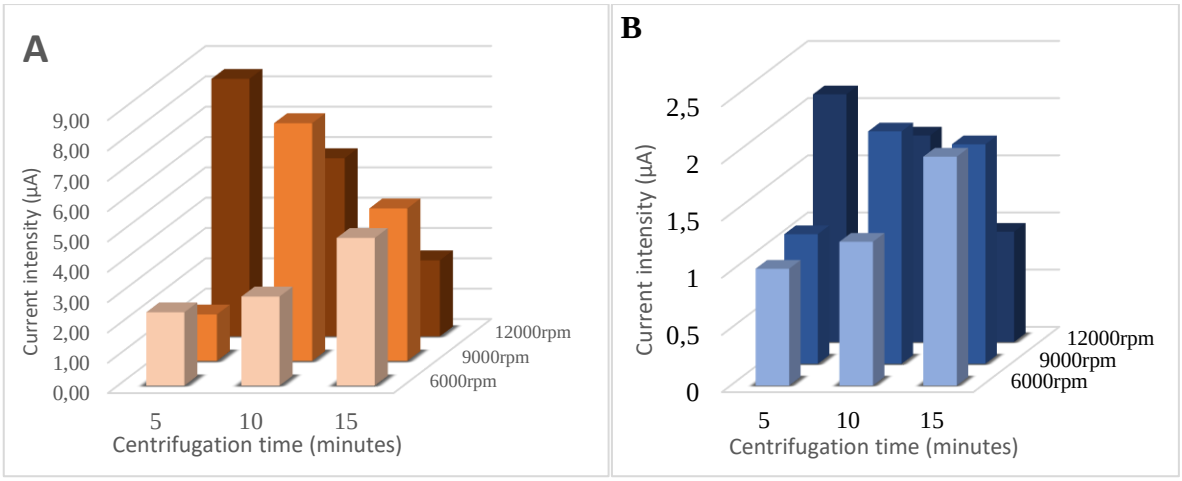

Figure 4.26 Effect of rotation speed and centrifugation time on the peak intensity relative to EVOO samples strengthened with A) caffeic acid and B) vanillic acid.

The highest intensity of current for both phenolic compounds (caffeic acid and vanillic acid) was obtained employing a rotational speed of 12000 rpm for 5 minutes, but at this speed, the centrifuge was subject to considerable heating. Since heating is known to cause degradation of phenolic compounds in EVOO, the rotational speed of 9000 rpm for 10 minutes was chosen as operative conditions, being the response only slightly lower and without heating effect.

The extraction procedure of polar antioxidants from EVOO used in all the following measurements was: EVOO:DES=1:2, sonication time=10 minutes, and centrifugation at 9000 rpm for 10 minutes.

4.4.3. Electrochemical determination of phenolic compounds

As far as we know DES has not been used in any electrochemical determination of phenolic compounds. In order to obtain a higher sensitivity for CA and VA determination, optimum SWV conditions were searched. Varying the square wave amplitude from 5 to 40 mV an increase of the peak intensity for CA and VA was observed. Setting the square wave amplitude above 40 mV no significant effect on the CA and VA responses resulted. Regarding frequency, starting from 10 Hz, a decrease in peak signals relative to CA and VA has been observed when the frequency was increased. Therefore, all the following measurements were conducted at 10 Hz frequency. The potential step increment was 2.5 mV since, for both analytes, any increase led to a decrease in signal intensity. For all the following measurements, amplitude = 40 mV, frequency = 10 Hz, and potential step increment = 2.5 mV were employed.

The calibration graphs, shown in Figure 4.27, were constructed by adding different quantities of antioxidants (CA or VA) dissolved in DES to the GC/MWCNT/TiO_2 platforms and to the bare GC electrodes. It can be seen that there is a linear dependence of current intensity with analytes concentration for both electrodes. The linear equations relative to the electrochemical response for CA and VA using the bare GC electrode are respectively

$$I(\mu A) = 0.0033 \cdot C_{CA}(\mu M) + 0.0851$$

$$I(\mu A) = 0.0003 \cdot C_{VA}(\mu M) + 0.0644$$

The GC/MWCNT/TiO_2 modified electrode provided higher sensitivity, better linearity, and lower limit of detection for CA and VA. The regression equations obtained are respectively

$$I(\mu A) = 0.0055 \cdot C_{CA}(\mu M) + 0.8900$$

$$I(\mu A) = 0.0016 \cdot C_{VA}(\mu M) + 0.2117$$

The detection limits for CA and VA determination were found to be 1.82 and 5.32 μmol L^{-1} respectively with GC. In the case of GC/MWCNT/TiO_2 platform, the

detection limits found were 0.6 and 1.03 μmol L^{-1} for CA and VA respectively. The electrode modified with MWCNT and TiO_2 showed 1.7 times higher sensitivity for CA and 5.3 times higher sensitivity for VA when compared to the unmodified electrode (GC).

It must be noted that the developed electrode shows a higher sensitivity towards CA than VA. However, the GC/MWCNT/TiO_2 can be applied to determine both CA and VA with high sensitivity, good linearity, and low detection limit.

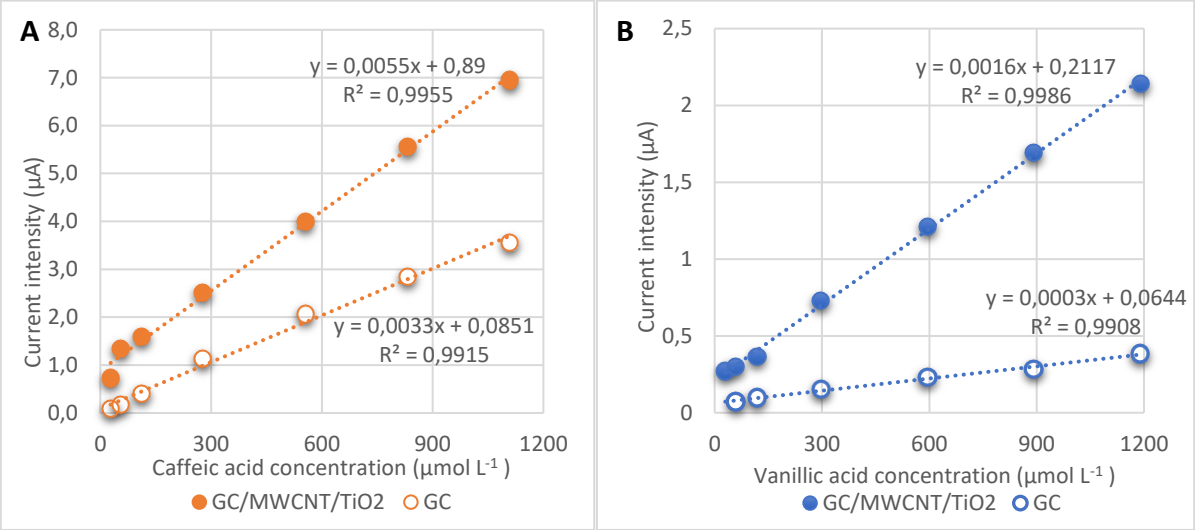

Figure 4.27 Comparison of A) caffeic acid and B) vanillic acid determination using GC/MWCNT/TiO_2 or bare GC electrode by square wave voltammetry.

The purpose of this study was to determine total polar phenolic compounds in EVOO and they can be divided into two groups: phenolic compounds oxidizing at low potential (about 220 mV) and phenolic compounds oxidizing at high potential (about 570 mV). Since in EVOOs there are a relatively high number of polar phenolic compounds with similar structures, their oxidation potentials may be similar but not the same. Therefore, to avoid the problem of peak overlap due to many compounds with similar potentials, the signals corresponding to CA and VA are calculated as total electric charge (Coulomb) exchanged in the redox process.

Since the software employed for the measurements provides the area of the peaks as V × mA, the area was divided by the scan rate used (expressed as V s^{-1}) to convert the value in Coulombs. For measurements performed employing SWV technique, the scan rate was calculated with the equation:

$$Scan\ Rate\ (V\ sec^{-1}) = \frac{E_{step}}{t}$$

Since the potential step employed was 2.5 mV, with a frequency of 10 Hz, the scan rate is 25 mV s^{-1}.

Figure 4.28 shows the linear dependence between the calculated electric charge and the concentrations of CA and VA. The respective ranges of linearity are 0,028-1.110 mmol L^{-1} for CA and 0.030-1.190 mmol L^{-1} for VA.

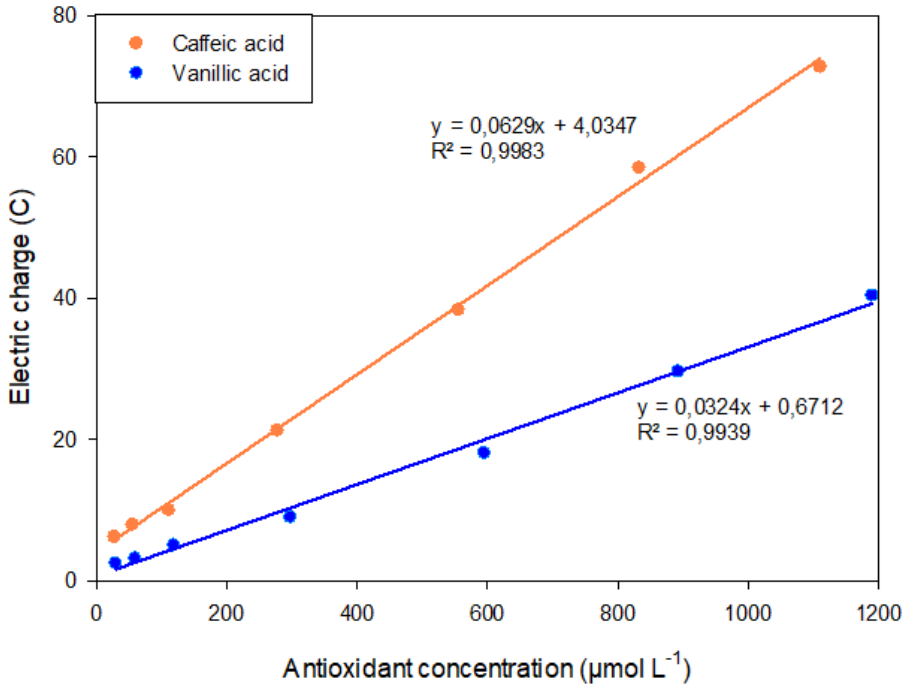

Figure 4.28 Electric charge variation vs concentrations of CA and VA.

4.4.4. Recovery and EVOO samples analysis

Under optimized conditions, a recovery test was performed for both groups of phenolic compounds. The model system for the group of compounds oxidizing at about 220 mV (1st Group) was constituted by CA and gallic acid (GA) in DES, while for the group oxidizing at about 570 mV (2nd Group) the mixture contained VA, p-coumaric acid (p-CA) and tyrosol (TS) (Figure 4.29).

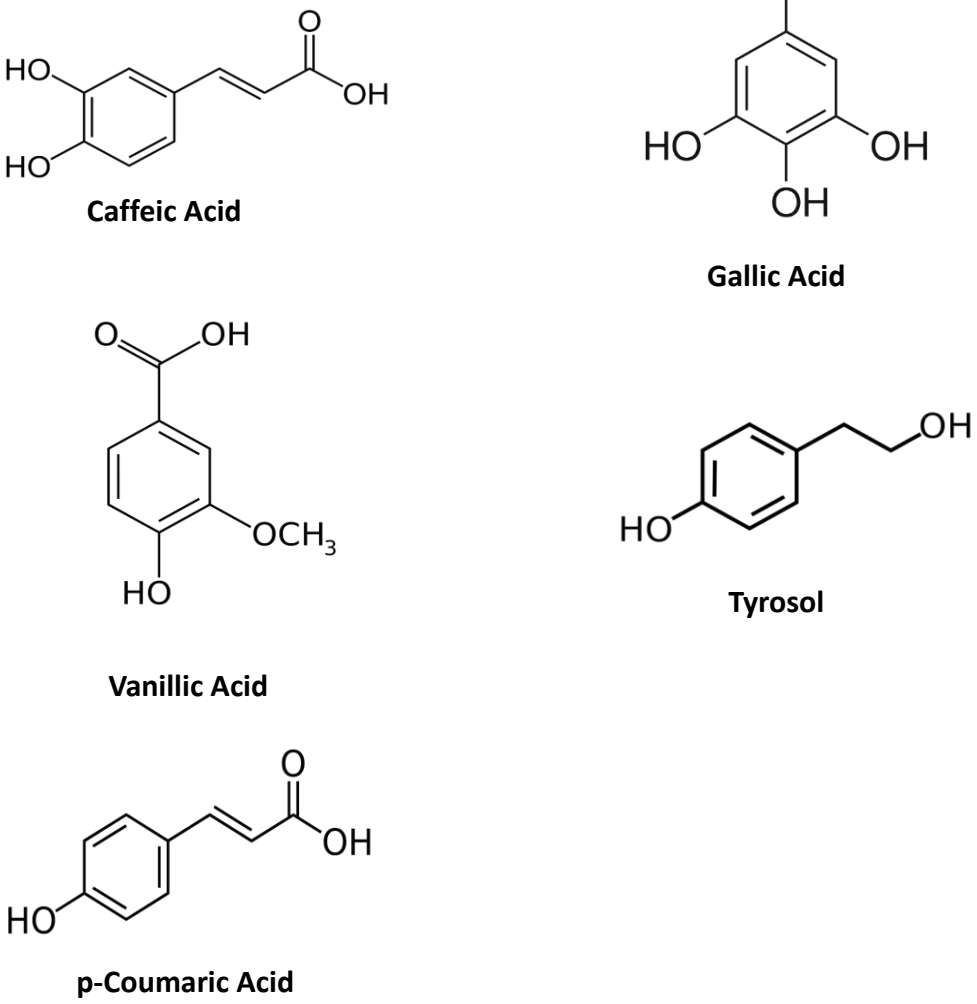

Figure 4.29: Antioxidants used for recovery test of developed platform: caffeic acid and gallic acid for antioxidant group oxidizing at about 220 mV (top row); vanillic acid, tyrosol and p-coumaric acid for antioxidant group oxidizing at about 550 mV (middle and lower row)

The obtained results are listed in Table 4.16. The percentage of recovery indicates that, although different phenolic compounds are present in different ratios of concentrations, the determination of total phenolic compounds added can be made.

Group	C_{CA} (μmol L^{-1})	C_{GA} (μmol L^{-1})	Total CA_{add}* (μmol L^{-1})	Total CA_{found} (μmol L^{-1}±*SD*)	Recovery (%)
1st	416.30	416.30	809.39	805.55 ± 0.02	99.52
	277.53	555.07	801.67	788.65 ± 0.01	98.37
	555.07	277.53	817.14	807.21 ± 0.02	98.78

	C_{VA} (μmol L^{-1})	$C_{p\text{-}CA}$ (μmol L^{-1})	C_{TS} (μmol L^{-1})	Total VA_{add}** (μmol L^{-1})	Total VA_{found} (μmol L^{-1}±*SD*)	Recovery (%)
2nd	297.37	297.37	297.37	964.04	941.51 ± 0.02	97.66
	148.69	446.06	297.37	967.76	967.19 ± 0.01	99.94
	446.06	148.69	297.37	960.34	946.44 ± 0.03	98.55
	297.37	148.69	446.06	992.60	926.69 ± 0.02	93.36
	297.37	446.06	148.69	935.50	919.04 ± 0.01	98.24
	148.69	297.37	446.06	996.31	990.15 ± 0.03	99.38
	446.06	297.37	148.69	931.76	901.75 ± 0.02	96.78

Table 4.16 Recovery results on model systems.

* The concentration of GA was converted to CA equivalents and then the phenolic compounds were calculated as total CA added.
**The concentrations of p-CA and TS were converted to VA equivalents, and then the total VA added was calculated.

Recovery tests were also performed on pure EVOO samples and results are shown in Table 4.17. The electrochemical determinations of polar phenolic compounds in several samples were compared with those obtained with the reference spectrophotometric method [89]. The results are in good agreement with those obtained with the spectrophotometric method. Since this last provides results expressed as GA equivalents, the values obtained by the electrochemical method are converted to GA equivalents.

Oil cultivar	This method (μmol L^{-1} ± *SD*)	Reference method (μmol L^{-1}± *SD*)	Recovery (%)
LECCINO	373.13 ± 0.03	385.23 ± 0.04	96.76
NOSTRALE	229.35 ± 0.02	235.67 ± 0.05	97.24
MORAIOLO	353.30 ± 0.02	356.54 ± 0.03	99.08

Table 4.17 Results comparison between the proposed electrochemical method and the reference spectrophotometric one.

Finally, the proposed method was also applied to different seed oil samples, in order to verify if the platform could be useful to discriminate them from olive oils. The results obtained for three seed oils (with known apolar antioxidant concentration) are shown in Table 4.18.

Samples	Tocopherol concentration (mg L^{-1} – labeled value)	Developed method (μmol L^{-1})
Sunflower oil	600	0
Corn oil	540	0
Soybean oil	690	0

Table 4.18 Analysis of seed oil samples with the proposed method and comparison with antioxidant concentration reported on the label

No significant peaks are observed for the three seed oils, confirming that polar antioxidant compounds are not present in seed oils. These results prove again that the proposed method is specific for polar antioxidant compounds as observed for the EVOO samples.

Furthermore, the method is useful for easily discriminate olive oils from oils obtained from oil of other seeds. This is particularly important since, to our knowledge, no screening method exists that allows such analysis to be performed on the field. It is possible to envisage the use of the proposed system in a situation in which is necessary to quickly analyze a massive amount of edible oils in a short time, such as at custom offices of major seaports.

4.5. EDXD analysis of edible oils

Aim of this study is to perform a qualitative comparison of EDXD spectra of edible oils to classify the oil samples based on origin, cultivar, or composition.

Twenty-two extra-virgin olive oil samples have been selected from those reported in section 3.1.4, considering cultivar and year of production. Furthermore, two seed oils have been analyzed (a soybean oil and a sunflower oil).

The X-ray analysis of the oil was performed using, as sample holder, a Kapton capillary with 2mm diameter. After each measure, the capillary was emptied and thoroughly cleaned, then used for the next measure. In this way, the influence of the capillary on the comparison of oils diffractometer data can be ignored.

A fixed amount of each oil sample was poured in the Kapton capillary, previously sealed at one end, with a single-use glass Pasteur pipette.

For each oil sample, X-ray diffraction measurements were performed at four angles (θ): 1°, 3°, 8°, and 30° in order to acquire data in the interval $0 \leq q \leq 25$. The X-ray absorption data for each oil was also recorded.

After the acquisition, each oil diffraction spectrum was normalized by dividing by the acquisition time. One example of the obtained spectrum is reported in Figure 4.30.

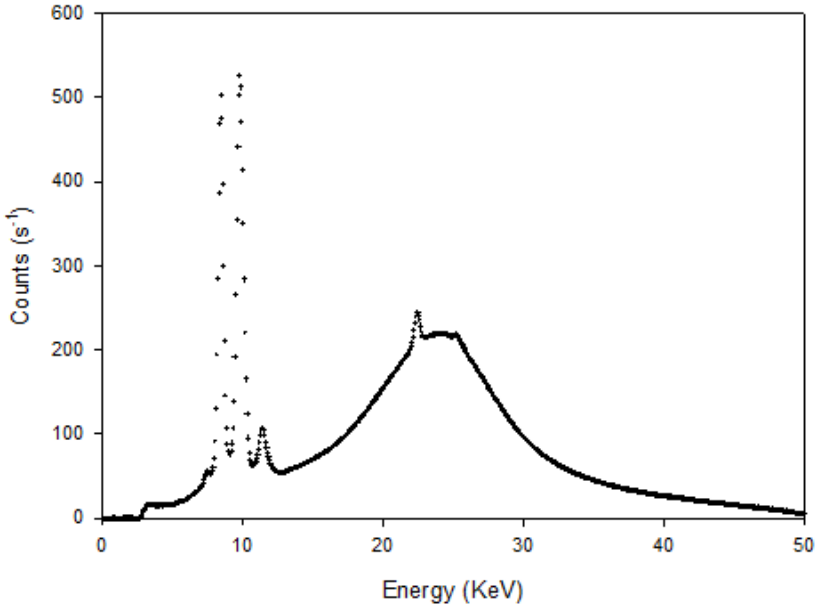

Figure 4.30 X-ray diffraction spectrum of an extra-virgin olive oil sample, θ = 3°.

Assuming the interaction between X-ray photons and the examined sample is elastic, the momentum of the scattered photon (q) will be:

$$q = \frac{4\pi \sin\theta}{\lambda}$$

From Bragg's Law, we know that the angle θ at which an X-ray photon is scattered depends by the distance between scattering centers (d):

$$\lambda = 2d \sin\theta$$

Thus, the momentum q of the scattered photon and the distance between scattering centers (d) are inversely proportional:

$$q = \frac{2\pi}{d}$$

From the literature, it is known [13] that vegetal edible oils have fatty acids with different chain lengths and degree of unsaturation. Thus, oils obtained from different plants should give different X-ray diffraction profiles due to different packing of the triglyceride molecules. Since our samples are liquids, we expect this difference to be more evident in the range of q corresponding to a scattering angle of 3°.

The variability of the EDXD spectra obtained for olive oils of the same cultivar is low, far less than the spectra variability in comparison to different cultivar oils. Therefore an average spectrum for each cultivar could be calculated. As an example in Figure 4.31 are reported the spectra of the selected Leccino cultivar oils.

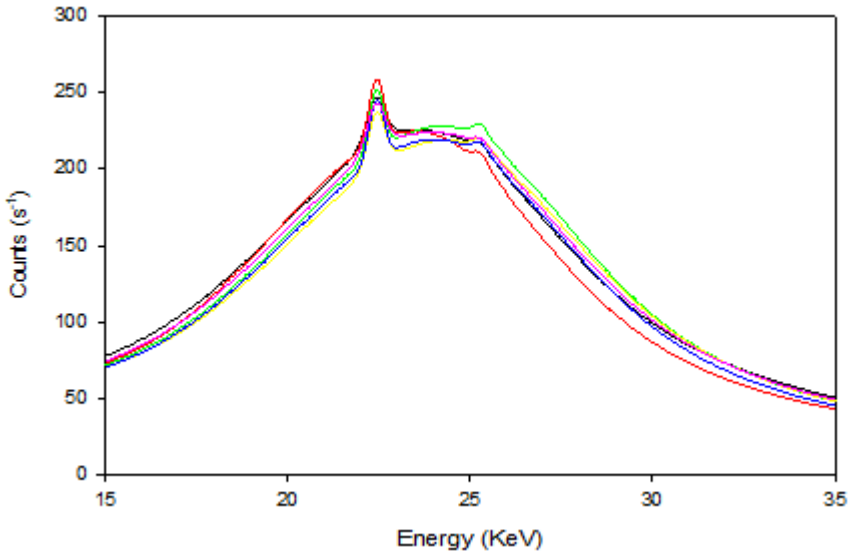

Figure 4.31 Comparison of EDXD spectra obtained for EVOOs of Leccino cultivar

The resulted average spectra of the different cultivar are shown in Figure 4.32. In the figure are also reported the data for the two selected seed oils.

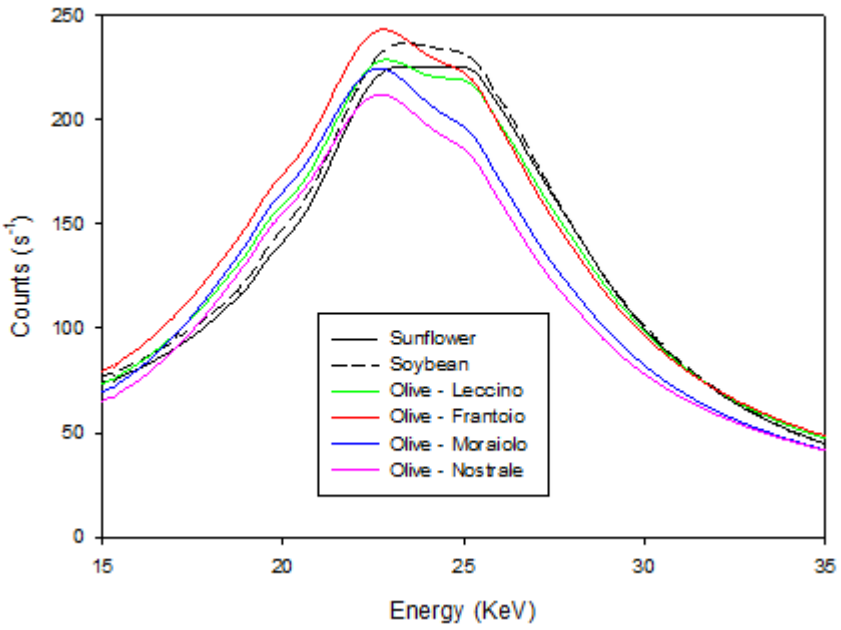

Figure 4.32 Comparison of EDXD spectra of the edible oils analyzed

In Figure 4.29, the spectra shown no sufficient differences to allow the prompt discrimination of the samples analyzed. The profiles are similar, but not equal and their complexity requires more accurate data analysis. Nonetheless, the figure shows that the profiles of olive oils spectra are quite different from those of sunflower and soybean oils, both in shape and position of the peak. It is thus possible to suppose that, with proper mathematical processing of the data, a more clear separation could appear.

5. Conclusions

Aim of this work was to develop one or more screening systems, easy to use for untrained personnel which could allow quick discrimination of edible oils based on composition, origin, and cultivar. Various analytical techniques have been developed and investigated in order to create a sensing platform reliable, easy to use, and with minimal impact on the environment.

The first sensing solution is a screen-printed electrode, modified with multi-walled carbon nanotubes, titanium oxide nanoparticles, and green ionic liquids. The ionic liquid-nanomaterial combinations and proportions were thoroughly studied and optimized using an experimental design and chemometric analysis. The best performing platform has been used to analyze 42 monocultivar extra-virgin olive oil samples, after incubation with Lipase enzyme from *Candida Rugosa*. After optimization of the experimental conditions, it was possible to use the platform to classify the oil samples based on their cultivar.

The second developed system is a screen-printed electrode, modified using Nafion perfluorinated resin and a multiwalled carbon nanotubes / Titanium oxide nanoparticles mixture. The modified platform was used in conjunction with a green Deep Eutectic Solvent, based on glucose and lactic acid, which was able to selectively extract polar phenolic compounds from olive oil without organic solvents. After optimization, the platform was able to perform an electrochemical quantification of polar phenolic compounds in real olive oil samples. The results obtained are in good agreement with the reference spectrophotometric method. Furthermore, when seed oils containing only non-polar antioxidants were analyzed, no response was obtained, proving the specificity of the platform towards olive oils.

Finally, X-ray diffraction spectra of the monocultivar oils were acquired. The acquisition process was quick and no pretreatment of the sample required. The obtained data do not allow quick discrimination of the samples studied, however since olive oil diffraction spectra appear to be significantly different from those of seed

oils, it is possible to suppose that proper chemometric processing of the spectra could help to achieve a useful classification of the samples.

Bibliography

[1] D. Zappi, R. Caminiti, G. M. Ingo, C. Sadun, C. Tortolini, and M. L. Antonelli, "Biologically friendly room temperature ionic liquids and nanomaterials for the development of innovative enzymatic biosensors," *Talanta*, vol. 175, pp. 566–572, Dec. 2017.

[2] D. Zappi *et al.*, "Biologically friendly room temperature ionic liquids and nanomaterials for the development of innovative enzymatic biosensors: Part II," *Talanta*, vol. 194, pp. 26–31, Mar. 2019.

[3] D. Zappi, C. Sadun, L. Gontrani, D. Dini, and M. L. Antonelli, "A new electrochemical sensor for extra-virgin olive oils classification," *Food Control*, p. 106903, Sep. 2019.

[4] C. Newton, C. Lorre, C. Sauvage, S. Ivorra, and J.-F. Terral, "On the origins and spread of Olea europaea L. (olive) domestication: evidence for shape variation of olive stones at Ugarit, Late Bronze Age, Syria—a window on the Mediterranean Basin and on the westward diffusion of olive varieties," *Vegetation History and Archaeobotany*, vol. 23, no. 5, pp. 567–575, 2014.

[5] P. Fiorino and F. Nizzi Griffi, "The spread of olive farming," *Olivae*, vol. 44, pp. 9–13, 1992.

[6] D. Boskou, *Olive Oil: Chemistry and Technology, Second Edition*. AOCS Publishing, 2006.

[7] S. Chazau-Gillig, "The civilisation of olive trees and cereals.," *Olivae*, vol. 54, p. 14, 1994.

[8] P. Perez-Martinez, A. Garcia-Rios, J. Delgado-Lista, F. Perez-Jimenez, and J. Lopez-Miranda, "Mediterranean Diet Rich in Olive Oil and Obesity, Metabolic Syndrome and Diabetes Mellitus," *Current Pharmaceutical Design*, vol. 17, no. 8, pp. 769–777, Mar. 2011.

[9] J. Perona, "Virgin olive oil reduces blood pressure in hypertensive elderly subjects," *Clinical Nutrition*, vol. 23, no. 5, pp. 1113–1121, Oct. 2004.

[10] A. M. Borzì, A. Biondi, F. Basile, S. Luca, E. S. D. Vicari, and M. Vacante, "Olive Oil Effects on Colorectal Cancer," *Nutrients*, vol. 11, no. 1, Dec. 2018.

[11] P. Yaqoob, J. A. Knapper, D. H. Webb, C. M. Williams, E. A. Newsholme, and P. C. Calder, "Effect of olive oil on immune function in middle-aged men," *The American Journal of Clinical Nutrition*, vol. 67, no. 1, pp. 129–135, Jan. 1998.

[12] M. A. De Pablo, M. A. Puertollano, and G. Álvarez de Cienfuegos, "Olive oil and immune system functions: potential involvement in immunonutrition," *Grasas y Aceites*, vol. 55, no. 1, pp. 42–51, Mar. 2004.

[13] F. D. Gunstone, *Fatty acid and lipid chemistry*. Springer, 2012.

[14] "Designations and definitions of olive oils - International Olive Council." [Online]. Available: http://www.internationaloliveoil.org/estaticos/view/83-designations-and-definitions-of-olive-oils. [Accessed: 21-Aug-2019].

[15] *Commission regulation (EEC) No 2568/91*. 1991.

[16] *Commission delegated regulation (EU) 2015/1830*. 2015.

[17] L. Zolichová, "Committee for the Common Organisation of the Agricultural Markets – Arable crops and olive oil," European commission for Agriculture and rural development, Nov. 2018.

[18] A. Baiano, C. Terracone, I. Viggiani, and M. A. D. Nobile, "Effects of Cultivars and Location on Quality, Phenolic Content and Antioxidant Activity of Extra-Virgin Olive Oils," *J Am Oil Chem Soc*, vol. 90, no. 1, pp. 103–111, Jan. 2013.

[19] "150 000 litres of fake extra virgin olive oil seized from 'well-oiled' gang | Europol." [Online]. Available: https://www.europol.europa.eu/newsroom/news/150-000-litres-of-fake-extra-virgin-olive-oil-seized-%E2%80%98well-oiled%E2%80%99-gang. [Accessed: 21-Aug-2019].

[20] Autoridade de Segurança Alimentar e Económica (ASAE), "ASAE apreende 4 265 litros de azeite 'biológico' por suspeita de fraude alimentar." [Online]. Available: http://www.asae.gov.pt/espaco-publico/noticias/comunicados-

de-imprensa/asae-apreende-4-265-litros-de-azeite-biologico-por-suspeita-de-fraude-alimentar.aspx. [Accessed: 21-Aug-2019].

[21] "Économie | Arles : 120 tonnes d'olives espagnoles cachées dans l'huile provençale | La Provence." [Online]. Available: https://www.laprovence.com/article/papier/4052849/des-olives-despagne-cachees-dans-lhuile-provencale.html. [Accessed: 21-Aug-2019].

[22] "Olio pugliese venduto come Igp Toscano, 47 indagati - In breve - ANSA.it." [Online]. Available: http://www.ansa.it/canale_terraegusto/notizie/in_breve/2016/03/03/olio-pugliese-venduto-come-igp-toscano-47-indagati_c62b7e22-5ec5-4c7a-a8b2-f04cf4285a26.html. [Accessed: 21-Aug-2019].

[23] R. Aparicio-Ruiz, I. Romero, D. L. García-González, C. Oliver-Pozo, and R. Aparicio, "Soft-deodorization of virgin olive oil: Study of the changes of quality and chemical composition," *Food Chemistry*, vol. 220, pp. 42–50, Apr. 2017.

[24] H. Azizian, M. M. Mossoba, A. R. Fardin-Kia, P. Delmonte, S. R. Karunathilaka, and J. K. G. Kramer, "Novel, Rapid Identification, and Quantification of Adulterants in Extra Virgin Olive Oil Using Near-Infrared Spectroscopy and Chemometrics," *Lipids*, vol. 50, no. 7, pp. 705–718, 2015.

[25] R. Korifi, Y. L. Dréau, J. Molinet, J. Artaud, and N. Dupuy, "Composition and authentication of virgin olive oil from French PDO regions by chemometric treatment of Raman spectra," *Journal of Raman Spectroscopy*, vol. 42, no. 7, pp. 1540–1547, 2011.

[26] L. Mannina and A. P. Sobolev, "High resolution NMR characterization of olive oils in terms of quality, authenticity and geographical origin," *Magnetic Resonance in Chemistry*, vol. 49, no. S1, pp. S3–S11, 2011.

[27] P. Dais and E. Hatzakis, "Quality assessment and authentication of virgin olive oil by NMR spectroscopy: A critical review," *Analytica Chimica Acta*, vol. 765, pp. 1–27, Feb. 2013.

[28] R. Goodacre, S. Vaidyanathan, G. Bianchi, and D. B. Kell, "Metabolic profiling using direct infusion electrospray ionisation mass spectrometry for the characterisation of olive oils," *Analyst*, vol. 127, no. 11, pp. 1457–1462, Oct. 2002.

[29] J. O. Alves, M. M. Sena, and R. Augusti, "Multivariate calibration applied to ESI mass spectrometry data: a tool to quantify adulteration in extra virgin olive oil with inexpensive edible oils," *Anal. Methods*, vol. 6, no. 18, pp. 7502–7509, Aug. 2014.

[30] B. Cañabate-Díaz *et al.*, "Separation and determination of sterols in olive oil by HPLC-MS," *Food Chemistry*, vol. 102, no. 3, pp. 593–598, Jan. 2007.

[31] M. Holčapek and M. Lísa, "Statistical evaluation of triacylglycerol composition by HPLC/APCI-MS," *Lipid Technology*, vol. 21, no. 11–12, pp. 261–265, 2009.

[32] C. Ruiz-Samblás, F. Marini, L. Cuadros-Rodríguez, and A. González-Casado, "Quantification of blending of olive oils and edible vegetable oils by triacylglycerol fingerprint gas chromatography and chemometric tools," *Journal of Chromatography B*, vol. 910, pp. 71–77, Dec. 2012.

[33] A. Hulanicki', S. Geab, and F. Ingman, "CHEMICAL SENSORS DEFINITIONS AND CLASSIFICATION," p. 4.

[34] C. Tortolini, P. Bollella, M. L. Antonelli, R. Antiochia, F. Mazzei, and G. Favero, "DNA-based biosensors for Hg2+ determination by polythymine–methylene blue modified electrodes," *Biosensors and Bioelectronics*, vol. 67, pp. 524–531, May 2015.

[35] J. H. T. Luong, K. B. Male, and J. D. Glennon, "Biosensor technology: Technology push versus market pull," *Biotechnology Advances*, vol. 26, no. 5, pp. 492–500, 2008.

[36] M. Turemis, S. Silletti, G. Pezzotti, J. Sanchís, M. Farré, and M. T. Giardi, "Optical biosensor based on the microalga-paramecium symbiosis for improved marine monitoring," *Sensors and Actuators B: Chemical*, vol. 270, pp. 424–432, Oct. 2018.

[37] I. Mannelli, M. Minunni, S. Tombelli, and M. Mascini, "Quartz crystal microbalance (QCM) affinity biosensor for genetically modified organisms (GMOs) detection," *Biosensors and Bioelectronics*, vol. 18, no. 2–3, pp. 129–140, 2003.

[38] "A microcalorimetric enzymatic method for trehalose determination in food | SpringerLink." [Online]. Available: https://link.springer.com/article/10.1007/s10973-009-0415-7. [Accessed: 12-Aug-2019].

[39] M. L. Antonelli, F. Arduini, A. Laganà, D. Moscone, and V. Siliprandi, "Construction, assembling and application of a trehalase-GOD enzyme electrode system.," *Biosens Bioelectron*, vol. 24, no. 5, pp. 1382–1388, Jan. 2009.

[40] M. Júlia and M. Adélio, "Urea potentiometric biosensor based on urease immobilized on chitosan membranes," *Talanta*, vol. 47, no. 1, pp. 183–191, 1998.

[41] G. A. Zhylyak, S. V. Dzyadevich, Y. I. Korpan, A. P. Soldatkin, and A. V. El'skaya, "Application of urease conductometric biosensor for heavy-metal ion determination," *Sensors and Actuators B: Chemical*, vol. 24, no. 1–3, pp. 145–148, 1995.

[42] L. C. Clark and C. Lyons, "Electrode Systems for Continuous Monitoring in Cardiovascular Surgery," *Annals of the New York Academy of Sciences*, vol. 102, no. 1, pp. 29–45, 1962.

[43] M. Pohanka and P. Skládal, "Electrochemical biosensors - principles and applications," *J Appl Biomed*, vol. 6, no. 2, pp. 57–64, Jul. 2008.

[44] W. Zhang and G. Li, "Third-Generation Biosensors Based on the Direct Electron Transfer of Proteins," *Analytical Sciences*, vol. 20, no. 4, pp. 603–609, 2004.

[45] R. P. Feynman, "There's Plenty of Room at the Bottom," *Engineering and Science*, vol. 23, no. 5, p. 22, 1960.

[46] W. Bollmann and J. Spreadborough, "Action of Graphite as a Lubricant," *Nature*, vol. 186, no. 4718, pp. 29–30, Apr. 1960.

[47] S. Iijima, "Helical microtubules of graphitic carbon," *Nature*, vol. 354, no. 6348, pp. 56–58, Nov. 1991.

[48] H. W. Kroto, J. R. Heath, S. C. O'Brien, R. F. Curl, and R. E. Smalley, "C 60 : Buckminsterfullerene," *Nature*, vol. 318, no. 6042, pp. 162–163, Nov. 1985.

[49] M. Brust, M. Walker, D. Bethell, D. J. Schiffrin, and R. Whyman, "Synthesis of thiol-derivatised gold nanoparticles in a two-phase Liquid–Liquid system," *J. Chem. Soc., Chem. Commun.*, no. 7, pp. 801–802, Jan. 1994.

[50] H. Li, S. Liu, Z. Dai, J. Bao, and X. Yang, "Applications of Nanomaterials in Electrochemical Enzyme Biosensors," *Sensors (Basel)*, vol. 9, no. 11, pp. 8547–8561, Oct. 2009.

[51] C. Lanzellotto *et al.*, "Nanostructured enzymatic biosensor based on fullerene and gold nanoparticles: Preparation, characterization and analytical applications," *Biosensors and Bioelectronics*, vol. 55, pp. 430–437, May 2014.

[52] K. S. Novoselov *et al.*, "Electric Field Effect in Atomically Thin Carbon Films," *Science*, vol. 306, no. 5696, pp. 666–669, Oct. 2004.

[53] Z. Tehrani *et al.*, "Generic epitaxial graphene biosensors for ultrasensitive detection of cancer risk biomarker," *2D Mater.*, vol. 1, no. 2, p. 025004, Sep. 2014.

[54] D. Reyes-Coronado, G. Rodríguez-Gattorno, M. E. Espinosa-Pesqueira, C. Cab, R. de Coss, and G. Oskam, "Phase-pure TiO2nanoparticles: anatase, brookite and rutile," *Nanotechnology*, vol. 19, no. 14, p. 145605, Mar. 2008.

[55] S. M. Gupta and M. Tripathi, "A review of TiO2 nanoparticles," *Chin. Sci. Bull.*, vol. 56, no. 16, p. 1639, May 2011.

[56] H. Shi, R. Magaye, V. Castranova, and J. Zhao, "Titanium dioxide nanoparticles: a review of current toxicological data," *Particle and Fibre Toxicology*, vol. 10, no. 1, p. 15, Apr. 2013.

[57] S. Pandey, "Analytical applications of room-temperature ionic liquids: A review of recent efforts," *Analytica Chimica Acta*, vol. 556, no. 1, pp. 38–45, Jan. 2006.

[58] P. Walden, "Molecular weights and electrical conductivity of several fused salts," *Bulletin of the Imperial Academy of Sciences (Saint Petersburg)*, vol. 1800, pp. 405–422, 1914.

[59] J. D. Holbrey and K. R. Seddon, "Ionic Liquids," *Clean Products and Processes*, vol. 1, no. 4, pp. 223–236, Dec. 1999.

[60] J. A. Crank and D. W. Armstrong, "Towards a second generation of ionic liquid matrices (ILMs) for MALDI-MS of Peptides, proteins, and carbohydrates," *J Am Soc Mass Spectrom*, vol. 20, no. 10, pp. 1790–1800, Oct. 2009.

[61] S. Ahrens, A. Peritz, and T. Strassner, "Tunable Aryl Alkyl Ionic Liquids (TAAILs): The Next Generation of Ionic Liquids," *Angewandte Chemie International Edition*, vol. 48, no. 42, pp. 7908–7910, 2009.

[62] J. Arning *et al.*, "Qualitative and quantitative structure activity relationships for the inhibitory effects of cationic head groups, functionalised side chains and anions of ionic liquids on acetylcholinesterase," *Green Chem.*, vol. 10, no. 1, pp. 47–58, Jan. 2008.

[63] A. Romero, A. Santos, J. Tojo, and A. Rodríguez, "Toxicity and biodegradability of imidazolium ionic liquids," *Journal of Hazardous Materials*, vol. 151, no. 1, pp. 268–273, Feb. 2008.

[64] T. Welton, "Room-Temperature Ionic Liquids. Solvents for Synthesis and Catalysis," *Chem. Rev.*, vol. 99, no. 8, pp. 2071–2084, Aug. 1999.

[65] S. D. Santis *et al.*, "Cholinium-amino acid based ionic liquids: a new method of synthesis and physico-chemical characterization," *Phys. Chem. Chem. Phys.*, vol. 17, no. 32, pp. 20687–20698, Aug. 2015.

[66] Z.-M. Jiang, L.-J. Wang, Z. Gao, B. Zhuang, Q. Yin, and E.-H. Liu, "Green and efficient extraction of different types of bioactive alkaloids using deep eutectic solvents," *Microchemical Journal*, vol. 145, pp. 345–353, Mar. 2019.

[67] H. Lores, V. Romero, I. Costas, C. Bendicho, and I. Lavilla, "Natural deep eutectic solvents in combination with ultrasonic energy as a green approach for solubilisation of proteins: application to gluten determination by immunoassay," *Talanta*, vol. 162, pp. 453–459, Jan. 2017.

[68] X. Peng *et al.*, "Green extraction of five target phenolic acids from Lonicerae japonicae Flos with deep eutectic solvent," *Separation and Purification Technology*, vol. 157, pp. 249–257, Jan. 2016.

[69] I. A. Lawal, M. M. Lawal, M. A. Azeez, and P. Ndungu, "Theoretical and experimental adsorption studies of phenol and crystal violet dye on carbon nanotube functionalized with deep eutectic solvent," *Journal of Molecular Liquids*, vol. 288, p. 110895, Aug. 2019.

[70] Z. Chen, B. Zhou, H. Cai, W. Zhu, and X. Zou, "Simple and efficient methods for selective preparation of α-mono or α,α-dichloro ketones and β-ketoesters by using DCDMH," *Green Chem.*, vol. 11, no. 2, pp. 275–278, 2009.

[71] E. Habibi, K. Ghanemi, M. Fallah-Mehrjardi, and A. Dadolahi-Sohrab, "A novel digestion method based on a choline chloride–oxalic acid deep eutectic solvent for determining Cu, Fe, and Zn in fish samples," *Analytica Chimica Acta*, vol. 762, pp. 61–67, Jan. 2013.

[72] J. T. Gorke, F. Srienc, and R. J. Kazlauskas, "Hydrolase-catalyzed biotransformations in deep eutectic solvents," *Chem. Commun.*, no. 10, p. 1235, 2008.

[73] A. P. Abbott, K. S. Ryder, and U. König, "Electrofinishing of metals using eutectic based ionic liquids," *Transactions of the IMF*, vol. 86, no. 4, pp. 196–204, Jul. 2008.

[74] T. Cai and H. Qiu, "Application of deep eutectic solvents in chromatography: A review," *TrAC Trends in Analytical Chemistry*, vol. 120, p. 115623, Nov. 2019.

[75] Y.-F. Lin and I.-W. Sun, "Electrodeposition of zinc from a Lewis acidic zinc chloride-1-ethyl-3-methylimidazolium chloride molten salt," *Electrochimica Acta*, vol. 44, no. 16, pp. 2771–2777, Apr. 1999.

[76] W.-G. Xu, X.-M. Lü, Q.-G. Zhang, J.-S. Gui, and J.-Z. Yang, "Studies on the Thermodynamic Properties of the Ionic Liquid BMIGaCl4," *Chinese Journal of Chemistry*, vol. 24, no. 3, pp. 331–335, 2006.

[77] J.-Z. Yang, P. Tian, L.-L. He, and W.-G. Xu, "Studies on room temperature ionic liquid InCl3–EMIC," *Fluid Phase Equilibria*, vol. 204, no. 2, pp. 295–302, Feb. 2003.

[78] A. P. Abbott, G. Capper, D. L. Davies, and R. K. Rasheed, "Ionic Liquid Analogues Formed from Hydrated Metal Salts," *Chemistry – A European Journal*, vol. 10, no. 15, pp. 3769–3774, 2004.

[79] A. P. Abbott, G. Capper, D. L. Davies, K. J. McKenzie, and S. U. Obi, "Solubility of Metal Oxides in Deep Eutectic Solvents Based on Choline Chloride," *J. Chem. Eng. Data*, vol. 51, no. 4, pp. 1280–1282, Jul. 2006.

[80] A. P. Abbott, P. M. Cullis, M. J. Gibson, R. C. Harris, and E. Raven, "Extraction of glycerol from biodiesel into a eutectic based ionic liquid," *Green Chem.*, vol. 9, no. 8, pp. 868–872, Aug. 2007.

[81] A. P. Abbott, T. J. Bell, S. Handa, and B. Stoddart, "Cationic functionalisation of cellulose using a choline based ionic liquid analogue," *Green Chem.*, vol. 8, no. 9, pp. 784–786, Sep. 2006.

[82] M. Gambino, P. Gaune, M. Nabavian, M. Gaune-Escard, and J. P. Bros, "Enthalpie de fusion de l'uree et de quelques melanges eutectiques a base d'uree," *Thermochimica Acta*, vol. 111, pp. 37–47, Feb. 1987.

[83] P. Zhou *et al.*, "Enhanced phenolic compounds extraction from Morus alba L. leaves by deep eutectic solvents combined with ultrasonic-assisted extraction," *Industrial Crops and Products*, vol. 120, pp. 147–154, Sep. 2018.

[84] P. S. Saravana, Y.-N. Cho, H.-C. Woo, and B.-S. Chun, "Green and efficient extraction of polysaccharides from brown seaweed by adding deep eutectic solvent in subcritical water hydrolysis," *Journal of Cleaner Production*, vol. 198, pp. 1474–1484, Oct. 2018.

[85] P. T. Kissinger and W. R. Heineman, "Cyclic voltammetry," *J. Chem. Educ.*, vol. 60, no. 9, p. 702, Sep. 1983.

[86] R. Caminiti, C. Sadun, V. Rossi Albertini, R. Felici, and F. Cilloco, "Brevetto Diffrattometro," RM 01261484.

[87] Y. Dai, J. van Spronsen, G.-J. Witkamp, R. Verpoorte, and Y. H. Choi, "Natural deep eutectic solvents as new potential media for green technology," *Analytica Chimica Acta*, vol. 766, pp. 61–68, Mar. 2013.

[88] Y. Dai, G.-J. Witkamp, R. Verpoorte, and Y. H. Choi, "Natural Deep Eutectic Solvents as a New Extraction Media for Phenolic Metabolites in Carthamus tinctorius L.," *Anal. Chem.*, vol. 85, no. 13, pp. 6272–6278, Jul. 2013.

[89] V. M. Paradiso, A. Clemente, C. Summo, A. Pasqualone, and F. Caponio, "Towards green analysis of virgin olive oil phenolic compounds : Extraction by a natural deep eutectic solvent and direct spectrophotometric detection," *Food Chemistry*, vol. 212, pp. 43–47, 2016.

[90] A. de Romo, "Tallow and the time capsule: Claude Bernard's discovery of the pancreatic digestion of fat," *Hist Philos Life Sci.*, vol. 11, no. 2, pp. 253–274, 1989.

[91] P. Desnuelle, "The Lipases," in *The Enzymes*, vol. 7, P.D. Boye, 1972, p. 575.

[92] H. L. Brockman, "General features of lipolysis," in *Lipases*, Amsterdam: Borgstrom, Elsevier, 1984, pp. 3–46.

[93] Carlos Andrés Galán-Vidal, "Monoenzymatic Lipase Potentiometric Biosensor for the Food Analysis Based on a pH Sensitive Graphite-epoxy Composite as Transducer," *J. Mex. Chem. Soc.*, vol. 59, no. 1, Oct. 2017.

[94] R. Pauliukaite, A. P. Doherty, K. D. Murnaghan, and C. M. A. Brett, "Application of room temperature ionic liquids to the development of electrochemical lipase biosensing systems for water-insoluble analytes," *Journal of Electroanalytical Chemistry*, vol. 656, no. 1, pp. 96–101, Jun. 2011.

[95] M. Tiina and M. Sandholm, "Antibacterial effect of the glucose oxidase-glucose system on food-poisoning organisms," *International Journal of Food Microbiology*, vol. 8, no. 2, pp. 165–174, May 1989.

[96] D. Dobbenie, M. Uyttendaele, and J. Debevere, "Antibacterial Activity of the Glucose Oxidase/Glucose System in Liquid Whole Egg," *Journal of Food Protection*, vol. 58, no. 3, pp. 273–279, Mar. 1995.

[97] V. Leskovac, S. Trivić, G. Wohlfahrt, J. Kandrač, and D. Peričin, "Glucose oxidase from Aspergillus niger: the mechanism of action with molecular oxygen, quinones, and one-electron acceptors," *The International Journal of Biochemistry & Cell Biology*, vol. 37, no. 4, pp. 731–750, Apr. 2005.

[98] J. E. Frew and H. A. O. Hill, "Electrochemical Biosensors," *Anal. Chem.*, vol. 59, no. 15, pp. 933A-944A, Aug. 1987.

[99] Y. Degani and Adam. Heller, "Direct electrical communication between chemically modified enzymes and metal electrodes. I. Electron transfer from glucose oxidase to metal electrodes via electron relays, bound covalently to the enzyme," *J. Phys. Chem.*, vol. 91, no. 6, pp. 1285–1289, Mar. 1987.

[100] F. Patolsky, Y. Weizmann, and I. Willner, "Long-Range Electrical Contacting of Redox Enzymes by SWCNT Connectors," *Angewandte Chemie International Edition*, vol. 43, no. 16, pp. 2113–2117, 2004.

[101] J. Liu, A. Chou, W. Rahmat, M. N. Paddon-Row, and J. J. Gooding, "Achieving Direct Electrical Connection to Glucose Oxidase Using Aligned Single Walled Carbon Nanotube Arrays," *Electroanalysis*, vol. 17, no. 1, pp. 38–46, 2005.

[102] V. Leskovac, S. Trivić, and D. Pericin, "The three zinc-containing alcohol dehydrogenases from baker's yeast, Saccharomyces cerevisiae," *FEMS Yeast Res.*, vol. 2, no. 4, pp. 481–494, Dec. 2002.

[103] K. Nakamura and T. Matsuda, "Asymmetric Reduction of Ketones by the Acetone Powder of Geotrichum candidum," *J. Org. Chem.*, vol. 63, no. 24, pp. 8957–8964, Nov. 1998.

[104] F. Salimi, M. Negahdary, G. Mazaheri, H. Akbari-dastjerdi, and S. Javadi, "A novel Alcohol Biosensor Based on Alcohol Dehydrogenase and Modified Electrode with ZrO2 Nanoparticles," *Int. J. Electrochem. Sci.*, vol. 7, p. 10, 2012.

[105] J.-K. Park *et al.*, "Determination of breath alcohol using a differential-type amperometric biosensor based on alcohol dehydrogenase," *Analytica Chimica Acta*, vol. 390, no. 1, pp. 83–91, May 1999.

[106] *A Bleachers Handbook*. Widnes, Cheshire, UK,: Interox Chemicals Ltd., 1980.

[107] O. Röe and P. Enoksson, "Species Differences in Methanol Poisoning," *CRC Critical Reviews in Toxicology*, vol. 10, no. 4, pp. 275–286, Jan. 1982.

[108] Y. Yao, G. Li, S. Ciston, R. M. Lueptow, and K. A. Gray, "Photoreactive TiO2/Carbon Nanotube Composites: Synthesis and Reactivity," *Environ. Sci. Technol.*, vol. 42, no. 13, pp. 4952–4957, Jul. 2008.

[109] S.-Z. Kang, Z. Cui, and J. Mu, "Composite of Carboxyl-Modified Multi-walled Carbon Nanotubes and TiO2 Nanoparticles: Preparation and Photocatalytic Activity," *Fullerenes, Nanotubes and Carbon Nanostructures*, vol. 15, no. 2, pp. 81–88, Mar. 2007.

[110] T. J. MacCormack *et al.*, "Inhibition of enzyme activity by nanomaterials: Potential mechanisms and implications for nanotoxicity testing," *Nanotoxicology*, vol. 6, no. 5, pp. 514–525, Aug. 2012.

[111] P. O. of the E. Union, *Commission Regulation (EEC) No 000/90 of 17 September 1990 determining Community methods for the analysis of wines, CELEX1*. 2005.

[112] J. M. Bosque-Sendra, L. Cuadros-Rodríguez, C. Ruiz-Samblás, and A. P. de la Mata, "Combining chromatography and chemometrics for the characterization and authentication of fats and oils from triacylglycerol compositional data—A review," *Analytica Chimica Acta*, vol. 724, pp. 1–11, Apr. 2012.

[113] J. Van Durme and J. Vandamme, "Non-thermal plasma as preparative technique to evaluate olive oil adulteration," *Food Chemistry*, vol. 208, pp. 185–191, Oct. 2016.

[114] N. Merchak, T. Rizk, V. Silvestre, G. S. Remaud, J. Bejjani, and S. Akoka, "Olive oil characterization and classification by 13C NMR with a polarization transfer technique: A comparison with gas chromatography and 1H NMR," *Food Chemistry*, vol. 245, pp. 717–723, Apr. 2018.

[115] M. Tasioula-Margari and E. Tsabolatidou, "Extraction, Separation, and Identification of Phenolic Compounds in Virgin Olive Oil by HPLC-DAD and HPLC-MS," *Antioxidants*, vol. 4, no. 3, pp. 548–562, Aug. 2015.

[116] Y. C. Chukwumah, L. T. Walker, M. Verghese, and S. Ogutu, "Effect of frequency and duration of ultrasonication on the extraction efficiency of selected isoflavones and trans-resveratrol from peanuts (Arachis hypogaea)," *Ultrasonics Sonochemistry*, vol. 16, no. 2, pp. 293–299, Feb. 2009.

Bibliography of the Author

[1]

D. Zappi, R. Caminiti, G. M. Ingo, C. Sadun, C. Tortolini, and M. L. Antonelli, "Biologically friendly room temperature ionic liquids and nanomaterials for the development of innovative enzymatic biosensors," *Talanta*, vol. 175, pp. 566–572, Dec. 2017.

[2]

D. Zappi, G. Masci, C. Sadun, C. Tortolini, M. L. Antonelli, and P. Bollella, "Evaluation of new cholinium-amino acids based room temperature ionic liquids (RTILs) as immobilization matrix for electrochemical biosensor development: Proof-of-concept with Trametes Versicolor laccase," *Microchemical Journal*, vol. 141, pp. 346–352, Sep. 2018.

[3]

D. Zappi *et al.*, "Biologically friendly room temperature ionic liquids and nanomaterials for the development of innovative enzymatic biosensors: Part II," *Talanta*, vol. 194, pp. 26–31, Mar. 2019.

[4]

D. Zappi, C. Sadun, L. Gontrani, D. Dini, and M. L. Antonelli, "A new electrochemical sensor for extra-virgin olive oils classification," *Food Control*, p. 106903, Sep. 2019.

[5]

D. Zappi *et al.*, "The effect of ionic strength and phosphate ions on the construction of redox polyelectrolyte–enzyme self-assemblies," *Phys. Chem. Chem. Phys.*, vol. 21, no. 41, pp. 22947–22954, Oct. 2019.